Robust liver vessel segmentation in medical images using 3-D deep learning approaches

Abir Affane

Robust liver vessel segmentation in medical images using 3-D deep learning approaches

Abir AFFANE

PHD thesis
To obtain the Doctor of Computer sciences grade of the
University Clermont Auvergne

Name	Affiliation
Pr. Antoine VACAVANT (Supervisor)	Pascal Institute, University of Clermont Auvergne
Dr. Marie-Ange Lebre (Supervisor)	Pascal Institute, University of Clermont Auvergne
Pr. Nicolat PASSAT (Examiner)	University of Reims Champagne-Ardenne (EA 3804 CReSTIC)
Pr. Benoît NAEGEL (Referee)	University of Strasbourg and ICube, IMAGeS team
Dr. Carole LARTIZIEN (Referee)	CNRS Research Director at CREATIS (Lyon)
Pr. Chafiaa HAMITOUCHE (Examiner)	LATIM Medical Information Processing Laboratory, Brest CHRU
Mr. Julien FINET (Examiner)	Manager at KITWARE Europe, Villeurbanne-Lyon

Doctoral school
Engineering sciences SPI

Discipline
Computer science

Date of the defense: 09/11/2022

Abstract

The evolution of computer science in research on vascular networks has revealed interest in the reconstruction and interpretation of these complex structures. The robust and automatic segmentation of the vessels can be used for many applications such as the resection of the liver in sub-regions. This definition of Couinaud segments was a good initialization for the researchers to solve several problems related to liver diseases, and also to facilitate the interpretation of images by radiologists. The exploration of the liver vessels in medical images is based on the correct acquisition during an examination. Nowadays, deep learning is providing new solutions for medical image segmentation problems and becomes a key point for future clinical application. The study of vascular structures is a challenging task due to the extremely small size of the vessel structure, low Signal to Noise Ratio (SNR), and varying contrast in medical image data. Since the arrival of deep learning, several methods based on pixel intensity have been tested to reduce more segmentation errors, but these intensity information were still not sufficient to preserve connectivity within branches, and may give poor segmentation outcomes in bifurcations. This is mainly due to the complexity of these structures and inhomogeneous contrast throughout the vascular network in medical images.

This thesis is dedicated to develop novel 3-D deep learning methods based on topological information for liver vessel segmentation from CT (Computerized Tomography) scans, which can help in improving segmentation decisions from vascular patterns. These approaches integrate both pixel wise intensity and topological signatures of vessel shapes by training a 3-D model with a specific topological loss function, which calculates the similarity between the likelihood map predicted by the 3-D model of segmentation and the ground-truth vessels. Our 3-D topological deep learning model gives better segmentation in terms of bifurcations and topology.

The first part of the work presents our different approaches used for vessel extraction. More precisely, 3-D U-Net, Dense U-Net, and MultiRes U-Net are pitted against each other in the vessel segmentation task on the CT scan public dataset from IRCAD. For each model, three alternative setups that allow adapting the selected architectures to volumetric data are tested. Namely, full 3-D, slab-based, and box-based setups are considered. These methods enable detecting bifurcations,

this comparison of 3-D models allows to choose the best approach based on the intensities of the image.

In the second part, a vesselness based method is introduced into the deep learning architecture to segment liver vessel in 3-D images. This approach enhances vessel in the whole 3-D volume of images in order to obtain more accurate segmentation. several vesselness filters were used and compared.

The third part of the thesis is devoted to introduce the topological signature. This information can help improve segmentation decision. The hierarchical study of the skeleton allows giving a graphic description of the hepatic vascular network. The incorporation of graph convolutions in the U-Net provides nodes in the graph with information that is based on node connectivity. Another topological approach is proposed to segment accurately liver vessel based on continuous-valued loss function, which can help in improving segmentation decisions from vascular patterns. It integrates both pixel wise intensity and topological structure of vessel shapes by training a 3-D U-Net with this specific topological loss function, by calculating the similarity between the likelihood map predicted by the 3-D U-Net and the ground-truth vessels.

Thus the complete processing pipeline developed leads to a precise 3-D reconstruction of the liver vascular network. It allows a better understanding of the hepatic vessel structure and provides the possibility to radiologists to better interpret medical images and liver desease.

Finally, we expose a comparative evaluation of the results with the state of the art methods, by a quantitative and qualitative assessment for clinical validation of the 3-D segmentation and reconstruction of hepatic vessels.

Resumé

L'évolution de l'informatique dans la recherche sur les réseaux vasculaires a permis d'améliorer la reconstruction et l'interprétation de ces structures complexes. L'extraction robuste de ces structures sur des images biomédicales nécessite une bonne acquisition lors d'un examen d'imagerie.

La segmentation des vaisseaux peut être utilisée pour de nombreuses applications telles que la division du foie en sous-régions. Cette définition des segments de Couinaud a été une bonne initialisation pour les chercheurs pour résoudre plusieurs problèmes liés aux maladies du foie, faciliter l'interprétation des images par les radiologues et même pour des planifications chirurgicales. L'exploration des vaisseaux hépatiques repose sur la bonne acquisition lors d'un examen. Le deep learning apporte de nouvelles solutions aux problèmes de segmentation des images médicales et devient une méthodologie de pointe pour de futures applications cliniques. L'étude des structures vasculaires est une tâche difficile en raison de la taille extrêmement petite de la structure du vaisseau, du faible SNR (Signal to Noise Ratio) et du contraste variable des données d'imagerie médicale. L'étude des structures curvilignes est une tâche difficile, en particulier compte tenu des applications d'imagerie médicale telles que la reconstruction des vaisseaux. Depuis l'arrivée des methodes d'apprentissage profond, plusieurs approches basées sur l'intensité des pixels ont été proposées pour réduire les erreurs de segmentation, mais ces informations ne sont toujours pas suffisantes pour préserver la connectivité au sein des branches et peuvent donner de mauvais résultats de segmentation dans les bifurcations. Ceci est principalement dû à la complexité de ces structures et au contraste inhomogène dans tout le réseau vasculaire des images médicales.

Cette thèse est consacrée au développement d'une nouvelle méthode d'apprentissage en profondeur 3-D basée sur des informations topologiques pour la segmentation des vaisseaux hépatiques à partir des images médicales, qui peut aider à améliorer les décisions de segmentation à partir des modèles vasculaires. Ces approches intègrent à la fois l'intensité du pixel et la structure topologique des vaisseaux en developpant des modèles 3-D avec une fonction de perte topologique spécifique, qui calcule la similarité entre la carte de vraisemblance prédite par un modèle 3-D de segmentation et les vaisseaux de vérité de terrain. Notre modèle d'apprentissage topologique profond 3-D est une technique prometteuse avec une meilleure qualité de segmentation sur les bifurcations notamment.

Dans une première partie, des modèles de segmentation U-Net 3-D sont revisités et comparés. Plus précisément, 3-D U-Net, Dense U-Net et MultiRes U-Net sont opposés les uns aux autres dans la tâche de segmentation des vaisseaux sur le jeu de données scanner public de l'IRCAD. Pour chaque modèle, trois configurations alternatives permettant d'adapter les architectures du réseau neuronal convolutif adaptées aux données volumétriques sont testées. À savoir, les configurations 3-D complètes, basées sur des groupes de coupes (slabs) et sur des patches 3-D sont prises en compte. Ces méthodes permettent de mieux détecter les bifurcations. Cette comparaison des modèles 3-D permet de choisir la meilleure approche basée sur les intensités de l'image.

Dans une seconde partie, une méthode basée sur la combinaison des modèles d'apprentissage profond avec des filtres de rehaussement est introduite pour segmenter les vaisseaux hépatiques sur des images 3-D. Cette approche améliore les resultats de segmentation. Plusieurs filtres de rehaussement ont été utilisés et comparés.

Enfin la troisième partie de la thèse est consacrée à introduire les signatures topologiques. Ces informations peuvent aider à améliorer la décision de segmentation. L'étude hiérarchique du squelette (sous forme de graphe) permet de donner une description graphique du réseau vasculaire hépatique. L'incorporation de convolutions de graphe dans le U-Net fournit grâce aux nœuds du graphe des informations basée sur la connectivité des nœuds. Une autre approche topologique est proposée pour segmenter avec précision les vaisseaux hépatiques basée sur une fonction de perte, ce qui peut aider à améliorer encore les décisions de segmentation. Il intègre à la fois l'intensité au niveau des pixels et la structure topologique des vaisseaux en combinant un 3-D U-Net avec cette fonction de perte topologique spécifique, qui calcule la similarité entre la carte de vraisemblance prédite par le 3-D U-Net et les vaisseaux de vérité de terrain.

Ainsi, le pipeline proposé conduit à une reconstruction 3D précise du réseau vasculaire hépatique. Il permet une meilleure compréhension de la structure des vaisseaux hépatiques et offre la possibilité aux radiologues de mieux interpréter les images médicales et les maladies du foie.

Enfin, une étape de comparaison des résultats avec les approches proposées dans la littérature est effectuée, en proposant une analyse quantitative et qualitative pour la validation des resultats de segmentation 3-D obtenus.

Acknowledgments

First of all, I would like to express my deep and respectful gratitude to my thesis director: Mr. **Antoine VACAVANT**, professor in computer science at Clermont Auvergne University and Pascal institute, for the trust they have placed in me by accepting to supervise my work. This thesis would not be possible without his endless help and selfless guidance. His kindness, generosity, patience and encouragements have accompanied me all the way during the past three years. My acknowledgements of his supports are indeed beyond words.

I would also like to thank my thesis supervisor, Mrs. **Marie-Ange LEBRE**, professor in computer science at IUT du Puy, Institut Pascal, Clermont-Ferrand, France, for the efforts made, the advice given, her patience, her tireless encouragement and her perseverance. I have been lucky enough to spend these years under her supervision. She is such a nice, amiable person, who is always here for me. It is truly great pleasure to work with her. I really appreciated all the efforts she has made, her directives and her advice which guided me in the elaboration of this thesis.

I would also like to address my special acknowledgments to all the personnel from the **"IUT du Puy en Velay"**, for welcoming me and guiding me during these three years.

I am truly grateful to every committee member of my thesis defense. I would particularly like to thank Prof. **Benoît NAEGEL** Professor in Computer Science at University of Strasbourg and ICube, IMAGeS team and Mrs. **Carole LARTIZIEN** CNRS Research Director at CREATIS (Lyon) for agreeing to be my thesis rapporteurs.

Furthermore, I would also like to thank Dr **Chafiaa HAMITOUCHE**, LATIM Medical Information Processing Laboratory, Brest CHRU and Prof. **Nicolas PASSAT** from the University of Reims Champagne-Ardenne (EA 3804 CReSTIC), and Mr **Julien FINET**, manager at KITWARE Europe, Villeurbanne-Lyon. It is truly a great honor to have them as examiners.

My gratitude also goes to all those who helped me to complete this work. I would also like to express my thanks to the whole team of the **Pascal Institute** laboratory and the whole members of the university of Clermont Auvergne.

Finally, I am indebted to my parents, **Samia** and **Abderrahmane**, for their unfailing moral and material support and their unfailing confidence in my choices,

their encouragement in the face of the trials of life. Without you I would not be here writing these few lines.

I would like to thank each member of my family, my sisters, Nadine, and Mebarka, my brothers Sohaib, Houssam, for supporting me these three years despite the distance.

Contents

List of Figures

List of Tables

1 Introduction

1.1 Working framework

This doctoral thesis entitled "Robust Liver vessel segmentation in biomedical images using 3-D deep learning approach" is carried out as part of the research work of the R-Vessel-X project funded by the French National Research Agency (ANR). The R-Vessel-X project proposes original and robust developments of image analysis and machine learning algorithms integrating strong mathematical frameworks, e.g. digital geometry and topology, mathematical morphology, or graphs for reconstructing vessels of the liver beyong medical image content. Another objective of R-Vessel-X is to diffuse research works in an open-source way, with the developments of plug-ins compatible with the ITK and VTK librairies largely popularized by the KITWARE company. This project also include benchmarks composed of images, associated ground-truth and quality metrics, so that researchers and engineers evaluate their novel contributions. The consortium of R-Vessel-X is composed of the following laboratories: Institut Pascal (coordinator, Le Puy-en-Velay/Clermont-Ferrand), LIRIS (Lyon), CReSTIC (Reims), working together with the KITWARE company (Lyon). This is a highly pluridisciplinary group composed of researchers in computer science-related topics (biomedical image processing, numerical simulation and analysis), applied mathematics (digital geometry and topology, mathematical morphology), working with medical doctors (radiologists, hepatologists) and young researchers and developers enrolled for the project.

1.1.1 The National Research Agency "ANR"

The National Research Agency (ANR) is a public administrative institution, placed under the supervision of the Ministry of Education, Research and Innovation. The Agency implements the financing of research on projects, for public operators in cooperation with each other or with companies.

The ANR was created in 2005 to promote French research on projects, and to stimulate innovation by promoting the emergence of multidisciplinary collaborative projects and by encouraging "public-private" collaborations. It is also a question of strengthening the positioning of French research at European and global level.

1.1.2 Pascal institute

The Institut Pascal, UMR 6602, is a joint research and interdisciplinary training unit of 400 people placed under the supervision of the University of Clermont Auvergne (UCA) and the CNRS. The Clermont-Ferrand University Hospital is the unit's secondary guardianship. Institut Pascal is a member of Clermont Auvergne INP, which brings together three engineering schools ISIMA, POLYTECH Clermont and SIGMA Clermont.

The Pascal Institute was born from the successive merger (2012, 2017, 2021) with a structuring vocation of seven laboratories covering the disciplines of Engineering Sciences and Systems of the Clermont site: Process Engineering, Mechanics, Robotics, Physics of Sciences Information, Health.

The laboratory develops knowledge and technologies contributing to three areas of application: the factory (including ecosystems), transport and the hospital of the future.

Institut Pascal is a member of FACTOLAB, a joint laboratory with MICHELIN. It is the bearer of the IMobS3 laboratory of excellence and a member of the CNRS EquipEx ROBOTEX network and of the LabEx GaNeX (PIA1) and PRIMES. The unit is a member of the CIMES competitiveness cluster, and of the AXELERA, MINALOGIC, POLYMERIS and XYLOFUTUR clusters through a partnership with UCA. The Institut Pascal is a member of the Institut Carnot MECD.

1.2 Technical context

Liver vessel disorders are increasing worldwide 5/10000 patients are affected, according to the "European Association of the Study of Liver". The visualization and the segmentation of liver vessels is a difficult task because of their very variable, tortuous and small shapes. The evolution of computer science in research on vascular networks has revealed interest in the reconstruction and interpretation of these complex structures. Their robust extraction from biomedical images requires good acquisition during an imaging examination. Liver blood vessel disorders are usually due to poor blood flow, either to the liver or leaving the liver. Extracting topological and geometric information from the data can provide an alternative perspective on the problems of segmentation of complex structures such as hepatic vessels. Topological data analysis methods allow us to obtain information, usually in the form of graphical representations of topological features. Moreover, these topological signatures are very little used in most machine learning techniques for segmentation problems. Graphs are structures used for modeling problems in

many fields (such as the representation of complex structures). Network analysis has experienced a new boom over the past twenty years, which has produced significant results, both in the analysis of specific cases and in terms of modeling large graphs. However, graphs bring a complexity that classic learning data does not have. Indeed, if the order of the pixels in an image is fixed and immutable, there is, for example, no natural order to traverse the neighbors of a node in a graph. Architectures based on convolution cannot be used directly and must be adapted. Various techniques have recently been developed to overcome these obstacles, starting with learning representations for each node "embeddings" [73]. They evolved into Graph Convolutional Networks [37] and Graph Neural Networks [74].

Since the hepatic vascular network is highly complex, the interpretation of liver disease is a difficult task that may last several hours. A prior knowledge of network structure is thus indispensable for a successful treatment development and surgical planning.

Deep learning has shown in recent years an impressive efficiency in solving many problems in medical imaging. Extracting topological information from the data can provide an alternative perspective on segmentation issues of complex structures such as hepatic vessels.

In this study we will propose a framework with the aim of developing a methodology for reconstructing the hepatic vascular network from medical images using deep learning techniques based on knowledge of shape. Our main objective is to find a new deep learning approach based on topological and morphological knowledge to have a correct and robust segmentation of the vascular structures of the liver in order to help experts in the exploration of liver diseases. We can deduce that the missions of radiologists and biomedical engineers are complementary, because engineers facilitate the interpretation of images and pathologies by radiologists, but they cannot validate their methods without taking advantage of the medical and anatomical knowledge of clinicians (see Figure 1.1).

1.3 Clinical context

Among the essential activities of a radiologist is to visualize organs and structure and also identify tumors on different medical images to define a treatment given his diagnosis knowledge, but the interpretation by a radiologist of data acquired by different modalities in order to detect tumors or some deep structure such as vessel and small tumors that are hardly or not visible in raw data is very difficult. Also, the interpretation of medical data is hard because of the large amount of data, and here is why the biomedical engineers interfere to facilitate the exploration of

images by analysing data, develop automatic algorithms to deal with problem of data quantity, and to detect automatically tumors structures and organs. From all that we can deduce that the collective effort not only allows to transfer diagnostic knowledge from radiologists to engineers but also to facilitate the interpretation of raw medical data by radiologists (see Figure 1.1).

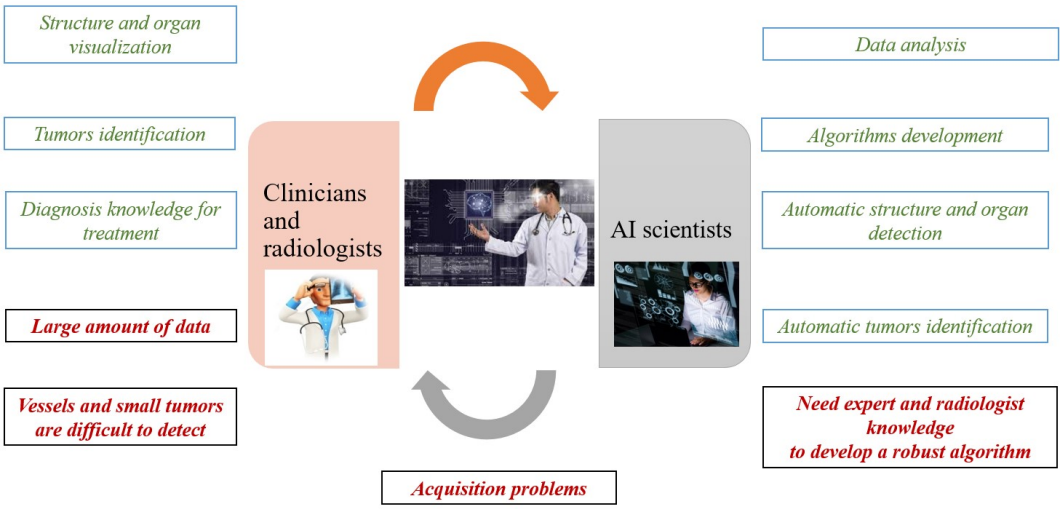

Figure 1.1: Diagram shows the complementary missions between biomedical engineers and radiologists

1.4 Organization of manuscript

This thesis consists of seven chapters:

Chapter 1 "Basic concepts: Binary segmentation and deep learning": in this chapter, we are interested in the basic notions of the two main concepts of our thesis: Segmentation and deep learning. We first present a general view of segmentation problems: their characteristics, definition, objectives and the presentation of standard methods proposed in the literature. Secondly, we expose the techniques of machine learning, focusing mainly on aspects related to deep learning: architectures, their efficiency, ..., then we will present the notion of graphs and their integration into deep learning architectures.

Chapter 2 "Liver anatomy and hepatic imaging": in this chapter, we present the liver functional and structural anatomy including liver Couinaud classification, and also liver vessel anatomy. This chapter presents also the hepatic vascular

pathology's and several hepatic imaging modalities. Finally we present the vessel enhancement filters existing in the literature that we will use later in this thesis.

Chapter 3 "State of the art": Segmentation of vascular tree using different deep learning approaches": This chapter presents a state of the art on the integration of topological signature in models based segmentation to improve the liver vessel extraction. It also presents studies works using machine learning techniques for the detection of liver vessel tree from different medical images as well as the different methods based on machine learning and the topology of vessels. Finally, we will deal with the methods of evaluating the results obtained by some segmentation methods.

Chapter 4 "Segmentation of liver vessel by combining 3-D U-Net approaches": This chapter studies algorithms based on deep learning for hepatic vessel segmentation from CT scan sequences. We present in the first part of this chapter the steps of the construction of a standard 3-D U-Net model allowing the segmentation of the vascular network of the liver on raw CT scan images. In the second part, we develop models on the base of this model which will be more robust, and we compare the results of the three models obtained on three 3-D configurations (full liver volume, slabs, boxes).

Chapter 5 "Robust deep 3-D architectures based on vascular patterns for liver vessel segmentation": this chapter will be devoted to the presentation and evaluation of the methodological contribution made by this work. For this, we will present a first approach applied to the segmentation of the vascular network of the liver in 3-D CT scan images, by developing an architecture based on vascular filters for the segmentation of these structures. We will then detail the comparative approach that we have implemented to validate the best combination filter + deep learning (DL) model to extract liver vessels in 3-D medical image. This approach significantly improves the approaches proposed in the literature.

Chapter 6 "Liver vessel extraction in CT scans using 3-D topological deep learning approach": This chapter is dedicated to introduce the topological signature into our DL model. This information can help improving segmentation decision. The incorporation of graph convolutions in the U-Net provides information that are based on node connectivity. Based on the "GNN" architecture, we present a novel U-Net GNN based segmentation for liver vessel segmentation. We will also present a novel 3-D deep learning method based on topological information for liver vessel segmentation. To do so, we employed a continuous-valued loss function, which can help in improving segmentation decisions from vascular patterns, the results will be compared with state of art approaches.

Chapter 7 "Conclusion and perspectives": We will discuss the results obtained using the methods presented above, to demonstrate the contribution of the in-

tegration of vascular filters and topological information into DL models. This thesis ends with a general conclusion on our work including our contributions and perspectives.

1.5 The Deep learning

Deep learning is a field of machine learning (ML) and artificial intelligence (AI) that mimics the way humans acquire certain types of knowledge (see Figure 1.2). Deep learning is an important part of data science, which includes statistics and predictive modeling. It is extremely useful for scientists responsible for collecting, analyzing and interpreting large amounts of data; Deep Learning makes this process faster and easier.

In its simplest form, Deep Learning can be thought of as a way to automate predictive analytics. While traditional machine learning algorithms are linear, deep learning algorithms are stacked in a hierarchy of increasing complexity and abstraction.

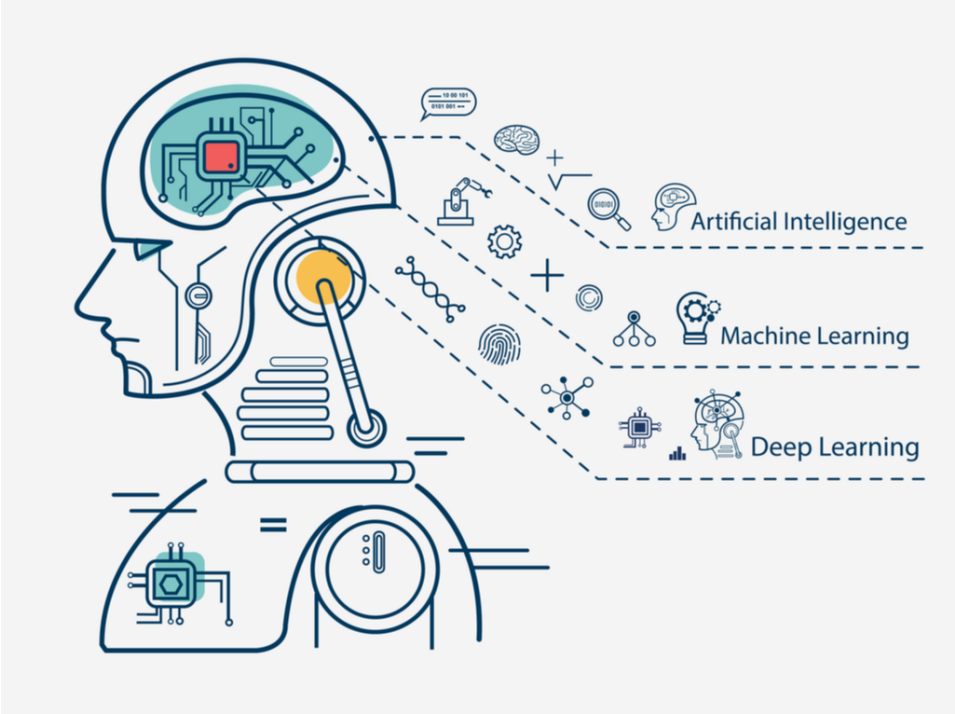

Figure 1.2: Deep Learning definition [29]

Deep learning has proven particularly effective in medical imaging, thanks to the availability of high-quality images and the ability of convolutional neural networks to classify images. For example, deep learning can be as effective (or even more effective) than a dermatologist at classifying skin cancers. Several vendors have already received FDA approval to use deep learning algorithms to perform diagnostics, including image analysis for oncology and retinal diseases. Deep learning is also making major advances in improving the quality of healthcare services by anticipating medical events through electronic medical records.

1.5.1 Neural networks

A type of advanced machine learning algorithm, known as artificial neural networks, is the basis of most deep learning models. Therefore, Deep Learning can sometimes be referred to as deep neural learning or deep neural network.

Neural networks (see Figure 1.3) come in several different forms, including recurrent neural networks, convolutional neural networks (CNN), artificial neural networks (ANN), and feedforward neural networks (FNN), and each has advantages for specific use cases. However, they all work quite similarly, feeding in the data and letting the model determine for itself whether it made the correct interpretation or decision about a given piece of data.

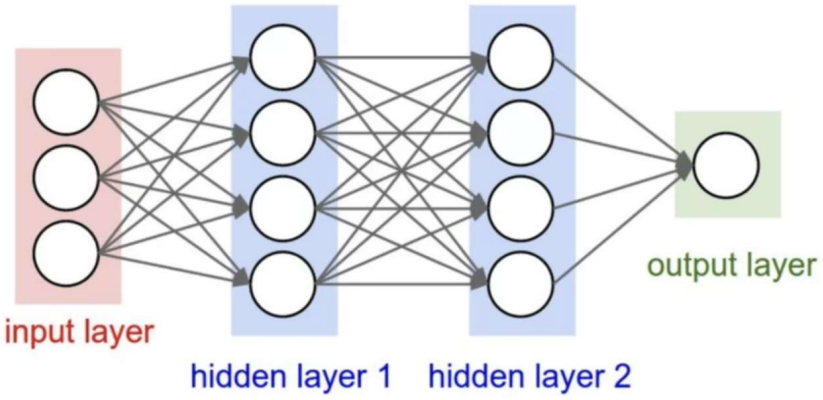

Figure 1.3: Neural network representation [14]

This kind of network is defined by layers of neurons, these being interconnected.

– Each neuron in the network is assigned a coefficient. – Each input data will be multiplied by this coefficient and will apply a certain function to this result. – If the sum obtained is negative, the neuron does not activate, because the data is not interesting.

If this sum is positive, then the neuron will send the information to the neuron of the next layer (hidden layer), until the ultimate data reaches the last neuron. We will then have a final result "output" (see Figure **??**).

1.6 Segmentation based models

In image processing, segmenting an image corresponds to the action of dividing it into a set of disjoint domains whose union is equal to the complete domain. This division is carried out according to one or more criteria defined on or between these regions. This division operation can be performed using many approaches. All these methods, whether low level such as thresholding methods or high level such as methods using an atlas or a deformable model, formalize this concept of criteria. Ideally, these criteria should make it possible to characterize the regions in an unambiguous way.

1.6.1 Binary segmentation

Binary images are images whose pixels have only two possible intensity values. They are normally displayed as black and white. Numerically, the two values are often 0 for black, and either 1 or 255 for white. Binary images are often produced by thresholding a grayscale or color image, in order to separate an object in the image from the background. The color of the object (usually white) is referred to as the foreground color. The rest (usually black) is referred to as the background color. However, depending on the image which is to be thresholded, this polarity might be inverted, in which case the object is displayed with 0 and the background is with a non-zero value. Binary image segmentation is the process of classifying the pixels of an image into two categories: pixels belonging to the foreground objects of an image and pixels belonging to the background objects of an image. Image segmentation is an important problem in image processing and computer vision with many application ranging from background substraction and removal to object tracking, *etc.*

1.6.2 What is U-Net

U-Net is a neural network model dedicated to computer vision tasks and more particularly to semantic segmentation problems. There are different computer vision tasks. One of the most common applications is image classification. It consists of letting the computer identify the main object of an image and assigning

it a label to classify this image. It is also possible to let the computer locate the location of the object on the image. It does this by surrounding the object with a "bounding box" that can be identified by numerical parameters relating to the edges of the image. Object classification is limited to one object per image. More complex, object detection goes further and requires the computer to detect and locate all the different objects within the same image. Semantic segmentation consists of labeling each pixel of an image with a class corresponding to what is represented. It is also called "dense prediction", because each pixel must be predicted. Unlike other computer vision tasks, semantic segmentation does not just produce labels and bounding boxes. It generates a high definition image, on which each pixel is classified. One of the most used neural networks for image segmentation is U-Net. It is a Fully Convolutional Neural Network Model (FCN). This model was initially developed by Olaf Ronneberger [69] in 2015 for medical image segmentation.

The architecture of U-Net is composed of two "paths". The first is the contraction path, also called the encoder. It is used to capture the context of an image. It is in fact an assembly of convolution layers and "max pooling" layers allowing to create a map of characteristics of an image and to reduce its size to decrease the number of network parameters. The second path is that of symmetric expansion, also called decoder. It also allows precise localization thanks to the transposed convolution

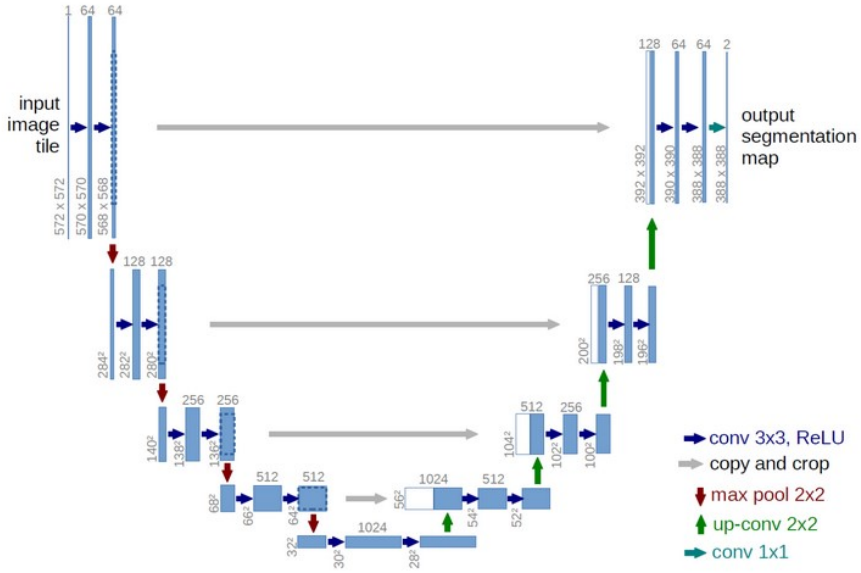

Figure 1.4: U-Net architecture [69]

1.7 The Graph Neural Network

1.7.1 Graph definition

Graph is a mathematical representation of a network and it describes the relationship between objects of interest such as concepts, graphical elements, *etc.* A graph consists of points (vertices or nodes) and lines (edges) between them.

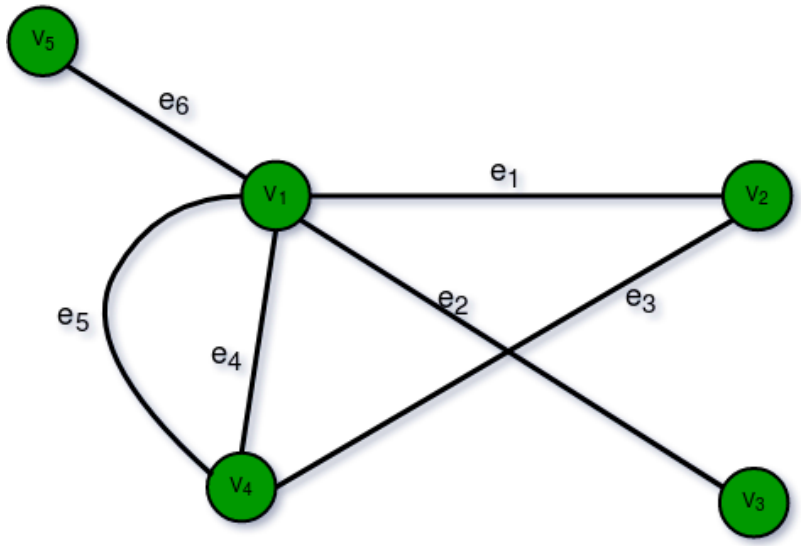

Figure 1.5: Illustration of graph representation [24]

A graph G is a set of vertices V which are connected by edges E. Thus

$$G = (V, E) \tag{1.1}$$

(see Figure 1.5). A node v is an intersection point of a graph. It denotes a location such as a city, a road intersection, or a transport terminal (stations, harbours, and airports). An edge e is a link between two nodes. A link denotes the connections between the nodes. It has a direction that is generally represented as an arrow. If an arrow is not used, it means the link is bi-directional.

1.7.2 Graph Neural Network GNN

Graph Neural Network (GNN) has a very specific meaning in deep learning literature. Thus, we will first talk about the difference between Graph Neural Networks GNNs [37] and Convolutional Neural Networks (CNN).

Convolutional Neural Networks (CNNs) were developed for grid-like data (essentially image) data where the images can be seen as pixels arranged in a grid-like structure. An image can be thought of as a graph where each pixel is a node and is connected to all its neighboring pixel. However, this graph has certain special characteristics - 1) It is nearly regular, that is all nodes have same amount of neighbors except those which are at boundary and 2) There is order in the arrangement of these nodes. Both of these characteristics are exploited by CNNs for learning good representations.

However, general graphs present certain challenges: 1) They are not always regular as in grids, *i.e.* they are irregular and 2) There is no ordering to the neighboring nodes and even if ordered, they do not really carry any semantic meaning. Consequently, traditional CNNs cannot be directly used in this case. Therefore, a generalization was needed to make CNNs work for general graphs. This gave rise to Graph Neural Networks or GNNs.

There are technical differences in CNNs and GNNs. CNNs are spatial convolution models, that is, loosely speaking, convolution operation is done on the spatial representation of the image. As discussed earlier, general graphs do not have a canonical spatial representation, thus GNNs perform convolution on the spectrum of the graph, given by the eigenvectors of its Laplacian. However, this convolution operation on the spectrum can be expensive. A first order approximation of this convolution was proposed in [20].

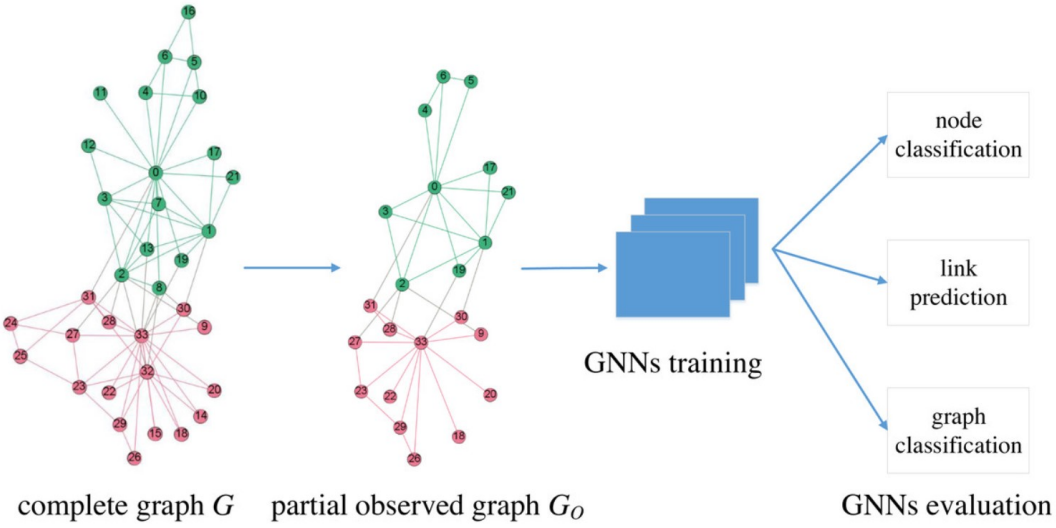

Figure 1.6: Example of GNN architecture [65]

If one looks at this approximated model GCN, it looks very similar to a CNN.

Indeed, every node information is learnt by aggregating weighted information from its neighbors. The only difference is that in CNNs, one learns a node-agnostic filter where the same filter matrix is applied to all nodes regardless of its position in the graph. However, in GCNs, we get node-specific filters governed by the Laplacian, it can also be learnt (see Figure 1.6).

Second difference is related to the concept of convolution: in CNN, convolution is similar to a sliding window to move through the images then the convolving process (multiply and sum the values pixel by pixel) makes the feature map. Afterward, it depends on the architecture to have pooling, normalization, dropout,..., after convolution layers. While this is totally distinct in GCN. As we mentioned above we have nodes and edges in GCN to generate them and then train them but in GCN, convolution is applied before all the actions because we plan to discover each pixel and then their edges and gradually all neighbors that are connected to a specific node. According to this, the role of convolution is summarised to cover the neighborhood of each node.

1.8 State of the art

Medical imaging systems such as Magnetic Resonance Imaging (MRI) and Computed Tomography (CT) provide useful information on the liver. Extraction of the organ and its vessels from images is essential for analysing disease and planning surgical operations.

Segmentation of the complete liver can be performed manually on images CT (2-D slices), moreover the division of liver volumes into eight sub-segments is crucial because it mainly requires visualization (3-D), it is important to explore the Couinaud segments. In the literature there are several articles on the segmentation of the whole liver. Gao et al. (1996) [21] used thresholding and morphological operations (morphological closure). Xu et al. (2010) [83] used the local entropy method to delineate the liver contour and tumor. Badakhshannoory and Saeedi (2011) [22] used principal component analysis (PCA) to segment the kidneys and the liver in each 2-D image section, and the results were combined to form a hepatic volume in 3-D. Oliveira et al 2011, [63] have also used an active contour method (levels sets) with parameters optimized by GA (Genetic Algorithm). Abdel-Massieh et al. (2010) [61] used a statistical model in the first part of their hepatic segmentation, followed by an active contour to improve the result. More recently, Chitsanupong Butdee et al. 2016 [7] used a region-based growth segmentation method. In all these previous methods they had good results but still need to be improved.

The manual segmentation is a long and tedious process, and becomes impossible with a large quantity of biomedical images. The automatic extraction of this information requires a very precise segmentation, which is difficult on medical images due to their low contrast and low signal to noise ratio. Classic methods are hardly reproducible or reach a low accuracy when confronted to more complex than limited private data sets. For the segmentation of the hepatic vessels, Lesage et al. [50], published a large and relevant overview. Some interesting techniques are the 3-D multiscale line filter of Sato et al. [72] improved locally adaptive region growing algorithm from Yi Ra et al. [85], Kawajiri et al. [34] proposed a thresholding segmentation approach after contrast enhancement steps, but this method lead to lot of false and negative segmentation. Oliveira et al. [63] used a region growing method based on a Gaussian mixture model for the segmentation of the vessels and nodules but the bifurcations or parts of vessels were not detected, especially when the nodules or the veins are close to the edge of the liver. Recently, Butdee et al. [7] proposed a 3-D segmentation method by region growing, they selected two seed points, some enhancement of the gray values was realized for optimal visualization, then a pixel within the hepatic vein in any slice was selected as a seed point for the 3-D region growing algorithm to extract the hepatic vein, it was selected at the main branch of the hepatic vein. The same process was repeated for segmentation of the portal vein to give vessels of liver at the end of processing.

All these methods failed to give a good reconstruction of hepatic vessels because they all used as information image intensities, which is generally not sufficient. Exploration of vascular images should consider the geometry and topology of vessels, the use of local appearance of the pixel is not sufficient, as illustrated by the methods we have described so far. Recently, deep learning architectures have been successfully applied to liver vessel segmentation challenges by automatically learning the hierarchies of relevant attributes directly from medical images.

1.9 Motivation of this work

The hepatic vascular network shape is very complex, the exploration of these structures by a radiologist is a difficult task and may last over time. A prior knowledge of network structure is essential for a successful treatment and surgical planning. Especially for vessel lesions detection, the required information include the precise position of the liver vessels, the identification of the veins and arteries, and the geometrical and topological parameters of the vessels.

From a practical perspective, the processing of data in medical images allows the clinician to observe on the same reconstructed image the different information from

each of the sources. This richer visualization provides the practitioner with more information on which he can rely in order to improve the quality of his diagnosis. From the point of view of image processing, this pooling makes it possible to make the numerical methods more robust by exploiting the available redundancy. Our work focused on the design of a relevant method to exploit the vessel. This approach allows each of them to bring their specificity while being enriched by that of the others.

1.9.1 Technical objectives

As we know segmentation of hepatic vessels is a difficult task. In the current state of the art, no method has been able to perform accurate segmentation, especially on CT images, due to acquisition issues such as: low spatial resolution, low contrast, the variability of acquisition parameters (acquisition is not reproducible for each patient). The reason why we are trying to solve this problem by providing a solution to help clinicians and radiologists in their diagnosis.

The main objectives of this work is to :

Develop accurate solution for hepatic vessels reconstruction on abdominal medical images using topological deep learning.

Train our models on CT scan images to predict a binary image of liver vessels tree.

1.9.2 Clinical objectives

Among the essential activities of a radiologist is the visualization of organs and structures, but also the identification of tumors on different medical images to define a treatment taking into account his medical knowledge. But the interpretation by a radiologist of data acquired by different modalities in order to detect tumors or certain deep structures such as vessels and small tumors which are hardly or not visible in the raw data is a very difficult task. We intervene to facilitate the exploration of data by analyzing them to develop automatic algorithms to deal with problems of large quantities of data, for example.

In this work, the focus is on the automatic detection of liver vessels from imaging data. The goal is to help the clinician detect liver tumors to reduce the need for biopsies.

Accurate segmentation of hepatic vessels helps radiologists interpret the data more easily and will help detect not only hepatic vessel diseases, but also most liver abnormalities that can be detected automatically using hepatic vessels.

1.10 Contribution

The main contributions presented in this thesis are as follows:

1. The proposal of a comparative study which considered three alternative setups that allow adapting popular encoder-decoder U-Net architectures to volumetric data. These setups, referred to as full 3-D, slab-based, and box-based, are depicted. The most methods on literature build their models on box especially to study 3-D images. In our case we test these three setups in order to validate the best model/configuration and then use them in further scientific studies to improve results of segmentation process.

2. The main contribution in this thesis : we proposed a complete framework with the aim of developing a methodology for detecting the hepatic vascular network from abdominal CT, in a 3-D approach, using topological deep learning techniques based on *a priori* knowledge of shape. Our main objective is to find a new deep learning approach based on vessel topology to obtain an accurate segmentation of the liver vascular network.

3. We proposed a novel approach which coupled a 3-D Dense U-Net with accurate weighted Dice loss function (focal weighting), and then we compare the results with ClDice [75]. This loss function is used and tested for segmentation tasks on 2-D images. Here we have created a loss function for binary segmentation in 3-D images instead of multi-class segmentation. The proposed topological model will be tested on preprocessed data using some vesselness filters to enhance the vascular structures prior to their segmentation, and to remove non vascular structures. This can give more accurate segmentation and can also eliminate the noise and positive false in results.

2 Clinical context and hepatic imaging

2.1 Liver anatomy

We can describe the anatomy of the liver using two principal aspects, morphological and functional anatomy. The morphological anatomy describes the shape of the liver and we can observe any internal features as vessels and nodules for example, that have an obvious importance in hepatic surgery. For the functional anatomy, the French anatomist Claude Couinaud [13] was the first who divided the liver into eight functionally segments allowing resection of segments without damaging any others in surgical transplantation for example.

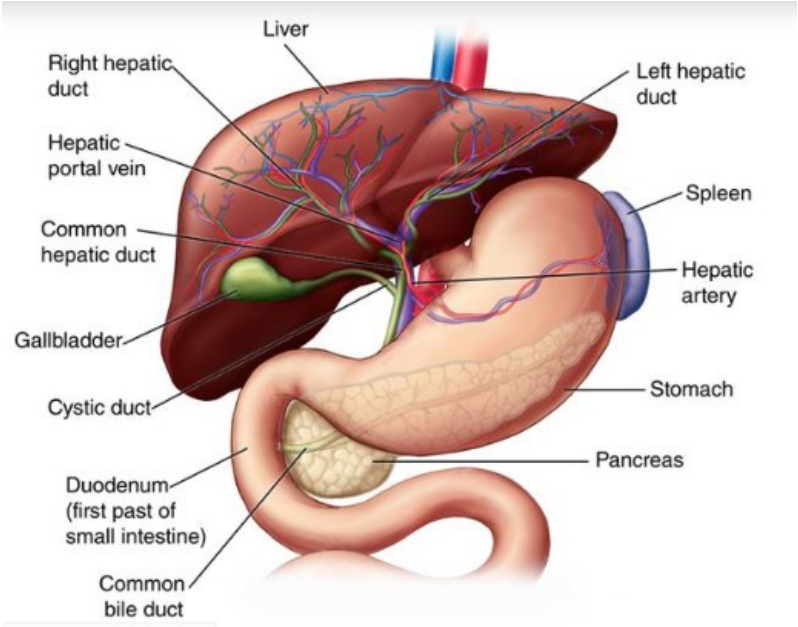

Figure 2.1: Detailed liver anatomy [6].

2.1.1 Structural anatomy of the liver

The liver is the largest solid organ in the body, it represents about 3 % of total body weight. It is in the part of the digestive system (see Figure 2.2), it has 2 lobes typically described in two ways, by morphological anatomy and functional anatomy. It is located under the diaphragm, in the upper right part of the abdominal cavity. It is above stomach and its weight is about 1.5 kg. The liver has the capacity to regenerate itself if it is damaged. This property makes it possible to carry out liver and resections. A healthy person can give a part of his liver to a relative who has a damaged part.

The liver is divided into four unequal lobes; the right hepatic lobe is the largest, the left hepatic lobe is the narrowest part of the organ. Between these two major lobes, we distinguish the square lobe and the caudate lobe. The gallbladder is attached to the liver at the border of the square lobe and the right hepatic lobe (see detailed anatomy in Figure 2.1).

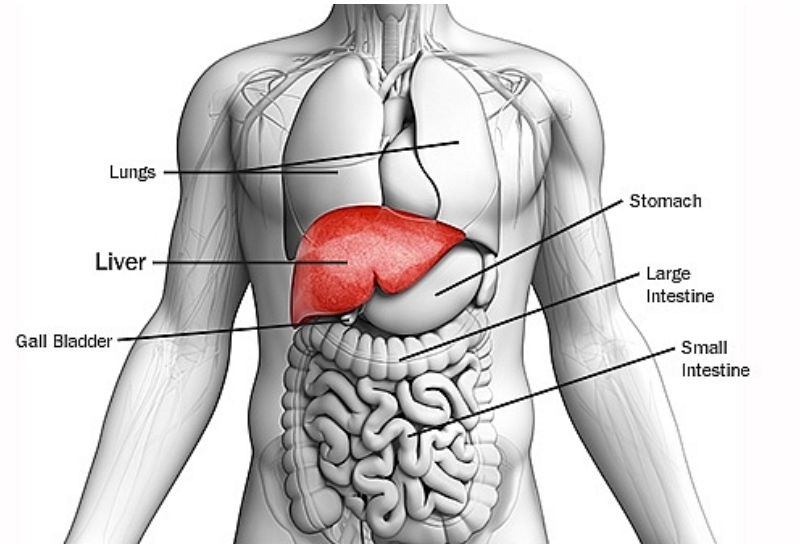

Figure 2.2: Liver position in humain body [70].

The square lobe and the caudate lobe are separated by a groove called the liver hilum. It is at the level of the hilum that the portal vein and the hepatic artery enter the liver, and that the major bile ducts pass.

The study of its vascular structures is essential when one wants to understand the functional anatomy of the liver, because the vascularization of the liver makes it possible to distinguish sectors which themselves are divided into segments: it is the segmentation of Couinaud. This segmentation allows the division of the liver

into 8 segments which are distributed, according to their localization, in the level of the right liver or the left liver and which are separated by the branches of the portal and hepatic veins.

The field of liver surgery has progressed recently, in the last years liver transplantation has become very essential for us to understand the vascular inflows in the liver. Consequently, it allowed the evolution of the concept of the functional anatomy of the liver.

2.1.2 Liver vessel anatomy

The blood vessels conveying blood to the liver are: the hepatic artery (30 %), and the portal vein (70 %). The hepatic artery brings oxygenated blood to the liver and the portal vein brings venous blood rich in the end products of digestion, which have been absorbed from the gastrointestinal tract. The venous blood is drained by two hepatic veins which drain into the inferior vena cava. The hepatic artery and portal vein terminate by dividing into right and left primary branches to the corresponding lobe of the liver. On penetrating the liver, these vessels divide until they form a very dense network of extremely fine vessels (see Figure 2.3). Depending on the person, the anatomy varies. The liver can have one to three arteries: the middle hepatic artery which arises from the celiac trunk, the right hepatic artery which arises from the superior mesenteric artery, the left hepatic artery which originates from the left gastric artery (see Figure 2.3).

2.2 The segments of Couinaud

Couinaud's liver resection is used in order to facilitate their identification, whether for a follow-up, a biopsy, an interventional procedure or surgical removal. The problem arises when the lesion is at the edge of different segments, where the precision is poor. In case of doubt in the CT imaging, the use of thick MIP (maximum intensities projection) or slices projection, 3-D reconstructions imaging are of great help. In fact, projection and 3-D reconstructions of vessels may provide a good segment localization of the lesions in liver than simple axial images. The liver resection described by Claude Couinaud is based on the identification of the hepatic and the portal veins. Today, Couinaud's definition is the most used classification since it is better suited for surgery and more accurate for the localization of lesions. Comprehension of the anatomy of the venous system is essential. Exact information is required both in the location of the lesions and to estimate the segments volumes, to determine the best therapeutic, radiological or surgical treatment. Any

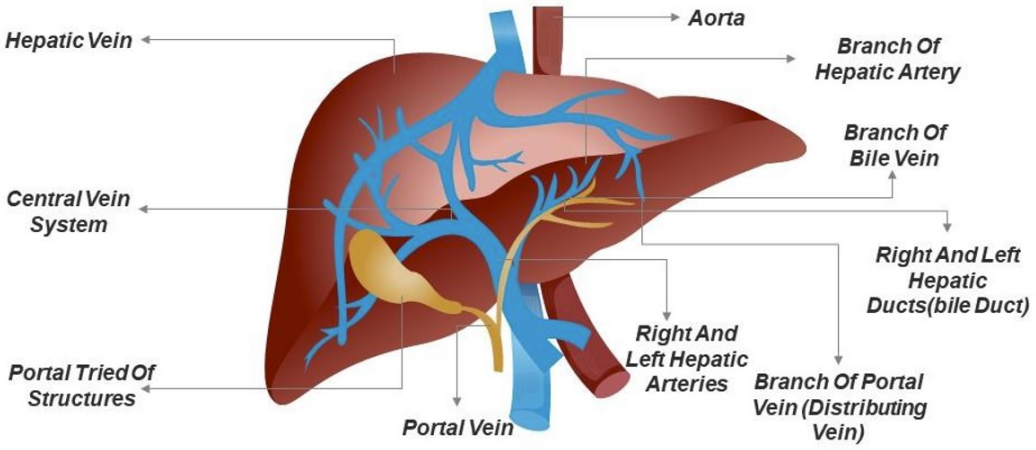

Figure 2.3: Detailed liver vessel anatomy [23].

venous or portal vascular anatomic variant should be exactly described, so as to let the interventional radiologist or surgeon plan their procedure in advance and, if necessary, modify their technique, by greatly reducing the inter and post-surgical difficulties and complications [19].

The anatomist Couinaud separated the liver into 8 functional segments, each containing, at its periphery, a branch of hepatic vein. For segments II, III and IV, left liver and segments V, VI, VII and VIII to the right liver as described in Figure 2.4: The Couinaud classification of liver anatomy divides the liver into eight functionally independent segments. Each segment has its own vascular inflow, outflow and biliary drainage. In the centre of each segment there is a branch of the portal vein, hepatic artery and bile duct. In the periphery of each segment there is vascular outflow through the hepatic veins.

Right hepatic vein divides the right lobe into anterior and posterior segments. Middle hepatic vein divides the liver into right and left lobes. This plane runs from the inferior vena cava to the gallbladder fossa. The falciform ligament divides the left lobe into a medial (segment IV) and a lateral part (segment II and III). The portal vein divides the liver into upper and lower segments. The left and right portal veins branch superiorly and inferiorly to project into the center of each segment.

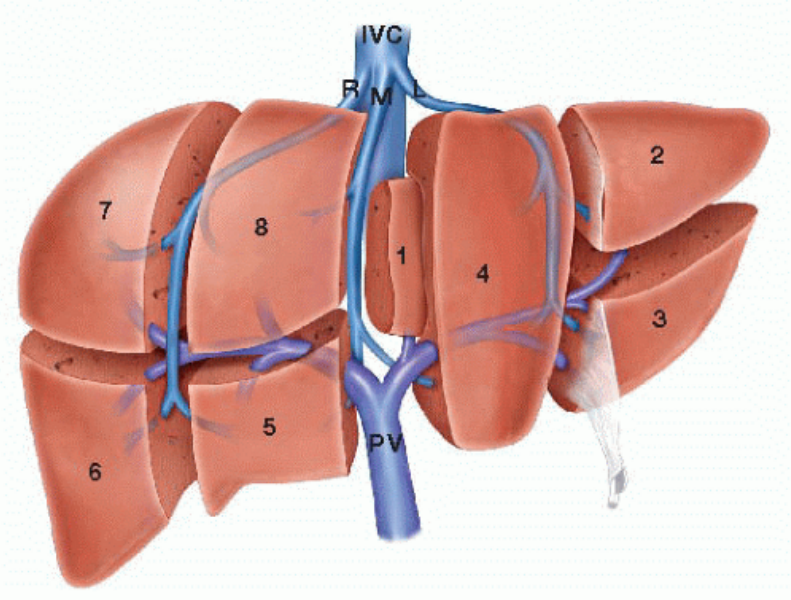

Figure 2.4: Diagram showing the segments (numbered 1 to 8) of the liver as described by Couinaud. [6]

2.3 Main vascular pathologies

Venous thrombosis constitutes the majority of vascular diseases of the liver. One or more risk factors for thrombosis - in particular a primary myeloproliferative syndrome - are often involved. Recent portal vein thrombosis, suspected in cases of abdominal pain, is recognized by imaging. The severity is linked to the distal involvement of the superior mesenteric vein, which increases the risk of intestinal infarction. The initiation of anticoagulant treatment is urgent. In the absence of reversal, a cavernoma develops, a late stage where the disease is sometimes only recognized, resulting in portal hypertension. Hepatic vein thrombosis can present as severe acute liver disease, such as cirrhosis, or be completely asymptomatic [64].

The diagnosis is made by imaging the hepatic veins and the inferior vena cava. Blood thinners are strongly recommended. In the absence of rapid improvement, percutaneous venous angioplasty, placement of a transjugular intrahepatic portosystemic shunt (TIPS), and finally liver transplantation are discussed. Portosinusoidal vascular disease corresponds to damage to the small hepatic vessels. It should be considered in case of unexplained liver test abnormalities, or portal hypertension without cirrhosis, and established by liver biopsy. It is often associated with general illnesses. Vascular diseases of the liver are divided into three main types depending

on the location of the attack: portal vein thrombosis, Budd-Chiari syndrome and portosinusoidal vascular disease [16].

2.3.1 Portal vein thrombosis

Extrahepatic portal vein thrombosis is characterized by the development of a thrombus in the trunk of the portal vein and/or one of its two branches, or by the permanent obliteration of the portal vein following a old thrombus [64].

2.3.2 Budd-Chiari Syndrome

Primary Budd-Chiari syndrome is a rare condition due to an obstacle to hepatic venous return unrelated to compression or neoplastic invasion. This obstruction, usually caused by thrombosis, can occur at any level from the small hepatic veins to the termination of the inferior vena cava at the level of the right atrium. Primary Budd-Chiari syndrome is closely associated with prothrombotic states. In a prospective and multicenter European study, at least one risk factor for thrombosis was identified in 84 % of patients [46].

2.3.3 Portosinusoidal vascular disease

Portosinusoidal vascular disease (PSVD) is a rare disease of the small vessels inside the liver. This term includes various disorders previously named from a histological point of view "nodular regenerative hyperplasia", "obliterating portal venopathy", "hepatoportal sclerosis", "incomplete septal fibrosis", "non-cirrhotic portal fibrosis" and from a clinical “idiopathic portal hypertension”, or “non-cirrhotic intrahepatic portal hypertension”. Indeed, there is a strong overlap between all these entities and to date no practical consequence to discriminate between them [46].

2.4 Vessel enhancement filters

Image filtering is one of the most fundamental operations in image processing and can improve image quality and provide a good visualization of pixels that are less enhanced in the image. Note that some filters are known to detect or preserve edges, while others are used for smoothing or denoising. You should also note that the performance of the filter depends on both the input image and the parameters selected for filtering, such as kernel shape and size, iterations, and interpretation.

To enhance the vascular structures prior to their segmentation and visualization, and to suppress non-vascular structures and image noise, several filters enhancing vascular structures are proposed.

In our case, we assume vessel enhancement as a filtering process that looks for geometric structures that can be considered tubular. The filters presented below were all tested for liver vessel enhancement by Lamy et al. [44].

2.4.1 Frangi filter

The Frangi filter [17] is typically used to detect vessel or tubular structures in volumetric image data. Most of Hessian-based vessel enhancement filters use eigenvalues extracted from the Hessian matrix to derive geometrical structures which can be regarded as tubular. Since vessels in the liver have different radius it is important to study these features in a multi-scale framework. This vessel enhancement filter was developed to improve the visualization of vessels which can reduce false positives during segmentation process, to obtain better segmentation results in vessel detection and airway wall exclusion.

2.4.2 Jerman filter

Jerman's filter [31] is a Hessian based tubular (vessel/vesselness) and spherical enhancement filters. It is an enhancement filter based on ratio of multiscale Hessian eigenvalues, which yields a close-to-uniform response in all vascular structures and accurately enhances the border between the vascular structures and the background.

2.4.3 Sato filter

It is a 3-D line enhancement filter which is developed in order to discriminate line structures from other structures and recovering line structures of various widths. The 3-D Sato filter [72] is based on a combination of the eigenvalues of the 3-D Hessian matrix. Multi-scale integration is formulated by taking the maximum among single-scale filter responses, and its characteristics are examined to derive criteria for the selection of parameters in the formulation.

2.4.4 Zhang filter

In the specific context of hepathic vascular networks, Zhang et al. [90] further proposed to improve Jerman vesselness by identifying the liver tissues and vessels

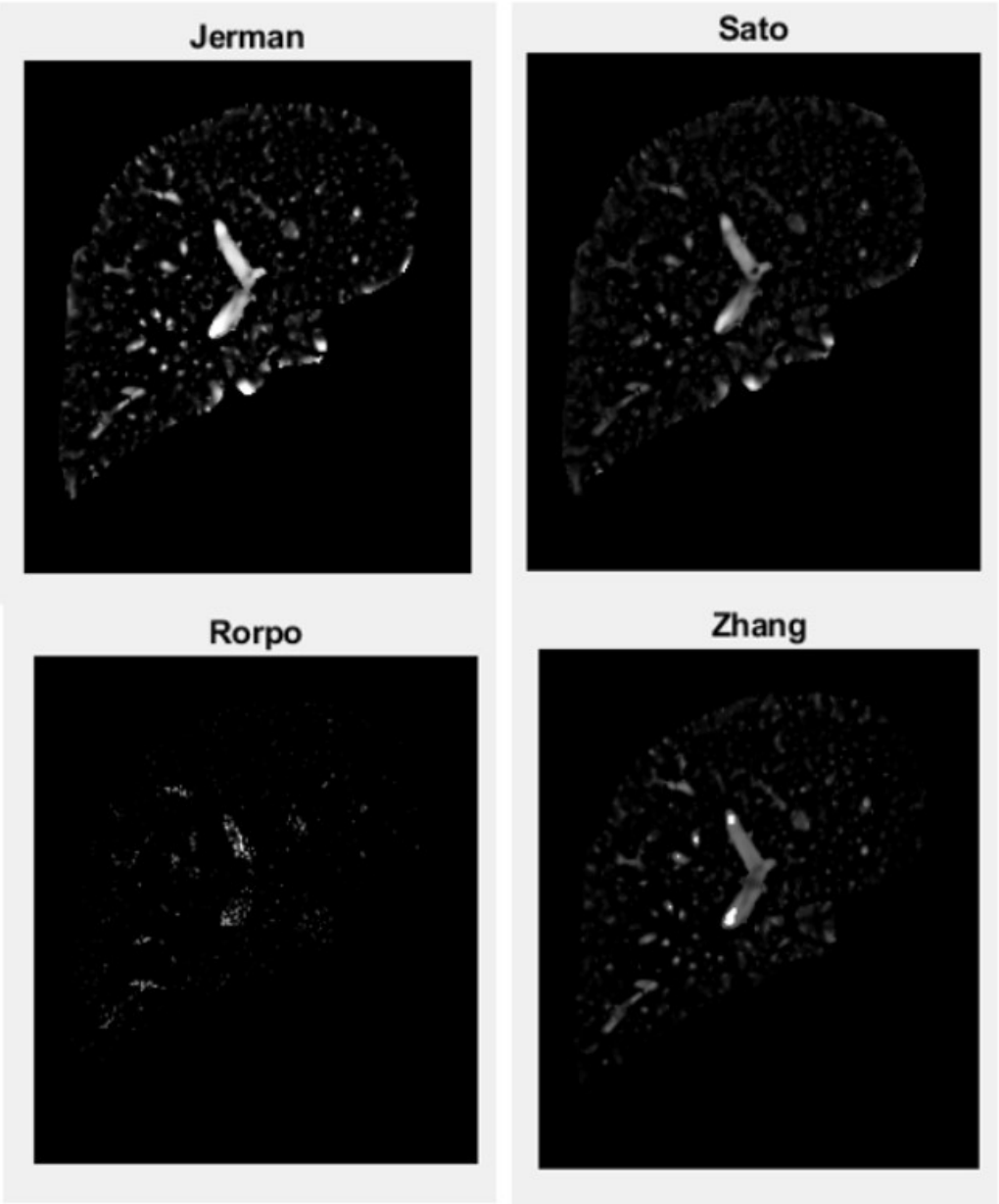

Figure 2.5: Illustration of the enhancement filters applied for liver vessel enhancement by [44].

mean intensity. A K-means classification was combined with a sigmoid filter dedicated to enhance the vessels whereas suppressing other tissues.

2.4.5 RORPO filter

Ranking the Orientation Responses of Path Operators is a non linear filter proposed by Merveille et al. [57] to deal with curvilinear structures. RORPO, unlike most methods in the literature, is a non-local, non-linear method and better adapted to the integrated anisotropy of curvilinear structures. This method is based on a recent notion of mathematical morphology: path operators. RORPO can be used directly to filter images containing curvilinear structures, in order to present them and preserve them, but also to reduce noise. But the two characteristics of RORPO can also be used as *a priori* information on curvilinear structures, in order to be integrated into a more complex method of image analysis. In a second step, the authors present a regularization term intended for variational segmentation, using the two characteristics of RORPO. The information transmitted by these two characteristics make it possible to regularize curvilinear structures only in the direction of their main axis. In this way, these structures are better preserved, and certain curvilinear structures disconnected by noise can also be reconnected.

2.5 Hepatic imaging modalities

2.5.1 Magnetic resonance imaging

The liver MRI protocol consists of several sequences before and post contrast. Post-contrast phases contain arterial phase, portal venous phase, delayed phase, and later delayed phase. The specific hepatobiliary contrast agents used in liver MRI are mangafodipir trisodium, gadobenate dimeglumine and gadoxetic acid. These contrast agents have specific characteristics such as specific receptors and transporters for absorption, different excretion percentage by biliary and renal routes, mode of administration and side effects. These hepatocyte-specific contrasts can help better identify and characterize small liver injury, especially well-differentiated hepatocellular adenoma (HCC). Contrast agents that are secreted into the bile can be used to differentiate hepatocellular adenoma (HCA) by early heterogeneous enhancement in the arterial phase MRI with fat suppression, then portal vein washout contrast. Because HCA has no bile ducts, biliary-specific contrast uptake is minimal in the delayed phase [4].

The standard method to evaluate the presence of inflammatory and early fibrotic changes is a liver biopsy [36]. However, a new technique called MR elastography is an MRI with low frequency vibration which measures liver. MR elastography does not have the possible bias of sampling present in liver biopsy. It has better

sensitivity and specificity compared to US elastography, which has limitations in obese patients and the presence of ascites.

2.5.2 Ultrasound imaging

Ultrasound is the main liver imaging technique to describe focal and diffuse liver injury due to its availability and low cost. It may exhibit different patterns in different liver lesions, malignant lesions, generalized hyperechogenicity, as seen in diffuse fatty liver disease, and lesions hyperechoic as seen in various benign and malignant lesions. Benign hyperechoic lesions contain hemangioma, hepatic adenoma, focal nodular hyperplasia, and focal fatty changes. Ultrasound has certain limitations because the proximity of the diaphragm to the liver makes it difficult to image the entire liver, inter-observer variability, less precision especially for patients suffering from obesity [4].

2.5.3 Tomographic nuclear imaging

Positron emission tomography (PET) and single-photon emission computed tomography (SPECT) are the nuclear imaging techniques used more frequently for diagnosis of liver malignancy and evaluation of response to treatment metastasis, recurrence, and prognosis. F-fluorodeoxyglucose (FDG)-PET and C-acetate PET are more common nuclear imaging modalities in diagnosing liver malignancy. Although it has high sensitivity, the false positive rate is high due to the detection of any focal hypermetabolism area. The sensitivity is low in the detection of lesions smaller than 1 cm.

2.5.4 Computed tomography imaging (CT scan)

CT of the liver can be done with different protocols, including unenhanced, single-phase, dual-phase, and triphasic contrast-enhanced. Each of these liver CT protocols is important in the evaluation of different liver pathologies. The single-phase contrast-enhanced CT is generally the modality of choice in the portal venous phase that is typically 70 seconds after intravenous contrast injection, the liver has the maximum enhancement. It can mainly provide information about diffuse liver pathologies, such as liver cirrhosis and hypovascular metastatic liver disease. The dual-phase contrast-enhanced CT is the primary imaging modality conducted in the portal venous phase and the late arterial phase, which can be obtained approximately 35 seconds after injection and might provide better information about hypervascular lesions [36]. This protocol can help hypervascular metastatic

lesions like renal cell carcinoma, breast cancer, melanoma, and endocrine tumors and preoperative evaluation for partial hepatic resection. It can provide information about liver anatomy and its vasculature to the surgeon.

Triphasic contrast-enhanced CT is non-enhanced, arterial and portal venous phase. Arterial phase enhancement begins approximately 20 to 25 seconds after contrast injection. Hypervascular pathologies, like most benign and malignant hepatic lesions, can be appreciated in this phase. Triphasic protocols are usually used for patients with possible cirrhosis [4]. HCC is a hypervascular lesion that enhances during the arterial phase, and it has a fast wash-out during the portal venous phase. Cholangiocarcinoma is one of the liver pathologies that can be appreciated better in triphasic CT, with non-enhanced, portal venous phase and delayed phase (10 to 15 minutes) hyperenhancement on the delayed phase because of the presence of plenty amount of fibrous tissue (see Figure 2.6).

Figure 2.6: In portal venous phase CT image shows strong enhancement of portal vein branches and hepatic veins [6].

2.6 Acquisition phases in hepatic imaging

Timing of CT-series is important in order to grab the right moment of maximal contrast differences between a lesion and the normal parenchyma. In the early

arterial phase: we clearly see the arteries, but we only see some irregular enhancement within the liver (see arterial phase in Figure 2.6). Portal venous phase is a post-contrast injection in which images have the following characteristics: Portal veins are very good enhanced. Hepatic veins are enhanced too (see Figure 2.6). In the late arterial phase, tumors are clearly observed (same figure).

2.7 Multimodal approaches in hepatic imaging

The good characterization of hepatic nodules and early diagnosis of liver disease such as HCC are very important steps. However, computed tomography (CT) and magnetic resonance (MR) imaging are the most useful modalities for the detection of new nodules detected after ultrasonography (US). Many studies presented the successful integration of contrast material-enhanced US into a multimodal approach for diagnosis of liver cancer HCC. Contrast-enhanced US also provides dynamic real-time assessment of tumor vascularity so that contrast enhancement can be identified regardless of its timing or duration, allowing for detection of arterial hypervascularity and portal venous washout. The purely intravascular nature of US contrast agents is valuable as the rapid washout of nonhepatocyte malignancies is highly contributory to their differentiation from HCC [4].

3 Segmentation and visualization of hepatic vascular network

3.1 Machine learning approaches for liver and vessels segmentation

Different architectures of DL are developed in order to segment precisely the liver vessels on different types and modalities of medical imaging. We will expose these approaches according to image types.

In recent years, Deep Learning (DL) has been increasingly applied in different areas such as object detection, medical images segmentation, classification, vessel extraction, [41, 42, 77, 89]. In particular, deep neural models have been proposed in order to segment the hepatic anatomy [3, 11, 59]. From this literature, the U-Net model proposed by Ronneberger et al. [69] and its extensions stand out as the most relevant for this task. In particular, the 3-D U-Net captures the volumetric features of the organs within medical images. This model is an extension of the 3-D FCN [55] (Fully Convolutional Neural network), which suffers from high computational cost and GPU memory consumption. To address these issues, the 3-D U-Net architecture was proposed, and is effective even with a limited image dataset. In the Table 3.1 we present the relevant reviewed vessel segmentation methods proposed in the literature.

3.1.1 Deep learning approaches

Liver segmentation

In recent years, many researchers developed DL methods to solve liver segmentation problems. Among the most widely used methods, various Convolutional Neural Networks (CNNs) have been proposed to learn feature representations for liver or lesions liver segmentation. Bencohen et al. [1] proposed to use a Fully Convolutional Neural networks (FCN) for liver segmentation and liver metastasis detection. They used three adjacent CT image slices to form a three-channel image service as input. Zhang et al. [92] train also a FCN for liver segmentation; then they make a comparative study on the post-processing step to refine their results. Christ et al. [10] proposed two cascaded FCNs to segment liver and tumors simultaneously. The final output was refined using a 3-D conditional random field. Sun et al. [80]

designed a multi-channel FCN to segment liver tumors. The probability maps were generated by the feature fusion from different channels. Lu et al. [56] used a 3-D CNN and a graph cut to refine their results. Qin et al. [66] proposed a super-pixel-based CNN which divides the CT-image into super-pixel by aggregating pixels according to their intensity. They classified them into three classes, liver boundary, and non-liver background and utilized the CNN to predict the liver boundary. Kushnure et al. [40] proposed to introduce multi-scale features in the CNN that extract global and local features at a more granular level. Chlebus et al. [8] use a U-Net in two models and filtered the false positives of tumor segmentation results by a random forest classifier. In Liu et al. [54], the authors proposed an improved U-Net model with a graph cutting. Jin et al. [32] present a basic architecture as U-Net with the extraction of contextual information which combines low-level feature maps with high-level ones. A hybrid method namely H-Dense U-Net presented by Li et al. [52], combined 2-D and 3-D models to segment livers and liver tumors. Rafiei et al. [68] also used 3-D and 2-D U-Net networks to segment livers. The 3-D encoding phase is for capturing 3-D surfaces while 2-D decoding phase reduces the complexity of the process.

Liver vessel segmentation

In this category the researchers tested their methods on CT scan data. Zeng et al. [87] proposed solution for liver vessel segmentation based on extreme learning machine (ELM) tested on 3-D CT scan images. They used an anisotropic filter to remove noise and to preserve vessel boundaries. Then, based on the knowledge of vessel shapes, 3 filters are introduced: Sato, Frangi and offset medialness filters to extract features of the vessel. Then the ELM is applied to extract liver vessels voxels from background voxels. Kitrungrotsakul et al. [38] proposed Multi Deep Convolution Network for robust hepatic vessel extraction from 2-D and 3-D (CT) images. It consists of three deep convolution neural networks to extract features from coronal, sagittal and transversal planes of CT data. The three networks have shared features at the first convolution layer, but will separately learn their own features on the second one. All three networks will join again at the top layer. Ibragimov et al. [27] proposed to combine DL with anatomical analysis for automatic segmentation of the liver portal vein. They applied CNN to learn the consistent appearance patterns of the portal veins using a training set with reference annotations. Yu et al. [84] presented a method of 3-D Residual U-Net for liver vessel segmentation on CT scan images. They introduced a residual block structure in the ResNet into the 3-D U-Net, and construct a new 3-D Residual U-Net architecture to segment the hepatic and portal veins from abdominal CT volumes.

To deal with the challenge of pixel imbalance they developed a weighted Dice loss function, which allows vessel boundary segmentation and small vessel detection.

The scientist tried also to segment hepatic vessels in images acquired by different modalities, but there are not many articles because they are generally less used in the clinical analysis and they are more complicated to explore. Thomson et al. [81] introduced a reduced filter 3-D U-Net for hepatic vessel reconstruction in 3-D ultrasound (US) images proposed to achieve accurate vessel segmentation in true 3-D and stuck 2-D US images. Recently Kitrungrotsakul et al. [38] proposed an automatic vessel segmentation approach that uses a multipathways DL network. The proposed framework learns a deep network for binary classification based on extracted training patches in 3 planes (sagittal, coronal, and transverse planes) of MRI scan images. It provides a good recognition performance on 3-D volumes. Their solution, VesselNet, products a vessel probability map for voxels to generate the final segmentation of liver blood vessels using a multi-scale method. Their results obtained on IRCAD data confirm that the solution improves previous works presented in the literature.

Table 3.1: Comparison of the main reviewed vessel segmentation methods, CTA: Computer Tomography Angiography. AP : average precisions. A: Accuracy. D: Dice

Method	Year	Modality	Region	Dimension	DL model	Precision
Butdee et al [7]	2016	CT	Liver	2D/3D	-	D=0.96
Sato et al [72]	1998	CT	Liver	3D	-	-
Fu et al [18]	2016	–	Retina	2D	CNN's/CRF	A=0.95
Oleivera et al [63]	2018	–	Retina	2D	FCN	A=0.96
Laibacher et al [43]	2019	–	Retina	2D	M2U-Net	A=0.78
Liskowski et al [53]	2016	–	Retina	2D	DNN	A=0.97
Zeng et al [87]	2016	CT	Liver	3D	–	A=0.9
Kitrungrotsakul et al [38]	2017	CT	Liver	3D	CNN	D=0.83
Ibragimov et al [27]	2017	CT	Liver	3D	CNN	D=0.83
Yu et al [86]	2019	CT	Liver	3D	3D ResU-NET	D=0.73
Thomson et al [81]	2019	US	Liver	2D/3D	3D UNet	D=0.78
Kitrungrotsakul et al [39]	2019	CT/MRI	Liver	3D	CNN	D=0.9
Shin et al [75]	2019	CTA	Retina	2D	CNN-GCN	AP=0.9
Yan et al [84]	2020	CT	Liver	3D	3D Residual U-Net	D=0.92
Zhai et al [88]	2019	CT	Lungs	3D	GCN-CNN	–

3.2 Machine learning approaches for other vessel segmentation

3.2.1 Deep learning approaches

Many DL methods have been introduced to reconstruct retinal vessel on 2-D images. Fu et al. [18] used the CNNs in combination with Conditional Random Field (CRF) to generate a vessel probability map. They developed this map to separate the vessels from the background even in the inadequate contrast regions, and is not sensitive to the presence of tumours. They tested their method on 2-D DRIVE and STARE public data sets. Oliveira et al. [63] proposed Fully Convolutional Neural Networks combining the multiscale analysis provided by the wavelet transform with a multiscale CNN to deal with the varying width and direction of the vessel structure in the retina. Their approach overtakes the results obtained by Fu et al. [18]. Liskowski et al. [53] proposed a supervised segmentation technique that uses a deep neural network tested on DRIVE and STAR public data sets their method solve the problem of the branch vessel disconnection. Laibacher et al. [43] presented a novel neural network architecture, called M2U-Net. This is a new encoder-decoder architecture that is inspired from the U-Net. It introduces pre-trained components in the encoder and contractive blocks in the decoder that are combined with bilinear up-sampling, the model was tested on the DRIVE data set. All existing methods using CNNs for retinal vessel segmentation are mainly based on local appearances learned on the image patches, without taking into account the topology and the shape of the vessels.

3.2.2 Topological deep learning approaches

Methods based on graph topology

GCN and GNN are used for segmentation problems especially for multi class segmentation (classification tasks), such as Shin et al. [75] who incorporated a GCN into a CNN architecture, where the final segmentation is inferred by combining the different types of features. They proposed a method that can be applied to expand any type of CNN-based retinal vessel segmentation method on 2-D images to enhance their performance. Zhai et al. [88] proposed a GCN-CNN by linking a CNN with GCN for pulmonary artery-vein separation in chest CT scan images. For binary segmentation, to the best of our knowledge, only one study was found in Juarez et al. [33]; they proposed a joint 3-D U-Net-Graph Neural Network-based method for airway segmentation from chest CTs. The dense feature maps at this

level are transformed into a graph input to the GNN module. The incorporation of graph convolutions in the U-Net provides nodes in the graph with information that is based on node connectivity.

Methods based on topological loss function

Another work based on loss functions such as Hu et al. [25] also proposes a topology-preserving loss function incorporated into end-to-end training of a deep neural network to improve segmentation results. They illustrate the effectiveness of their proposed method on a broad spectrum of natural images. Other approaches used loss functions to improve the multi class segmentation such as Banerjee et al. [5] who proposed a coupled 2-D U-Net architecture that allows training with topological priors and losses for segmentation of street scenes in adverse weather conditions with a neural network trained on images in good weather. Sudre et al. [78] investigated and compared the behavior of several loss functions and their sensitivity to learning rate tuning in the presence of different rates of label imbalance across 2-D and 3-D segmentation tasks. Clough et al. [12] used a topological loss function for deep learning based image segmentation using persistent homology; a CNN with loss function was used for semantic segmentation. Ngoc et al. [62] introduced the boundary-aware loss for deep image segmentation using CNN model for semantic segmentation. Sugino et al. [79] and Kervadec et al. [35] proposed loss weightings for improving imbalanced brain structure segmentation using fully convolutional networks. Finally, Hu et al. [26] developed a topology-aware segmentation by using discrete Morse theory for 2-D neuron image segmentation task. The closest method to our project is proposed by Shit et al. [76], where they presented a centerlineDice loss function that measures the similarity between skeleton of ground truth and the skeleton of likelihood map obtained by CNN network to segment tubular structures such as vessels, neurons, or roads. At the best of our knowledge, no studies propose to elaborate the topological approach for hepatic vessel segmentation, especially by a 3-D approach.

Part I

Segmentation of liver vessel by combining 3-D U-Net approaches

4 Models based on 3D U-Net approaches

4.1 Resume

Accurate liver vessel segmentation is crucial for the clinical diagnosis and treatment of many hepatic diseases. After the in-depth study of the state of the art in the previous chapter, hereafter, we focus on the hepatic vessel segmentation task for improving the results obtained in the literature. To the best of our knowledge, no comparative evaluation has been proposed to compare deep learning methods for the liver vessel segmentation task. Moreover, most research works do not consider the liver volume segmentation as a preprocessing step, in order to keep only inner hepatic vessels.

This chapter is dedicated to carry out a comparative study of 3-D deep learning method based segmentation for liver vessel segmentation from CT (Computerized Tomography) scans, to find an optimal method that can help in improving segmentation decisions. More precisely, 3-D U-Net, Dense U-Net, and MultiRes U-Net are pitted against each other in the vessel segmentation task on the public IRCAD data set. For each model, three alternative setups that allow adapting the selected CNN architectures to volumetric data are tested. Namely, full 3-D, slab-based, and box-based setups are considered.

The results showed that the most accurate setup is the full 3-D process, providing the highest Dice score for most of the considered models. However, concerning the particular models, the slab-based MultiRes U-Net provided the best score. With our accurate vessel segmentations, several medical applications can be investigated, such as the automatic and personalized Couinaud zoning of the liver.

First, we will start with the methodology, including the description of the different models with their parameters, then we will present the results obtained, and finally a discussion of the results and a general conclusion will be described.

4.2 Introduction

Hepatic blood vessel disorders usually result from inadequate blood flow, whether into or out of the liver, induced by cirrhosis and other liver diseases (HCC, for example). To help experts in diagnosis and treatment planning related to these

diseases, accurate segmentation methods of the liver and inner vessels are highly demanded in the clinical practice, whatever the image modalities used such as CT, MRI, or US for instance. The evolution of computer science in research on image segmentation has revealed interest in the reconstruction and interpretation of these complex organic structures [11, 89]. Their robust extraction from biomedical images requires good acquisition during an imaging examination and advanced image analysis developments.

In recent years, Deep Learning (DL) has been increasingly applied in different areas, for higher accurate segmentation, several automated methods have been based on neural networks. However, the used convolutional layers bring to a higher computational complexity. Particularly, the DL-based methods have always belonged to the studies providing higher liver vessel segmentation performances [3, 11, 59] compared to classic segmentation methods. Their architectures are based on convolution blocks that have ensured extracting vessel features even with the complicated details of hepatic vascular tree. They have provided higher accuracy rates that exceed 0.9 when performed with IRCAD database images. Moreover, the permanent rise of fundus image resolution allows illustrating a large gap of vessels details. Hence, DL models will be heavily needed with the aim of obtaining accurate results.

The famous U-Net model proposed by Ronneberger et al. [69] and its extensions stand out as the most relevant for segmentation tasks. The 3-D U-Net captures the volumetric features of the structures and organs in biomedical images. This architecture is the extension of the 3-D FCN proposed by Long et al. [55] (Fully Convolutional Neural network), which suffers from high computational cost and GPU memory consumption. To address these issues, the 3-D U-Net models were proposed, and they are pertinent even with a few image dataset.

Currently in the literature, no comparative evaluation has been found, in order to develop the best 3-D U-Net-based approaches for segmenting the liver volume and hepatic vessels. In general, authors focus either on the liver for future diagnosis analysis (*e.g.* tumor detection) or on the vessels, without taking the parenchymal volume as a region of interest. This question is however of high importance for several compter-aided medical applications, involving the Couinaud representation of the liver for instance [47, 48]. As a consequence, we first use an efficient Dense U-Net algorithm in order to segment the liver vessel. Hence, our study proposes to construct the optimal segmentation pipeline for the liver anatomy by comparing the accuracy of three 3-D DL architectures: 3-D U-Net, 3-D Dense U-Net, and 3-D Multi-res U-Net [60].

4.3 Input data preparation

This study considered three alternative setups that allow adapting popular encoder-decoder U-Net architectures to volumetric data. These setups, referred to as full 3-D, slab-based, and box-based, are described in detail in the following subsections. In all the considered setups, leave one out cross-validation was used to assess the model.

4.3.1 Data

The performance of the studied U-Net-based models in the three considered set-ups were tested on the IRCAD dataset [30]; a popular and publicly available benchmark for liver vessel segmentation. The IRCAD dataset is composed of 20 CT-scans (10 women and 10 men), in DICOM format with a variable number of slices ($512 \times 512 \times Z$ voxels) with hepatic tumors in 75% of cases. Binary masks of the venous system ground truth, done by radiologists, are available within a dataset (see Figure 4.1).

For training, Z was set to 120, which relates to the maximum number of slices within the considered liver volumes. Volumes with the number of slices smaller than 120 were extended to fix this size by zero paddings.

Particularly, the models were trained on 19 volumes (with 3 volumes used for validation) and tested on the remaining one from public IRCAD dataset. The training-testing procedure was repeated 20 times, with different volumes used for testing. In our case the data augmentation were not performed because we tried and the results were not accurate.

4.3.2 Data preprocessing and analysis

Depending on the medical imaging technique, the available GPU plays an important role in 3-D segmentation. For example, with standard computer hardware, it is not possible to fully fit a whole CT-scan with a size of $512 \times 512 \times Z$ into CNN or U-Net models due to the enormous GPU memory requirements; we thus decided to resize the data to $256 \times 256 \times Z$. Therefore, the 3-D medical imaging data can be either sliced into batches with little chunks of images, also called slabs, of $512 \times 512 \times 10$ slices with higher batch size, hence, the 3-D batches analysis can be used to test the three models. It should be noted that we did not use any data augmentation process in our study.

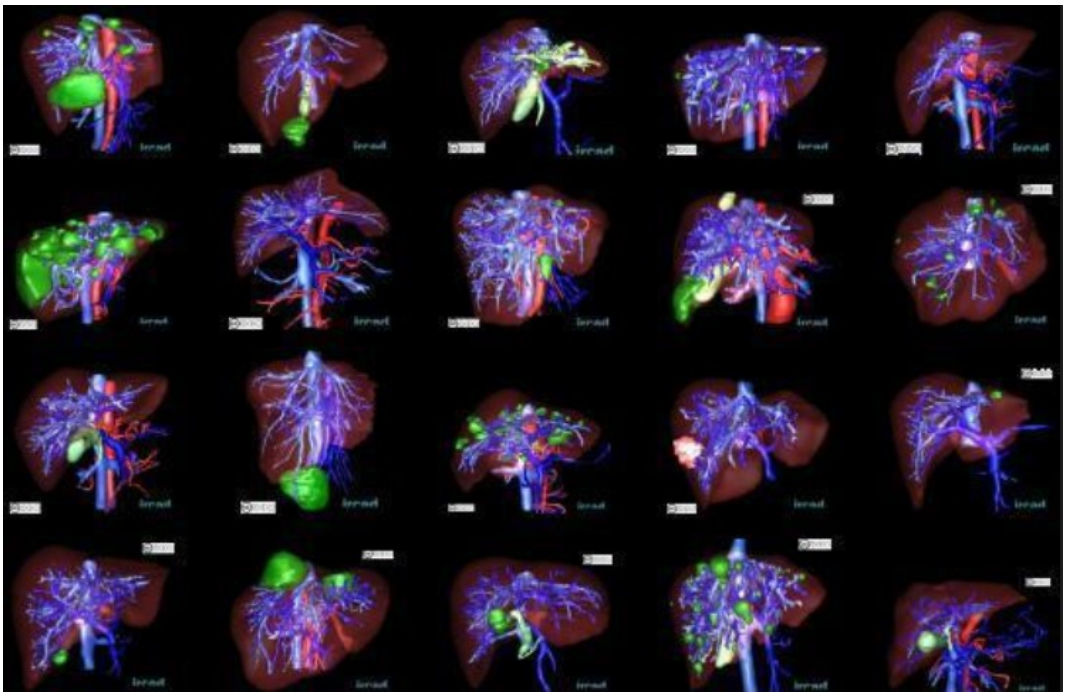

Figure 4.1: The 3-D-IRCADb-01 database. The 20 folders correspond to 20 different patients, which can be downloaded individually or conjointly.

4.3.3 Cross validation K-Fold

With this approach we divide the data into K partitions of the same size. For each partitioning i, we train the model on K-1 partitions, and we evaluate it on the partition i which has been excluded from the training, our final score is then the average of the K scores obtained. This method is useful when the performance of the models varies significantly depending on the partitioning chosen between the training set and the test set as for the validation with a single data set excluded.

Full 3-D approach

In the full 3-D setup, the models were trained using complete 3-D liver volumes (cf. Figure 4.2) to predict a vessel probability map for each input image. Each time 19 volumes of size $512 \times 512 \times 120$ voxels were used, 15 for training and three ones used for validation and one volume for test. Volumes with the number of slices smaller than 120 were extended to fix this size by adding zeros (zero paddings).

A full 3D approach allows taking advantage of complete spatial information contained in a volume. However, it also results in limited train data and requires

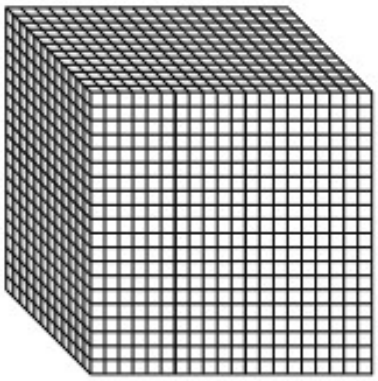

Figure 4.2: Full volumetric setup used for training and testing the considered U-Net-based CNN models.

the heaviest computational workload. Both the slab-based setup and the box-based setup diminish these limitations at the cost of limiting spatial information to selected sub-volumes.

Slab-based approach

In the slab-based setup, the models were trained with slabs, *i.e.*, sub-volumes comprising neighboring slices (cf. Figure 4.3). At the prediction stage, the trained models were applied to consecutive overlapping slabs. The resulting model outputs in the overlapping regions were next averaged to produce the seamless vessel probability map.

In the experiments we used 240 slabs in total. The slab size was $512 \times 512 \times 10$ voxels. Slabs for training were sampled equally from the 19 train volumes, resulting on average in 120 slabs per train volume. For prediction, slabs overlapping by 2 slices were considered.

Box-based approach

The box-based setup is somehow similar to a slab-based one. However, the sub-volumes used for training the model comprise neighboring and connected voxels composing a box (cf. Figure 4.4). The trained models were next applied to consecutive overlapping boxes at the prediction stage to produce a continuous edge probability map by averaging the model's output in the overlapping regions. In our experiments we used 320 000 train boxes of size $32 \times 32 \times 32$ voxels. The boxes for training were sampled randomly from the 19 train volumes, resulting on average

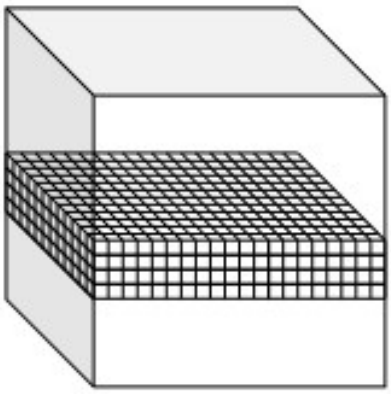

Figure 4.3: Slabs volumetric setup used for training and testing the considered U-Net-based CNN models.

in 17 000 boxes per volume. For prediction, boxes overlapping by 8 voxels in each direction were considered.

4.4 Models architecture

In this study, we compared three popular U-Net-based architectures, namely the basic U-Net as proposed by [69], Multi-res U-Net [28], and Dense U-Net [60]. The original models, after extending them to the third dimension (see Figure. 4.5), were used in the full 3-D and slab-based setup. The details of the models are given in the following subsections, and the models' hyperparameters are summarised in Table 4.1. Particularly, depth relates to the number of resolutions (poolings) implemented in the model. While dropout mentions dropout rate. These layer randomly sets input units to 0 with a frequency of rate at each step during training time, which helps prevent overfitting. The remaining parameters relate to the model training stage, and their names are self-explanatory.

For the box-based setup, the considered models needed to be reduced in terms of both depth and the number of filters in each layer. Such a change was imposed by the reduced input size. All amendments made to the considered U-Net-based models are also detailed in the following subsections. Models' hyperparameters used in the box-based setup for each of the considered models are summarised in Table 4.2.

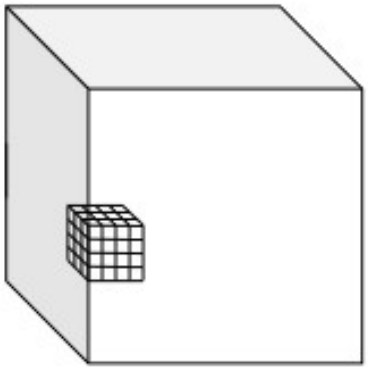

Figure 4.4: Box volumetric setup used for training and testing the considered U-Net-based CNN models.

Table 4.1: Models parameters on slabs and full volumes

Parameters	U-Net	MultiRes U-Net	Dense U-Net
Depth	4	4	4
Dropout	0.2	0.2	–
Epochs	100	100	100
Batch size (slabs)	8	8	8
Batch size (full)	1	1	1
Batch normalization	True	True	True
Loss	Dice loss	Dice loss	Dice loss
Optimizer	Adam	Adam	Adam
Momentum	0.99	0.99	0.99
Learning rate	0.0001	0.0001	0.0001

4.4.1 3-D U-Net model

The 3-D U-Net model used for the full 3-D and the slab-based setup comprises nine convolutional step blocks (see Figure 4.5a). Each convolutional step block contains two 3-D convolutions of size 3×3×3 followed by the ReLU activation and a dropout layer with a rate of 20% between them to reduce overfitting. The contracting path consists of four convolutional step blocks, each followed by max-pooling 3-D of size 2×2×1. The expanding path also consists of four step blocks, each followed by upsampling 3-D of size 2×2×1. The feature maps outputted by upsampling operation are concatenated with the corresponding ones from the contracting path.

Finally, the last convolutional step block is applied, followed by a convolution 3-D of size 1×1×1. A sigmoid activation is used to produce a final probability map.

To adapt the model to the box-based setup, the size of max-pooling and upsampling operations was changed from 2×2×1 to 2×2×2 to adapt the model to smaller input resolutions. Also, in the expanding path, the number of filters was reduced by half. Finally, the dropout rate was set to 25% to facilitate training.

4.4.2 3-D Dense U-Net model

3-D Dense U-Net is based on the original U-Net and 3-D U-Net version. The architecture adds residual and dense interconnections between layers processed in convolutional step blocks (see Figure. 4.5b). A single step block contains the 3-D convolution of size 3×3×3 followed by the ReLU activation and the batch normalization layer with a momentum of 0.99. The output of this operation is concatenated with an input. Then the process is repeated for the result of the previous concatenation. The contracting and expanding paths look the same as in the 3-D U-Net model. The contracting path consists of four convolutional step blocks, each followed by max-pooling 3-D of size 2×2×1. The expanding path also consists of four step blocks, each followed by upsampling 3-D of size 2×2×1. The produced feature maps by upsampling operation are concatenated with the corresponding ones from the contracting path. Finally, the last convolutional step block is applied, followed by a convolution 3-D of size 1×1×1. A sigmoid activation is used to produce a final probability map.

Again, the model as above was used for two set-ups - the full 3-D and the slab-based one. Also, it was used for the liver volume segmentation in the preprocessing step. In the box-based set-up, a shallow version of the Dense U-Net was used to adapt the model to the smaller resolution of inputs. Particularly, both the number of filters and the depth of the model were reduced. The latter was reduced from four to three. The number of filters for the contracting and the expanding path was reduced from (6; 12; 24; 48; 96; 48; 24; 12; 6) to (2; 4; 8; 16; 8; 4; 2) respectively.

4.4.3 3-D MutliRes U-Net model

3-D MultiRes U-Net is based on the original U-Net and 3-D U-Net version. However, the architecture is more complex. The model consists of nine resolution blocks and ten resolution paths.

The resolution path consists of two 3-D convolutions with eight filters each. The first is of size 1×1×1, the second has a size of 3×3×3 and is followed by the ReLU activation. Then, the result of both operations is added, and sigmoid activation

followed by batch normalization is performed. The resolution block consists of three connected 3-D convolutions of size 3×3×3 each, followed by the ReLU and dropout with a rate of 20% to reduce overfitting. The first convolution has 32 filters, and the next two have 16. Then the result of those three operations is concatenated, and after batch, normalization is added to the 3-D convolutions of 1×1×1 with 64 filters which are performed on the original input of the resolution block. Finally, sigmoid activation followed by batch normalization is performed. The contracting path consists of four resolution blocks, each followed by max-pooling of size 2×2×1 and resolution paths. The expansion also consists of four resolution blocks, each followed by upsampling of size 2×2×1. The output feature maps by upsampling operation are concatenated with the corresponding results of the resolution path from the contracting one. Finally, the last resolution block is applied, followed by a convolution 3-D of size 1×1×1. A sigmoid activation is used to produce final probability maps.

Similar to previous architectures, 3-D Multi-res U-Net model as described above was used in the full 3-D and slab-based setup but needed to be adapted to the box-based setup. Particularly, the number of filters in a resolution block was reduced to a quarter from (32; 16; 16; 64) to (8; 4; 4; 16).

Table 4.2: Models parameters on boxes

Parameters	U-Net	MultiRes U-Net	Dense U-Net
Depth	4	4	3
Dropout	0.25	0.2	–
Epochs	10	10	10
Steps per epoch	1000	1000	1000
Boxes per step	32	32	32
Batch normalization	False	True	True
Loss	Binary crossentropy	Binary crossentropy	Binary crossentropy
Momentum	–	0.99	0.99
Optimizer	Adam	Adam	Adam
Learning rate	0.0001	0.0001	0.0001

4.5 Post-Processing

Post-processing removes imperfections, noisy pixels or corrects them through image processing operations. It uses simple image processing operations to remove

errors resulting from the segmentation process. Automatic thresholding with morphological operations such as morphological closure are used to reduce noise and false negatives in the image. Thresholding is a method for finding the threshold(s) to segment the image into region(s), in order to make the analysing easier. In thresholding, we convert an image from colour or grayscale into a binary image.

To continue the segmentation process, it is necessary to know the opening and closing operations. Although erosion and dilation are very useful, these operations tend to change the size of the mask. The opening and closing morphological operations were used to solve this problem by keeping the same size of the objects in the mask. In our case, we used the close operation (see Figure 4.6). Morphological closure is a dilation followed by an erosion (which is the reverse of the operations for an opening). So the impact of the close operation is to remove background voxels, and this can help removing false negatives in images, also closing tends to fill in gaps in the image.

4.6 Results

4.6.1 Training convergence

In Figure. 4.7, we depict the learning of the tested models, by considering the Dice coefficient that we obtained for slab-based approaches, and the binary-crossentropy loss for box-based ones (with a different sliding window averaging). For a sake of clarity, we have chosen these configurations to evaluate the accuracy and loss curves and to validate the best setup configuration.

The 3-D U-Net stands as the less efficient architecture of our study, with the lowest Dice increase during training (approximately 0.4) and the highest loss (0.08) at the end of the training process. Moreover, its validation is the worst, without any significant increase during the optimization. The two other architectures lead to similar outcomes, with a better performance for the MultiRes U-Net, which reaches a Dice accuracy at 0.8 and loss value lower than 0.05. Validation accuracy is also optimized in a better way for this model.

4.6.2 Liver vessel segmentation results

The assessment of the vessel segmentation results was performed by means of the Dice score. The performance of each model was evaluated using the test set (one CT-scan following our distribution). Dice coefficient was used as an evaluation measure, which is written as:

$$Dice = 2\frac{|A \cap B|}{|A| + |B|}, \tag{4.1}$$

where A is the segmented vessel image and B is the ground truth vessel mask.

Models are designed for the largest possible input images that can fit the GPU memory. We used an NVIDIA GeForce GTX 1650 (12Gb) with 256 Gb of RAM, available on our local server.

The vessel probability maps output by the considered models were binarised with a global threshold of 0.5, cropped to the liver region, and then compared to the ground truth results provided within the IRCAD dataset. The average Dice scores resulting from the leave-one-out cross-validation are summarised in Table 4.3. Best scores (greater than 70%) are highlighted in bold face.

Table 4.3: Dice score results on slabs and full volumes.

Set-up	U-Net	MultiRes U-Net	Dense U-Net
Full 3D	0.734	**0.863**	**0.838**
Slabs-based	0.700	**0.880**	0.775
Box-based	0.551	0.764	0.625

Sample visual results of the first partient of the IRCAD data set using the full 3-D setup is presented in Figure 4.9. Presented results were obtained from the first patient of the IRCAD dataset using the full 3-D setups. The latter set-up was selected for presentation, since it performed best. A comparaison of the results obtained using the three developed models on different configuration setup are presented in Figure 4.8, were the best results are obtained using 3-D MultiRes U-Net on full liver volume.

Particularly, the top panel (see Figure 4.9 a) presents the ground truths provided within the IRCAD dataset, while the vessels provided by the considered U-Net-based models are presented below (see Figure 4.9b-d).

4.7 Discussion

The experimental results clearly show the differences between the performance of the considered models and the setups in which they were applied. The numerical results presented in Table 4.3 show clearly that the most accurate results were obtained when using a full 3-D setup. This manifests itself by the highest Dice scores obtained for each of the considered models. On the other hand, the box-based setup seems to be less accurate, with the lowest Dice scores. It is somehow

surprising since the amount of the training data was the largest in the box-based setup. However, these experiments show that the completeness of the information contained in the smaller amount of the whole volumes is more beneficial to the model than a large number of pieces of information sliced in the boxes. Probably for these reasons, the full 3-D setup performed visibly better than the competitive frameworks.

When the U-Net-based models are considered, the Multi-Res U-Net is the leader. This model performed best for all the considered setup, resulting in the most accurate segmentation for the slab-based approach. On the other hand, the original U-Net model performs worst, with the lowest Dice scores obtained for each of the considered frameworks. The training behavior observed in Figure 4.7 confirm the best performance of Multi-Res U-Net.

The above observations are also confirmed by the visual results presented in Figures 4.9 and 4.8. Mainly, the results of the U-Net model are visibly the most noisy, with many small regions distant and not connected to the main vessels (see Figure. 4.9b). On the other hand, the visually best representation of the liver vessels is obtained from the MultiRes U-Net. From Figures 4.9 and 4.8, we can see that that the resulting vessels are larger and more continuous, with the lowest amount of noise. Also, the MultiRes U-Net provides the best segmentation of the largest branches. This latter fact is a significant advantage to build automatically the Couinaud representation of the liver, which is commonly used by clinicians of various specialties to describe locations of the hepatic lesions.

The MultiRes U-Net is however the most expensive to train in terms of the computer resources. In all considered setups the time per epoch for this model, was about twice as much as in the case of the U-Net model, and slightly longer than the time required by the Dense U-Net.

4.8 Conclusions

In this chapter, we deal with the segmentation of hepatic vessels in 3D CT scan images. Three models based segmentation on three alternatives setup are proposed. Firstly, a standard 3-D U-Net model based segmentation is developed. Secondly, this model were tested on 3-D full liver volume images and, boxes and slabs to compare results and validate the best combination model/ volumetric setup

The obtained results with 3-D U-Net demonstrate the efficiency of this architecture that allows the reconstruction of the liver vascular structure with a good results especially on full volume but still gives poor response on small regions and bifurcations. After that, we proposed to use the modified 3-D Dense U-Net and 3-D

MultiRes U-Net which are new approaches to improve segmentation decision. Nevertheless, it is difficult to avoid the segmentation vessel issue with a simple U-Net model, especially when the propagation criterion is an intensity-based condition. For this reason, more performant models are expected. To provide a good extraction, a post-processing smoothing operation is necessary after the segmentation.

We have performed a comparative analysis of the three U-Net-based models in the liver vessel segmentation task. The analysis results clearly show that the leader in the considered task is a Multi-Res U-Net which provides the most accurate results in terms of the Dice coefficient.

When the 3-D setups used for liver vessel segmentation are considered, the better is a full 3-D approach, which provided the highest Dice scores for three out of two considered U-Net-based models. However, in our experiments, the slab-based setup used with the Multi-Res U-Net performed the best.

The results of the liver vessel segmentation using the Multi-Res U-Net are good and promising. However, they still probably could be improved. The possible ways of the improvement include adaptive thresholding applied for post-processing of the predicted vessel probability maps. Also, in the following chapter we will try to improve the segmentation results of Multi-Res U-Net using preprocessed data (vessel enhancement) to deal with segmentation errors.

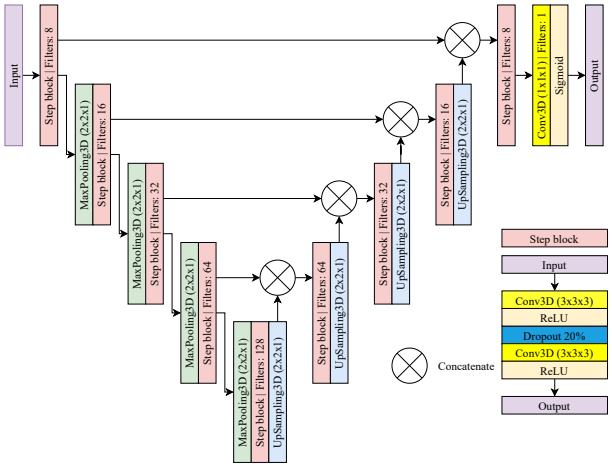

(a) 3-D U-Net model

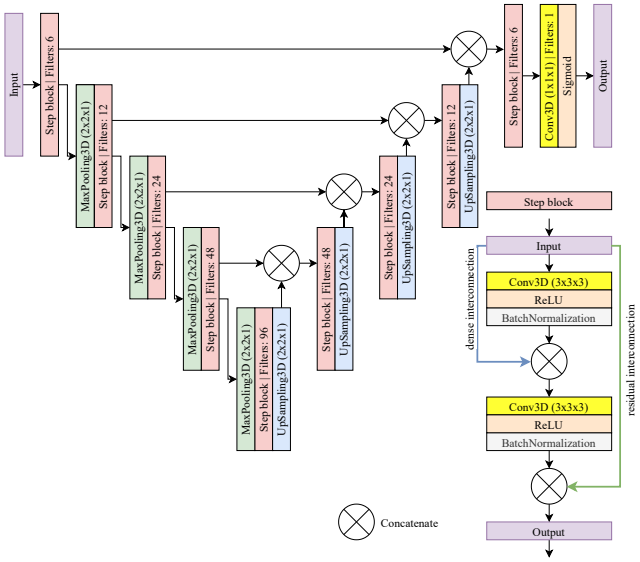

(b) 3-D Dense U-Net model

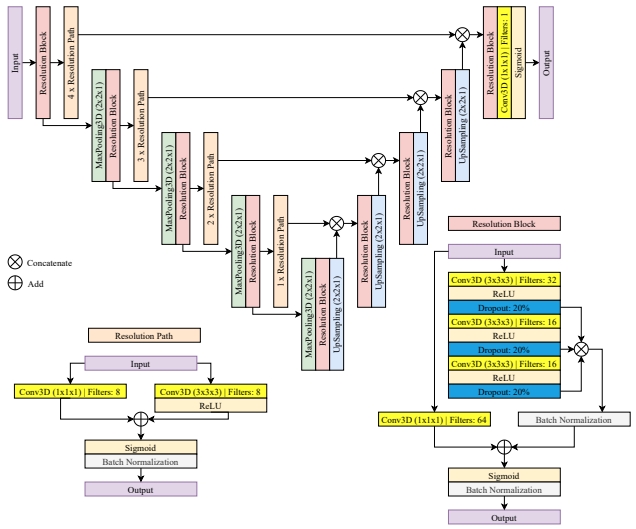

(c) 3-D Mutli-res U-Net model

Figure 4.5: The U-Net-based models considered in this study for full 3-D and slab-based setup.

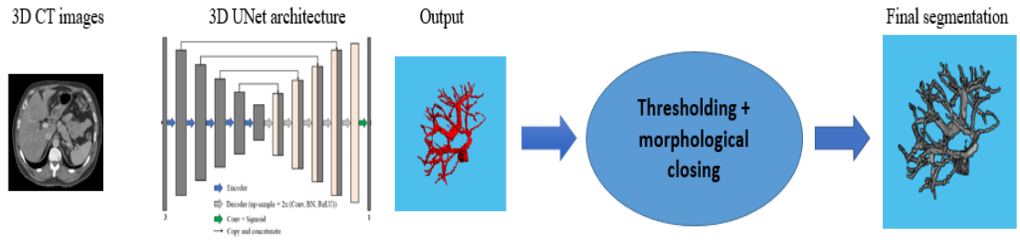

Figure 4.6: Steps of hepatic vessel segmentation and post-processing to improve segmentation results

(a) 3-D U-Net Dice coefficient

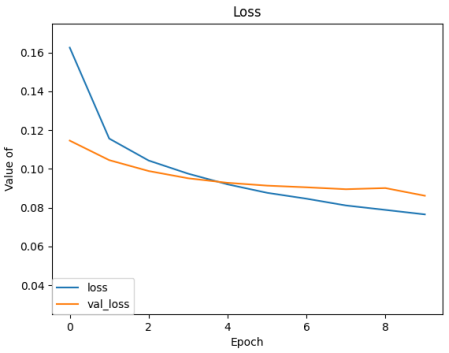

(b) 3-D U-Net binary-crossentropy loss

(c) 3-D Mutli-res U-Net Dice coefficient

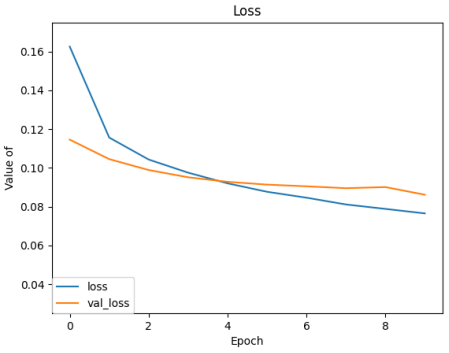

(d) 3-D Mutli-res U-Net binary-crossentropy loss

(e) 3-D Dense U-Net dice coefficient

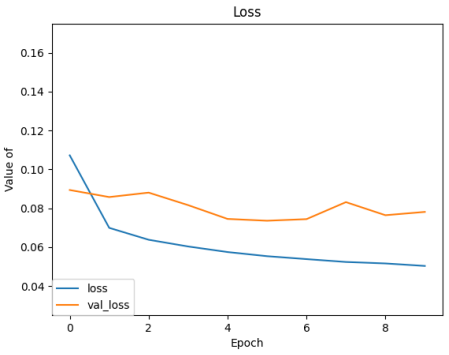

(f) 3-D Dense U-Net binary-crossentropy loss

Figure 4.7: Training and validation Dice values per epoch for slab-based models (a,c,e) and loss optimization for the box-based models with a sliding-window averaging (b,d,f).

(a) Box

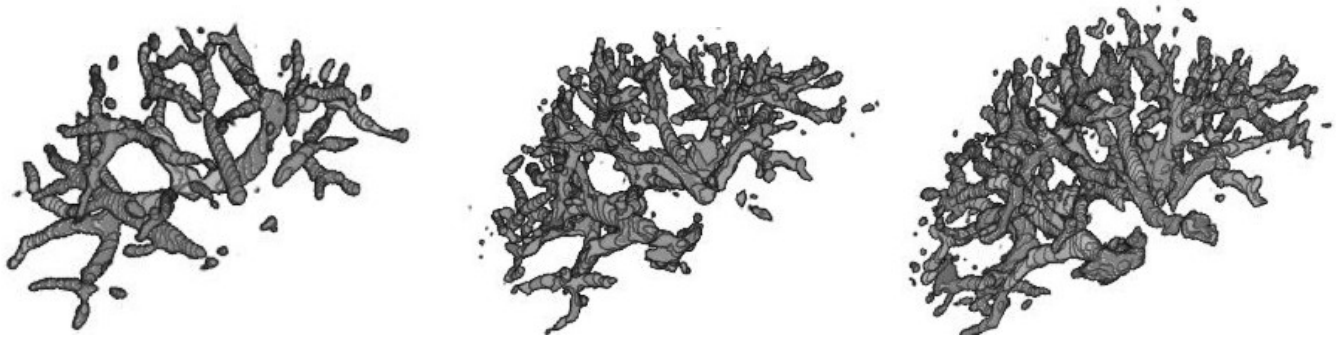

(b) Slabs

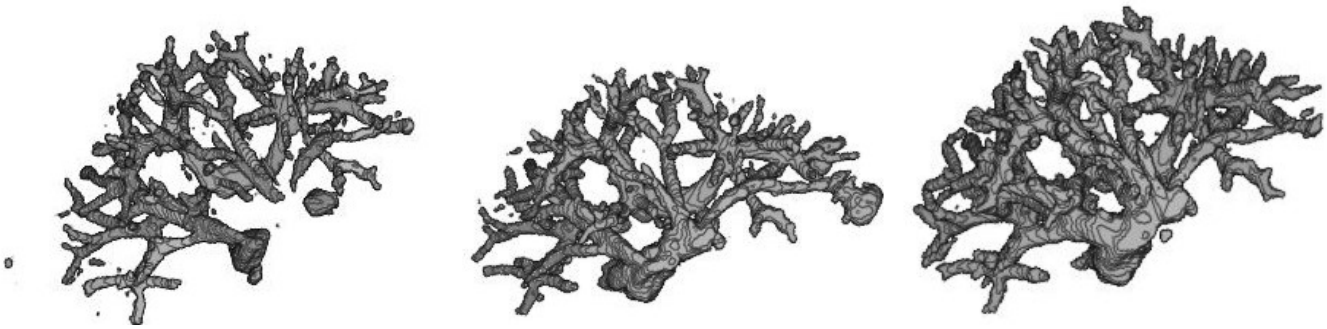

(c) Full

Figure 4.8: 3-D views of segmentations obtained from the first patient of IRCAD dataset, with the full 3-D volume and box and slabs based segmentation. The first column : Results obtained using 3-D U-Net, the second column: results obtained using 3-D Dense U-Net, the last column: results obtained using 3-D MultiRes U-Net.

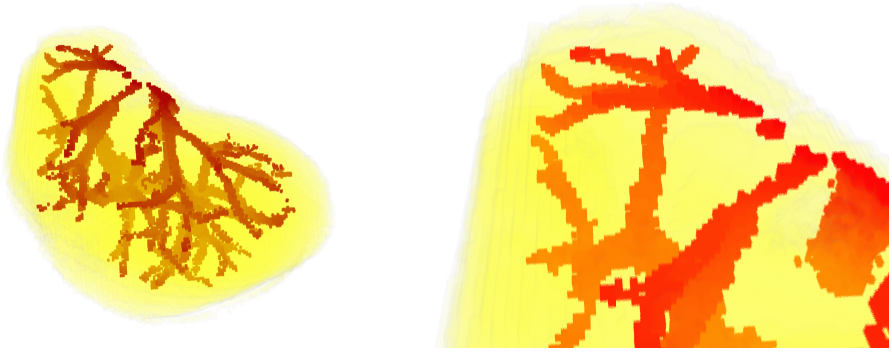

(a) Ground-truth

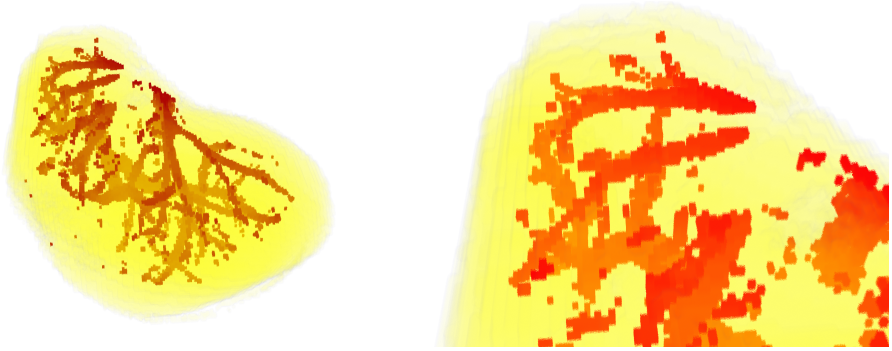

(b) U-Net

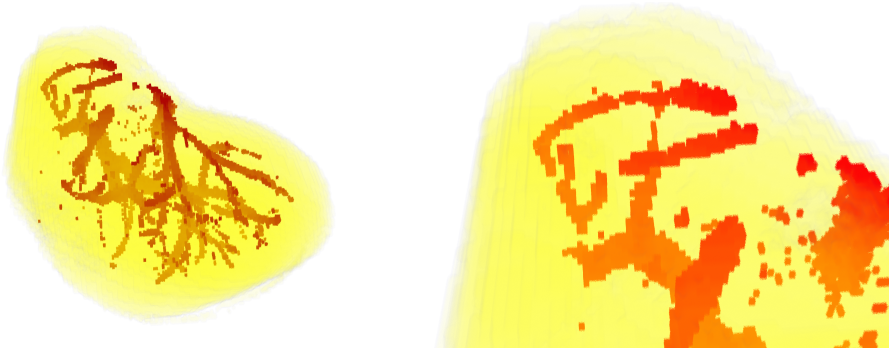

(c) Dense U-Net

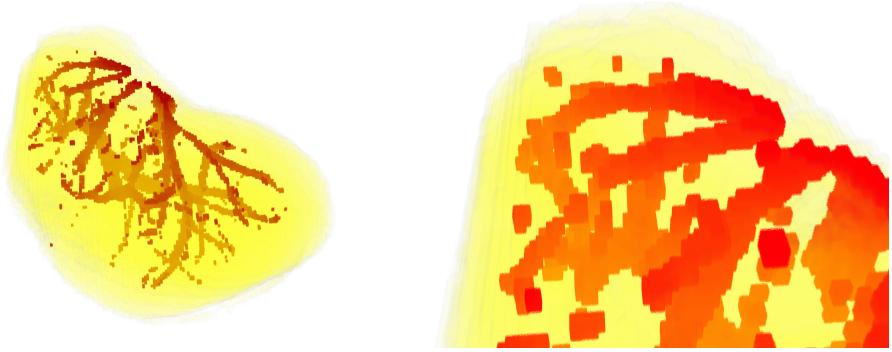

(d) MultiRes U-Net

Figure 4.9: 3-D views of segmentations obtained from the first patient of IRCAD dataset, with the full 3-D volume approach. The upper part of the visualization is also zoomed.

Part II

Hepatic vessel extraction using vesselness filters

5 Models based on vascular patterns

5.1 Resume

In the previous chapter we have carried out a comparative study of three U-Net architectures for the segmentation of the hepatic vascular network in order to validate the best model/configuration combination which will be useful in the following chapters to increase the performance of the segmentation process.

In this chapter, we will present an end-to-end deep learning segmentation method relying on the integration of vessel enhancement filters inside a 3-D U-Net based architecture described previously. In particular, the raw data used in the learning process or used as input, are preprocessed using enhancement filters. We assume that the use of these vesselness filters can significantly improve the vascular contrast in raw images, this step can also help to improve segmentation decision on small regions and bifurcations that are generally very hard to detect during segmentation process.

First of all, The 3-D U-Net, Dense U-Net and MultiRes U-Net presented in previous chapter are pitted against each other in the vessel segmentation task with the public IRCAD dataset. Considering the integration of vesselness filters, the model parameters were optimized in order to identify the optimal configuration for fully automatic segmentation of hepatic vessels tree.

Secondly, we propose an original comparative study of several deep learning models combined with vesselness filters (Jerman, Frangi, Sato and RORPO algorithms) as preprocessing step. 3-D U-Net, 3-D Dense U-Net, and 3-D MultiRes U-Net have been tested on CT-scans to extract the vascular networks with and without preprocessing on full liver volumes and on slabs (stacks of 2-D slices) that are validated in the previous chapter as better configurations compared to boxes. The models were evaluated on publicly available database, and the 3-D Dense U-Net achieved the best Dice score on preprocessed data with Jerman filter in particular, compared to raw data.

The results showed that the most accurate setup is the full 3-D process, providing the highest Dice for most of the considered models, however the 3-D Dense U-Net gives the best results compared to other models with or without vessel enhancement filters, and this model improve segmentation results compared to outcomes obtained in the previous chapter where we did not use vesselness filters.

5.2 Introduction

Blood vessel segmentation is crucial for many diagnostic and research applications. In recent years, CNN-based models have leaded to breakthroughs in the task of segmentation, hence, these approaches usually lose important information on object boundaries and small regions of complex structures which are useful in vessel segmentation process.

Enhancement and denoising are problems in the field of image processing, vascular enhancement as well as noise reduction with preservation of the structure of medical images is important for clinicians to diagnose vascular diseases, by reducing noise level and by enhancing some features in the image, some preprocessing techniques are adopted.

To enhance the vascular structures prior to their segmentation, and to remove positive false and image noise, the vesselness filters enhancing vascular structures are used in the literature. Even though several enhancement filters are widely used, the responses of these filters are typically not optimal especially on vessels of different radius and, compared to the response in the central part of vessels, their response is lower in the presence of vascular pathologies. In parallel, from the early age of medical image processing, vessel enhancement algorithms (or vesselness filters) have been very important techniques to improve the results of vessel segmentation. Recently, a benchmark from [44] has compared seven vesselness filters published the last 20 years in the literature on CT images for liver vessel exploration.

At the best of our knowledge, no comparative study has been proposed to elaborate the best combination between 3-D DL networks and vessel enhancement algorithms for vessel segmentation. In this chapter, we propose to combine the most useful and accurate U-Net architectures (3-D U-Net, 3-D Dense U-Net and 3-D MultiRes U-Net) with the four best vesselness filters of the benchmark mentioned above (Jerman, Sato, Frangi and RORPO algorithms), for the segmentation of liver vessels in CT-scans. For a better comparison, we also consider full volume analysis and with slabs (stacked 2-D slices). Thanks to this comparative study, we show that the use of these filters as a preprocessing steps improves significantly the accuracy of DL models for this task.

5.2.1 Vesselness filters

We propose to test the three 3-D U-Net architectures presented in chapter above with different parameters which are optimized in this case for hepatic vessel segmentation using different vessel enhancement filters (presented previously) as a

preprocessing step. We choose four filters that improve vessel contrasts, evaluated in study [45]. A variety of enhancement filters exists in the literature, but they are often difficult to compare as the applications and datasets differ from a study to another and the method is not totally described or the codes are rarely available. The Zhang, Sato, Jerman and RORPO filters were selected in this case, the choice of these filters was after testing the seven filters proposed in this article and after visual evaluation of the results we decided to select these four filters. In addition, we have different results of these filters, with different algorithm settings (see Table 5.1). One of these filters is specifically optimized for binary segmentation of vessels (see Table 5.2). Next, we compare the results obtained for three 3-D U-Net models on full liver volume CT images and on slabs (see Figure 5.1). We have tested Sato filter [72], Frangi filter [17] and Jerman filter [31], which are based on Hessian matrix analyses. Then Zhang filter [91] is an extension of Jerman's method for CT data with an improved fuzzy affinity function. Also, Merveille et al, [57] proposed RORPO (Ranking the Orientation Responses of Path Operators) filter using orientation-based path opening outcomes, combined with a voting policy. This benchmark showed that all these filters may be useful to improve liver vessel segmentation and especially on bifurcations.

5.2.2 Data generation

The data for this experiment where obtained using the benchmark framework from [45]. This framework allows to apply vesselness filters over a dataset and compute metrics in user defined regions of interest (ROI). In more details, the vesselness outputs are successively thresholded in the same way we would proceed to compute a ROC curve (Receiver Operating Characteristic). For each threshold, the MCC (Matthews Correlation Coefficient), Dice and usual metrics derived from the confusion matrix are evaluated. This framework make possible an automated optimization of the filters parameters over a dataset for a specific area of interest.

Several vesselness filters (Jerman, Sato, Zhang, RORPO) where computed over two optimization schemes. A first version use the results of the benchmark presented in [45]. In this version the optimization is set up to find the best parameters sets maximizing the mean MCC over the entire dataset. In practice, for the organ ROI and for each tested parameter set P_i, the mean MCC for all binary volumes would be computed for each threshold. Then the best parameter P_{best} is selected as the parameter set with the highest mean MCC. In the second version, the optimization is done differently. For each parameter set, we chose to optimize the MCC per volume (MCC_v). Then we chose the parameter set maximizing the mean over MCC_v.

In terms of clinical usage, the first strategy represents a use case in which a segmentation algorithm is set up once. In the second strategy, the vessels enhancement is fine tuned by the operator for each volume.

Table 5.1: MCC score and vesselness parameters for the first optimization strategy

Filters	MCC	Parameters
Zhang	0.356 ± 0.079	$\sigma_{min} = 1.4$ $\sigma_{max} = 2.4$ $nbScales = 4$ $tau = 1.0$
Sato	0.275 ± 0.066	$\sigma_{min} = 1.4$ $\sigma_{max} = 2.4$ $nbScales = 4$ $alpha1 = 0.3$ $alpha2 = 1$
Jerman	0.318 ± 0.081	$\sigma_{min} = 1.4$ $\sigma_{max} = 3.0$ $nbScales = 4$ $tau = 0.2$
RORPO	0.384 ± 0.077	$scale_{min} = 60$ $factor = 1.2$ $nbScales = 3$ $dilation = 0$

Table 5.2: MCC score and vesselness parameters for the second optimization strategy

Filters	MCC	Parameters
Jerman	0.350 ± 0.081	specific scale space per volume $tau = 0.1$

5.3 Methodology

This section is organised as follows: First, we present our material. Then, we compare the results of three different models presented before, with or without vessel enhancement as preprocessing step. A discussion of the results follows. Finally, we conclude and give some directions for further work.

We propose to test three 3-D U-Net architectures presented in the pervious chapter for hepatic vessel segmentation using different vessel enhancement filters as a preprocessing step. We choose four filters that improve vessel contrasts, evaluated in study [45], the Zhang, Sato, Jerman and RORPO filters. In addition, we have different results of these filters, with different algorithm settings (see Table 5.1). One of these filters is specifically optimized for binary segmentation of vessels (see Table 5.2). Next, we compare the results obtained for three 3-D U-Net models on full liver volume CT images and on slabs (as presented in pipeline of Figure 5.1). The models were implemented with the open source neural network libraries Keras [9] and Tensorflow [2]. Parameters were optimized to obtain the most accurate segmentation outcomes (see Table 5.3).

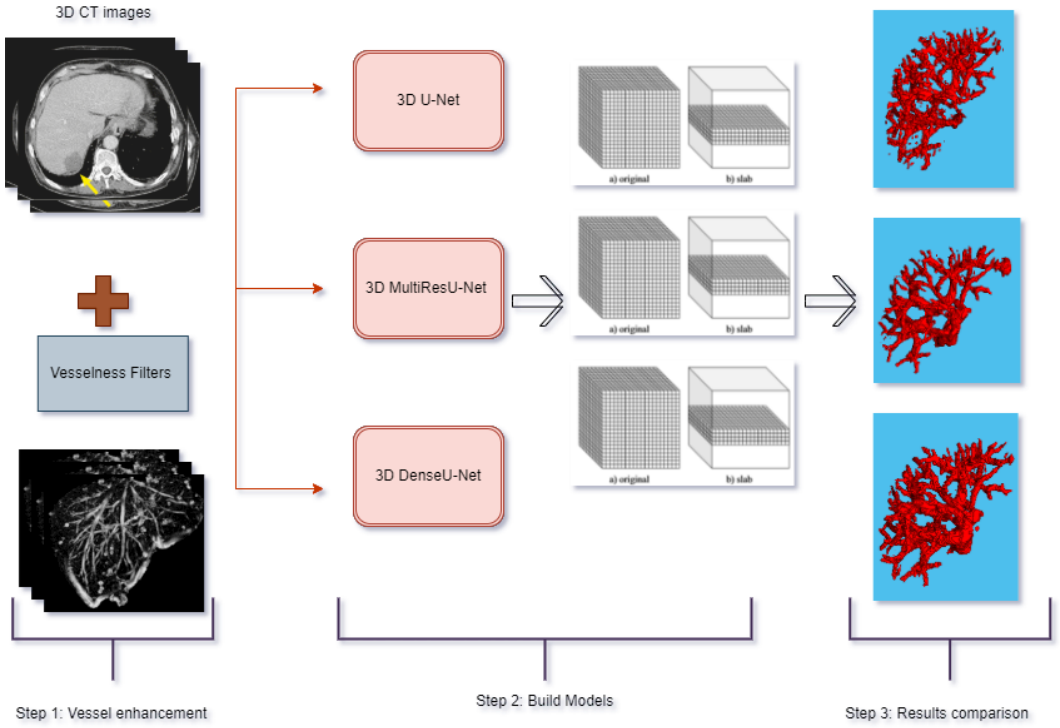

Figure 5.1: Pipeline proposed to carry out the comparative study

Table 5.3: Model parameters on slabs and full volume

Parameters	U-Net	MultiRes U-Net	Dense U-Net
Number of filters	256	256	256
Epochs	20	20	20
Dropout	0.25	0.25	–
Batch size (slabs)	8	8	8
Batch size (full)	1	1	1
Depth	4	4	4
Batch normalization	True	True	True
Momentum	0.99	0.99	0.99

5.3.1 Evaluation method

We evaluated our models by randomly selecting the data (preprocessed or not and coming from the IRCAD database) into the training, validation and testing sets in the ratio of 70%-20%-10% respectively in a cross-validation manner. For each

method, all data are performed to collect experimental results with a different training set.

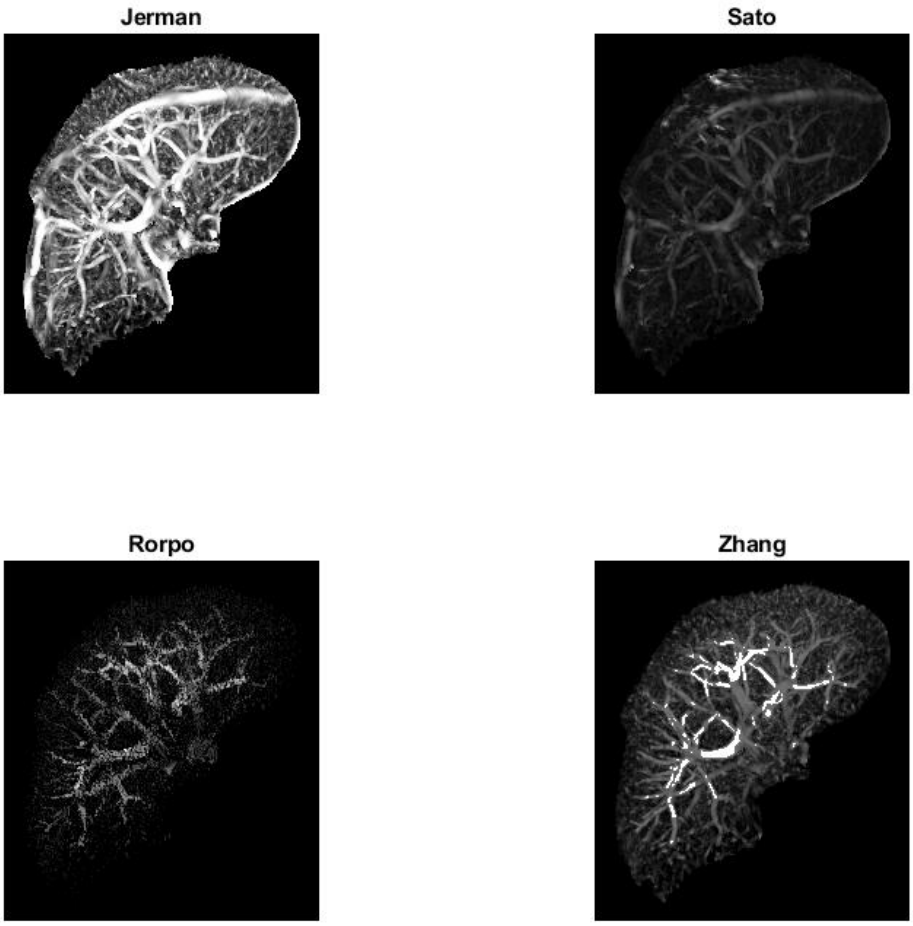

Figure 5.2: Maximum intensities projection of liver vessel enhancement using the selected filter.

5.4 Results

Generally, vessel segmentation is more accurate on full volumes than on slabs (see Figure 5.4). We also note that they are more precise after using the Jerman filter with an improvement in the Dice coefficients (see Table 5.4).

Table 5.4: Results of the Dice coefficient calculated on full volumes and slabs.

Volume	**Full volume**		
Preprocessing	**U-Net**	**Dense U-Net**	**MultiRes U-Net**
Without filter	0.784	**0.853**	0.811
Jerman filter	0.727	**0.942**	0.913
RORPO filter	0.417	**0.521**	0.492
Sato filter	0.719	**0.814**	0.731
Zhang filter	0.434	**0.642**	0.629
Volume	**Slabs**		
Preprocessing	**U-Net**	**Dense U-Net**	**MultiRes U-Net**
Without filter	0.518	**0.789**	0.771
Jerman filter	0.658	**0.936**	0.921
RORPO filter	0.410	**0.456**	0.411
Sato filter	0.713	**0.800**	0.689
Zhang filter	0.456	**0.714**	0.611

With data preprocessed using Zhang and RORPO filters, performance decreases especially on slabs (see Figure 5.5), and this may be due to the creation of noise when applying these filters, false positives appear especially using RORPO filter . In addition, we can note that the 3-D Dense U-Net gives a Dice score on the whole volume and slabs respectively of 0.853 and 0.789 without preprocessing; 0.814 and 0.800 using the Sato filter, 0.942 and 0.936 using a Jerman filter; these are the best scores compared to all other experiments with 3-D U-Net and 3-D MultiRes U-Net. We can deduce that the 3-D Dense U-Net gives the best results compared to other models with or without vessel enhancement filters. This can be justified by the fact that the 3-D MultiRes U-Net model is sensitive to noise generated by enhancement filters.

Our deep learning and vesselness filters based method significantly outperforms methods without preprocessing in accuracy. We have observed that our approach demonstrates more consistency in terms of bifurcations of liver vessels. It correctly segments liver vessel, in the other hand other models without preprocessing segments liver vessel but they generate positives false and negatives false especially on small regions.

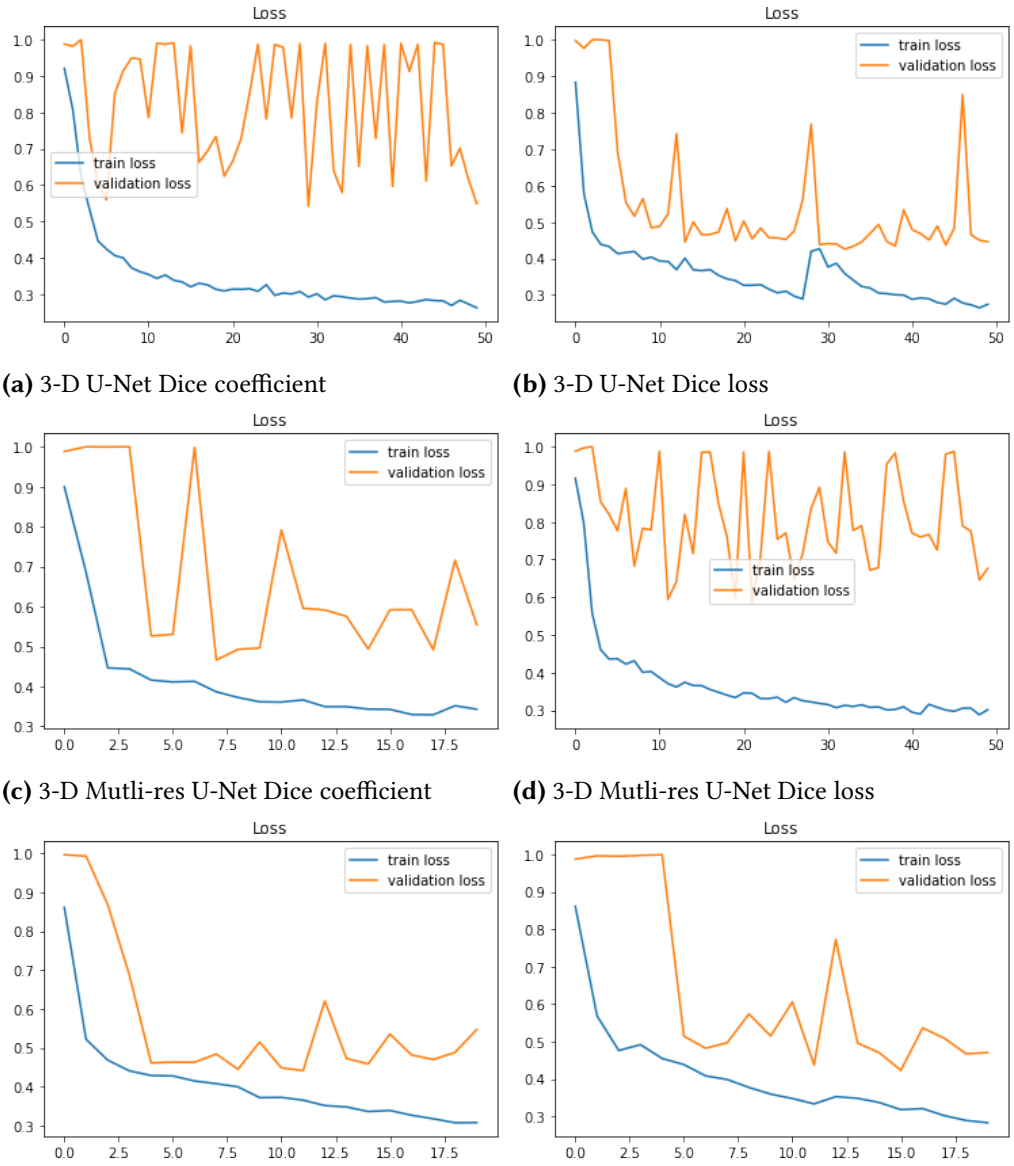

(a) 3-D U-Net Dice coefficient

(b) 3-D U-Net Dice loss

(c) 3-D Mutli-res U-Net Dice coefficient

(d) 3-D Mutli-res U-Net Dice loss

(e) 3-D Dense U-Net Dice coefficient

(f) 3-D Dense U-Net Dice loss

Figure 5.3: Training and validation Dice loss per epoch for slab-based models (a,c,e) and loss optimization for the full volume-based models with a sliding-window averaging (b,d,f), using the Jerman filter for vascular enhancement.

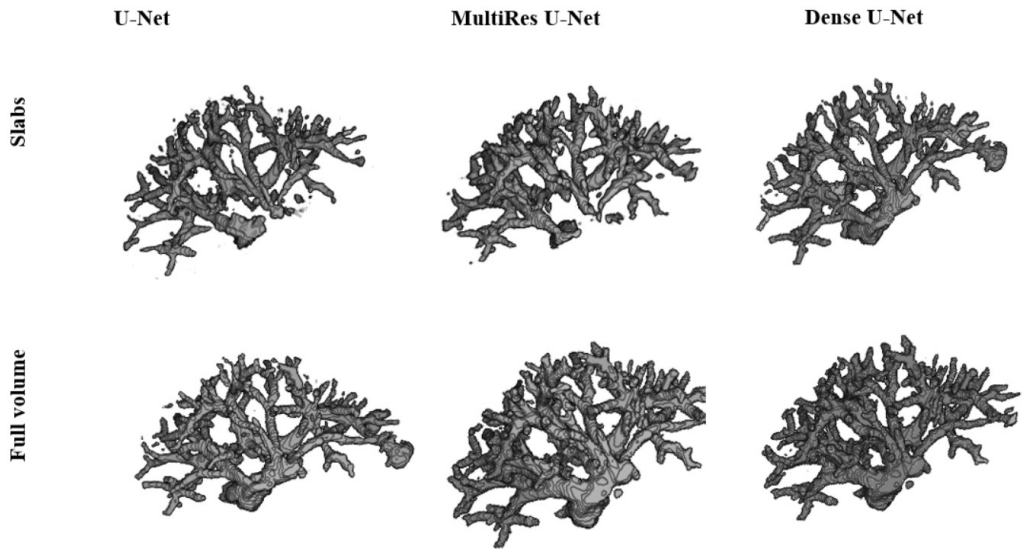

Figure 5.4: Results of 3-D models on full liver volume optimized for the segmentation of liver vessels using the Jerman filter for vascular enhancement

5.4.1 Comparison of our method with state of the art approaches

In this section, we compare the proposed 3 U-Net models with other vessel segmentation models on processed and raw data, the results and Dice are presented in Table 5.5.

Table 5.5: Quantitative results for different models in state-of-the-art on IRCAD public datasets for vessel segmentation.

Method	Datasets	Model	Dice
Kitrungrotsakul *et al.*, [38]	Processed data	DenseNet	**0.903**
Kitrungrotsakul *et al.*, [39]	Processed data	3-D CNN	0.879
Long *et al.*, [55]	Raw data	FCN	0.624
Ronneberger *et al.*, [69]	Raw data	3-D U-Net	0.723
Milletari *et al.*,[58]	Raw data	V-Net	0.689
Zhou *et al.*, [93]	Raw data	U-Net++	0.817
Yan *et al.*, [84]	Raw data	LVSNet	**0.904**
Our method	Processed data	Our MultiRes U-Net	**0.913**
Our method	Processed data	Our U-Net	0.727
Our method	Processed data	Our Dense U-Net	**0.942**

For this experiment, we listed most methods, which has previously been tested on

IRCAD public datasets. Our proposed models, 3-D Dense U-Net and 3-D MultiRes U-Net, processed using Jerman filter achieved higher Dice coefficients of 0.942, 0.913 respectively. Though there is no significant difference between our 3-D U-Net results and the model of the article [69], Dice coefficients are 0.727, 0.723 respectively. To conclude our Dense U-Net combined with Jerman filter achieved the best results.

We presented a combination of three Deep learning based segmentation with vesselness filters to extract liver vessel from abdominal CT scans. By introducing a vesselness filters into a 3-D U-Net architectures, the proposed approach shows significant improvement segmentation results with the reputed IRCAD dataset especially using Jerman filter, which indicates that the proposed model can segment more complete vascular trees. The Figure 5.6 shows a comparison between the results of 3-D U-Net obtained using Jerman filter, and we can see that the best combination was Jerman with 3-D Dense U-Net which gives a suitable outcomes especially on small regions and bifurcation and principal liver vessel branche. As presented in this study, without prepossessing the model ignored the small regions, while the Sato and Jerman filter is able to reduce the segmentation errors, the RORPO and Zhang gived poor response and this was maybe due to the important noise that these filters add to the original image compared to others.

5.5 Discussion and conclusion

We present in this chapter a joint 3-D U-Net based segmentation and vesselness filter method with an application to extract liver vessel segmentation from hepatic CT scans. By introducing enhancement filters, the proposed models are able to learn and segment vessel better than with raw images. The proposed 3-D Dense U-Net model shows a significant improvement in the false negative measure over the baseline 3-D U-Net. This indicates that the proposed combination can segment more complete liver vessel trees. Further, this is achieved with fewer trainable parameters.

To have an objective validation of the best vesselness filter to be employed in our pipeline, we have selected four filters that enhance contrast of the vessels, originally evaluated with a relevant performance in [45]: Zhang, Sato, Jerman and RORPO filters. Then, we have compared results obtained by three 3-D U-Net models on the full liver CT-scans and on image slabs, with and without the application of these filters as a preprocessing step.

As you can see for all three models, the training loss decreases at each epoch,

and the training accuracy increases at each epoch. but the curves obtained on the slabs are less precise compared to the complete volume (see Figure 5.3).

The prediction accuracy curve during validation seems smoother for using 3-D Dense U-Net on the full volume, we can see a significant improvement over the state of the art models. It should be noted that the loss curve does not show real improvements, what is displayed is an average of the point loss values but what is important for the accuracy of the prediction is the distribution of the loss values and not their average, because the accuracy of the prediction is the result of a binary thresholding of the probability per class predicted by the model, so that this model can continue to improve even if it is not reflected in the average loss. And in our case, we clearly see that our 3-D Dense U-Net model combined with the Jerman enhancement filter, has the best distribution compared to the other models even if the distribution was really not perfect, especially the distribution loss of validation. The segmentation results of (Figure 5.4 and Figure 5.5) and the Dice score of Table 5.5 confirm that our 3-D Dense U-Net is the most accurate. We show that the Dense U-Net with Jerman filter is the most suitable for extracting hepatic vessels on CT-scans. This is a promising result to promote vesselness filtering in DL pipelines for vascular segmentation. Furthermore, based on our results, it is possible to extract different biomarkers and use them for clinical experiments, especially for detecting liver's and hepatic vessels disorders. The proposed architecture can also be applied on other organs or vessels. The results of comparison between the results of 3-D U-Net obtained using jerman filter on full liver volume and the ground truth vessel, showed that the 3-D Dense U-Net segment more accuretly the liver vessel tree and reduce the noise and false negative in segmentation masks (see Figure 5.6).

In the next chapter, we will test our method using topological signature to improve segmentation results. Moreover, we would like to study the combination of DL models with other image features to enhance response in vessel bifurcations and to reduce the false positive and negative detection's.

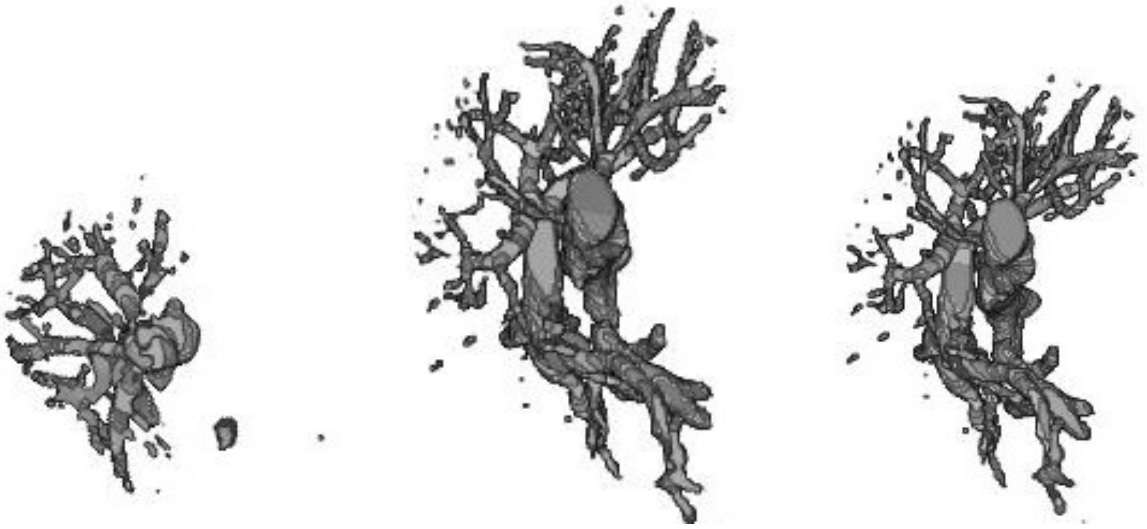

(a) Sato filter

(b) RORPO filter

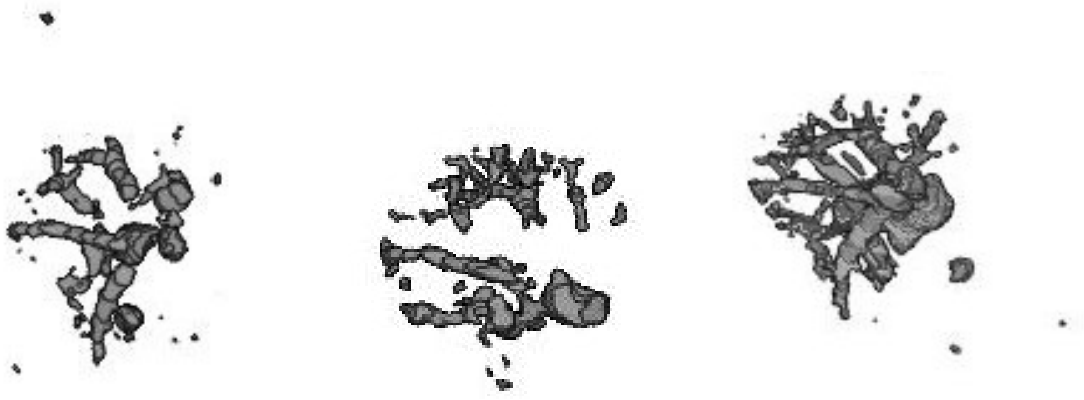

(c) Zhang filter

Figure 5.5: Results of 3-D models on full liver volume optimized for the segmentation of liver vessels using the Sato, Zhang, Roropo filters for vascular enhancement, the first column: using 3-D U-Net, the second column : using 3-D MultiRes U-Net, and the last column: using 3-D Dense U-Net

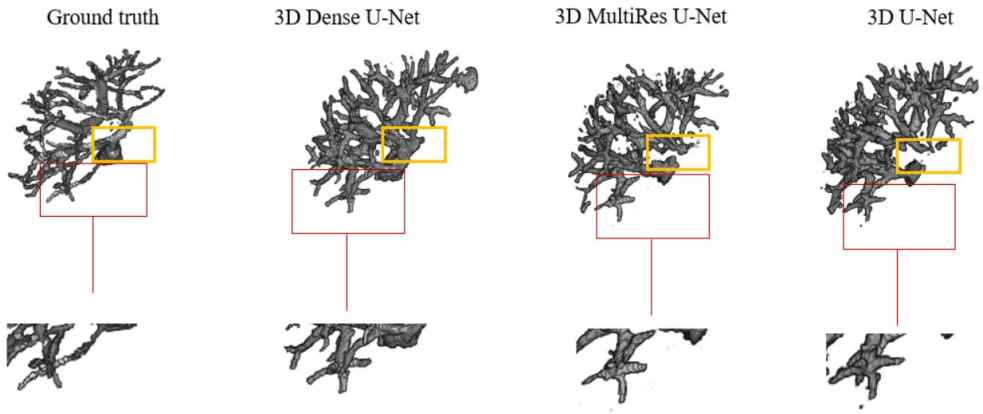

Figure 5.6: Comparison between the results of 3-D U-Net obtained using Jerman filter on full liver volume and the ground truth vessel.

Part III

Hepatic vessel extraction by topological DL approaches

6 Liver vessel extraction in CT scans using 3-D topological DL methods

6.1 Resume

DL for vessel extraction is currently an active research area since segmentation of these structures is becoming more mature, it is time to face the different challenges that will allow us to enhance it and make it more effective. The main purposes of the following chapter is to analyze the existed methods based on vessel topology that can be used for accurate hepatic vessel tree extraction.

In the previous chapters we presented the different methods proposed in the state of the art for segmentation problems, the aim was to realize a study of DL for liver vessel segmentation and to investigate and identify the methods which reconstruct the complex structure accurately. Then we proposed a pipeline that can perform segmentation of liver vessel by combining 3-D U-Net approaches. Results reveal that some of them need to be considered and others need to be improved. These approaches were not sufficient enough to reduce segmentation errors, especially on vessel bifurcations and small vessels.

We deducted that methods based on the shape and topology of complex data must be included to obtain more better segmentation outcomes. In this part, we proposed three topological approaches, the first one consists of combining feature map of a graph convolutional network with the feature map obtained using U-Net architecture. The second approach is a 3-D U-Net-GNN based method, where the convolutional layers at the deepest level of the 3-D Dense U-Net are replaced by a GNN module with a series of graph convolutions. In the third approach we propose to use the W-ClDice loss function with the 3-D Dense U-Net based segmentation method that can improve liver vessel segmentation.

The results obtained showed that the topological information can improve the segmentation of the vessels and reduce the noises and the false positives and the false negatives, a better segmentation of the vessels of the liver is obtained.

6.2 Introduction

The liver has a complex vascular structure, the analysis of the topology of this structure can help radiologist in surgical planning and other clinical practices.

But the study of liver vessel is a challenging task due to the extremely small size of the vessel structure, low SNR, and varying contrast in biomedical image data. Deep learning has shown in recent years an impressive efficiency in solving many problems in medical imaging. Extracting topological information from the data can provide an alternative perspective on segmentation issues of complex structures such as hepatic vessels.

The segmentation of tree structures is an essential problem in many fields, such as clinical and biological domain (segmentation of vascular networks and cells from microscopic images), real-time object detection applications (segmentation of the road network from satellite images). In the domains mentioned above, a topologically precise segmentation is necessary to guarantee obtaining adequate results without error in the small poorly enhanced regions.

In this chapter, we describe three topological approaches, the first one consists of the incorporation of a GCN into a standard U-Net architecture, where the final segmentation is obtained by combining the different types of features [88]. The second approach consist of coupling 3-D U-Net-GNN, where the convolutional layers at the deepest part of the U-Net architecture are changed by a GNN module [33], in the third approach we propose a coupled W-ClDice loss function with the 3-D Dense U-Net based segmentation method to improve hepatic vessel extraction from CT images. A focal weight were integrated into a topological Dice loss function to reduce segmentation errors on small regions.

6.2.1 Topology study

Topological data analysis methods allow us to obtain information, usually in the form of graphical representations of topological features. Furthermore, these topological signatures are very rarely used in most machine learning methods especially for segmentation problems. Graphs are structures used for modeling problems in many fields [76]. Graph analysis has experienced a new boom over the past twenty years, which has produced significant results, both in the analysis of specific cases and in terms of modeling large graphs. However, graphs offer complex discrete structures that classic machine learning data does not have basically. Indeed, if the order of the pixels in an image is fixed and immutable, there is, for example, no natural order to parse the neighbors of a node in a graph. Architectures based on convolution cannot be used directly and must be adapted for segmentation tasks

Recently, Graph Neural Network (GNN) architectures have been developed to accurately analyze complex-structured data such as vessel. Information that graphs contain can be formulated, by conditioning the learning models both on such data and the adjacency matrices of the underlying graphs. For retinal vessel detection,

graph convolution was first proposed by Shin et al [75] by an architecture, where the final segmentation is inferred by combining the different types of features. Their method can be applied to expand any type of CNN-based vessel segmentation method to enhance the performance.

As reviewed in the state of the art chapter, there has been significant recent interest in incorporating high-level shape and topological features within CNN, U-Net training, including the development of specialised segmentation loss functions. A fundamental obstacle is that this loss function must be differentiable with respect to the class probabilities assigned to each pixel, which is challenging when the presence or absence of particular global features is a poor quantity.

The topological study consists of transformation of segmented vascular network to a related graph representing it with different topological and geometrical descriptors. Multiple advantages can then be addressed for employing symbolic representation as a post-processing technique. This chapter gives a better visualization of the structure information, and the information is much more simplified, and exactly what the radiologist requires.

6.2.2 Skeletonization

Skeletonization is a morphological operation which represents an object by its central lines while preserving the initial shape of the object. It provides very important features in medical imaging for the analysis of curvilinear structures.

Thinning is a morphological operation used to eliminate foreground pixels in images, it is used in several fields of application, on the other hand it is useful for the calculation of central line or what is called the skeleton. So it is generally used for edge detection by reducing all lines to the thickness of a single pixel. Thinning must be applied to binary images and also output another binary image [15].

Topological thinning consists of gradually removing the points from the contour of the shape, while preserving its topological characteristics. The skeletal points are added progressively when a corner is formed "the contour curve becomes discontinuous" or when the contour points meet.

Thinning transforms objects in a binary image into a set of center lines, which run along the objects, the midline. The algorithm recursively removes edge points that have more than one neighbor. With this algorithm, thin ends are not removed.

6.2.3 Losses that deal with class imbalance

Class imbalanced is a frequent problem experienced when trying to train segmentation models. This is a common problem encountered in most image segmentation

tasks, where the background class is much larger than the other classes. In this part, we will go through the techniques used to deal with class imbalanced problems and why the W-Cldice loss might be the best option for us.

Dice coefficient

The Dice coefficient, given at Equation 4.1, is well-known for being the go-to evaluation metric for image segmentation, but it can also serve as a loss function. Although not as widely used as other loss functions like binary cross entropy, the Dice coefficient does wonders when it comes to class imbalance. Dice coefficient only considers the segmentation class and not the background class.

The Dice coefficient is a measure of overlap of the predicted mask and the ground truth. Since it does not account for the background class, it cannot dominate over the smaller segmentation class. The Dice coefficient outputs a score in the range [0,1] where 1 is a perfect overlap. However, (1-Dice) can be used as a loss function.

Tversky Index

The Tversky Index is a asymmetric similarity measure that is a generalisation of the Dice coefficient and the Jaccard index [82].

$$TI = \frac{|TP|}{|TP| + |\alpha FN| + |\beta FP|}, \tag{6.1}$$

where TP is the true positive and FN is the false negative and FP is the false positive .

The Tversky index adds two parameters, α and β where α+ β= 1. The case α = β= 0.5 simplifies into the dice coefficient. It simplifies to the Jaccard index if α = β = 1.

Although the Tversky index is only a simple improvement over the Dice coefficient, it can prove useful in edge cases where one need a finer level of control.

The Focal Tversky Loss

The Focal Tversky Loss (FTL) is a generalisation of the Tversky loss. The non-linear nature of the loss gives you control over how the loss behaves at different values of the Tversky index obtained [82].

$$FTL = (1 - TI)^{\gamma} \tag{6.2}$$

γ is a parameter that controls the non-linearity of the loss. The gradient of the loss tends to ∞ as the Tversky Index (TI) tends to 1. As γ tends to 0, the gradient of the loss tends to 0 as TI tends to 1.

Essentially, with a value of $\gamma < 1$, the gradient of the loss is higher for examples where TI > 0.5, forcing the model to focus on such examples. This behaviour can be useful towards the end of training as the model is still incentivised to learn even though TI is nearing convergence. However, at the same time, it will weight easier examples higher during the early stages of training, which can lead to poor learning.

Loss functions play an essential role in determining the model performance. For complex objectives such as segmentation, it is not possible to decide on a universal loss function. The majority of the time, it depends on the datasets properties used for training [82].

6.3 Proposed method

In the previous chapters the 3D Dense U-Net was validated as the best architecture for liver vessel segmentation compared to 3D MultiResU-Net and 3D U-Net; that is why we will use this models for following experimentation.

This section is organised as follows. First, we present our material, and we describe describe three topological methods: 3-D GNN U-Net, 3D U-Net GCN, 3D Dense U-Net with W-ClDice loss function applied for liver vessel segmentation. Then we will realize a comparative analysis of results. Finally, we will discuss results to validate the best approach for liver vessel extraction.

6.3.1 3-D U-Net GCN for liver vessel segmentation

In this section, we present a novel 3D U-Net architecture, which jointly learns the global structure of liver vessel shape together with local appearances. This novel architecture comprises three components, 1) a U-Net module for generating pixelwise features map and vessel probabilities, 2) a Graph Convolutional Network (GCN) that generates a topological features map learnt on graphs of liver vessel constructed using Skel2Graph (a Matlab framework), which constructs graph from skeletons constructed on liver vessel ground truth using standard parallel thinning algorithm, and 3) an inference module to produce the final segmentation.

This approach incorporates a GCN into a unified 3-D Dense U-Net architecture, where the final segmentation is inferred by combining the different types of features (see Figure 6.1).

6.3.2 Our contributions

Our work is based on the article of Shin et al [75] who proposed 2-D CNN GCN combination for retinal vessel segmentation on 2-D images, in our case we replaced the 2-D CNN by a 3-D Dense U-Net to deal with binary segmentation problems, and not for classification. We also modified the loss function of their method using a weighted Dice instead of Cross-Entropy, which can improve segmentation results, but this implementation did not work yet due to feature maps generated which can not be combined.

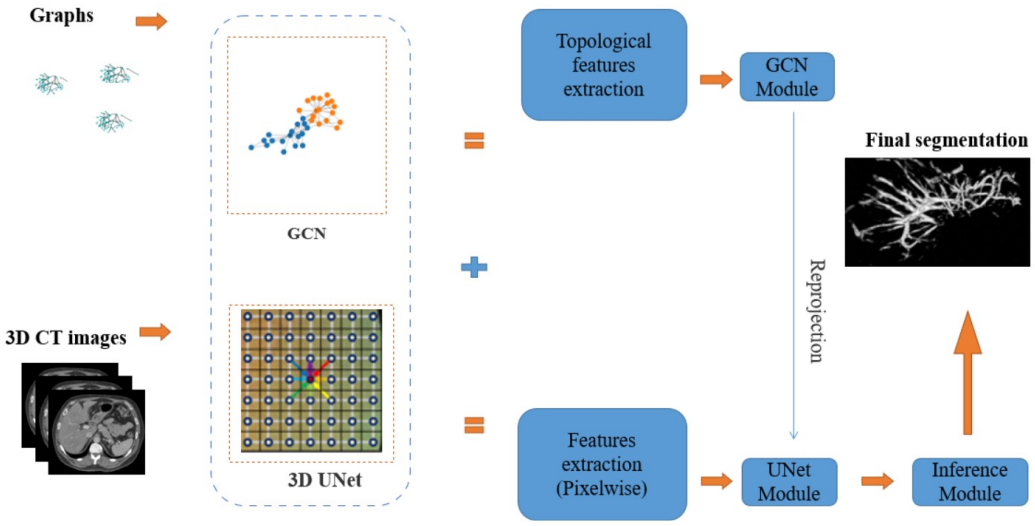

Figure 6.1: Schematic of the combined U-Net-GCN network

6.3.3 GNN-U-Net for vessel extraction

We also propose an extension of the article of [33]. They propose a joint 3D U-Net-Graph Neural Network-based method for airway segmentation from chest CTs, the deepest convolutionnal layer are replaced using two GNN layers.

The proposed 3-D U-Net-GNN architecture is described as follows: This approach puts a GNN module instead of the deepest layers of our 3-D U-Net (see Figure 6.2). The GNN module uses a graph structure obtained from the dense feature maps resulting from the contraction path of our U-Net. Each node of this graph will be considered as a supervoxel from the undersampled regions with the corresponding feature vector. The connectivity of nodes in the graph is described by the adjacency matrix and determines the neighborhood of each node when performing graph

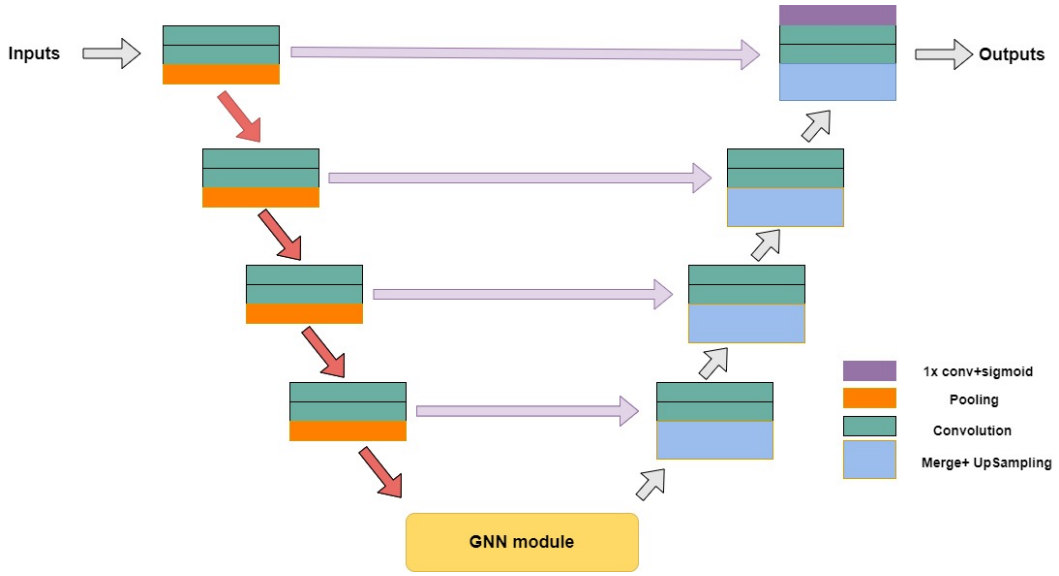

Figure 6.2: Schematic of the U-Net-GNN network

convolutions. The GNN module learns combinations of the input feature maps depending on the graph topology and results the same graph with the corresponding vector of learned features for each node. This output consists of feature maps that are fused to the oversampling path of our U-Net.

Graph Neural Network GNN

GNN module is composed of a series of graph convolutional layers, this operation can be seen as a generalisation of the Cartesian convolution to a graph setting [33].

A graph has been constructed and given as input for the GCN module. We assume a U-Net has been pretrained to generate the probability feature map , on which the following operations are performed:

1) Post-processing (thresholding).

2) Centerline extraction using standard parallel thinning algorithm [49].

3) Vertex generation by equidistant sampling, on the skeleton together with skeletal junctions and endpoints.

4) Edge generation between generated vertices based on geodesic distances on the vessel probability map.

The GNN uses these graph structures obtained from the dense feature maps resulting from the U-Net contraction path as previously described. The connectivity of nodes in the graph is described by the adjacency matrix. The GNN trains on

these input feature maps based on the graph topology and generates a learned feature vector for each node that will be merged to the U-Net up-sampling path. Each node in the output graph updates its features with information from higher order neighbourhood, which can improve the segmentation decisions (see Figure 6.3), The module will be integrated into the segmentation network (Decoder) as a multi-task branch, which we called the Embedding mode as presented in [67] and [71].

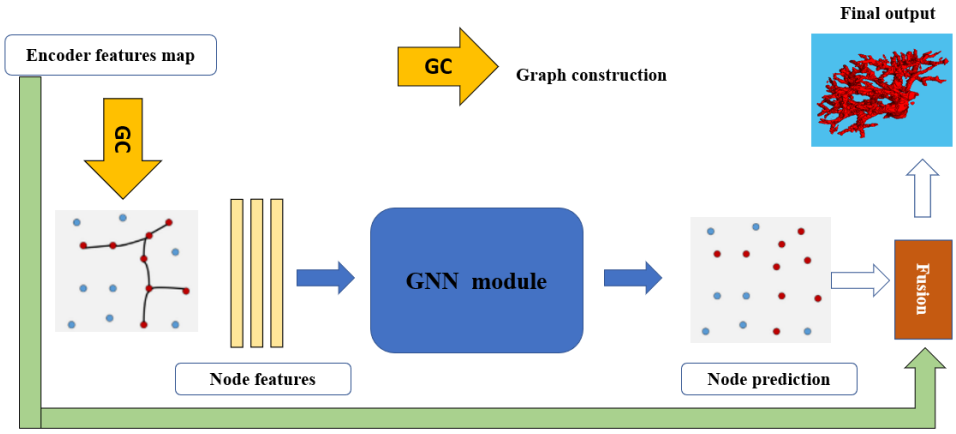

Figure 6.3: Combinaison of GNN and U-Net networks

Node connectivity was calculated during training based on nearest neighbors in node feature space. Aggregating multiple GNN layers allows nodes to access information beyond the initial neighborhood, which can improve segmentation results because features that include relevant information from distant nodes in the volume can be used.

Contributions

In our case we used our proposed 3-D Dense U-Net presented above, and we replaced the deepest layer using four GNN layers as presented in the Figure 6.2, and we used 3-D images instead of 2-D. We also modified the loss function by using Focal Tversky Loss and the way to calculate the skeletons and graphs compared to the method of the article [33].

6.3.4 Topological loss functions to improve liver vessel segmentation

In this section, we present a novel 3-D deep learning method based on topological information for liver vessel segmentation from CT scans. To do so, we employed a continuous-valued loss function, which can help in improving segmentation decisions from vascular patterns. It integrates both pixel wise intensity and topological structure of vessel shapes by training a 3-D U-Net with this specific topological loss function, by calculating the similarity between the likelihood map predicted by the 3-D U-Net and the ground-truth vessels. This approach was tested to the task of segmenting the hepatic vessel tree from CT scans provided by the IRCAD dataset. Our 3-D topological deep learning model inducing better segmentation in terms of bifurcations and topology. We show its accuracy by comparing with a baseline 3-D U-Net and 3-D U-Net-GNN models.

The objective of this part is to identify an efficient and intuitive loss function that allows the preservation of shape and topology after the segmentation step of vascular structures. We modify a connectivity-sensitive similarity measure named clDice [76] for the analysis of vascular structure segmentation algorithms by adding a focal weight. Importantly, we provide theoretical guarantees for the topological correctness of clDice for 3D binary segmentation. Due to its formulation based on morphological skeletons, our measure pronounces the topology of the network and allows to equally weight each voxel.

Proposed pipeline

Most loss functions proposed in literature are for binary classification (foreground / background) using CNN and FCN, they allow the quantification of class imbalance. Here, in our study, we introduce a weighted loss function for binary segmentation problems. To deal with this issue, a weighting strategy of Dice loss function has been proposed. We investigate the behavior of this loss functions in the presence of different rates of label imbalanced 3-D segmentation tasks. The proposed approach is based on 3-D Dense U-Net coupled with novel weighted Dice loss functions called W-ClDice for liver vessel segmentation on CT images (See Figure. 6.4). The loss function is designed for topological structure segmentation and to deal with common issue of connectivity within branches, and poor segmentation outcomes in bifurcations.

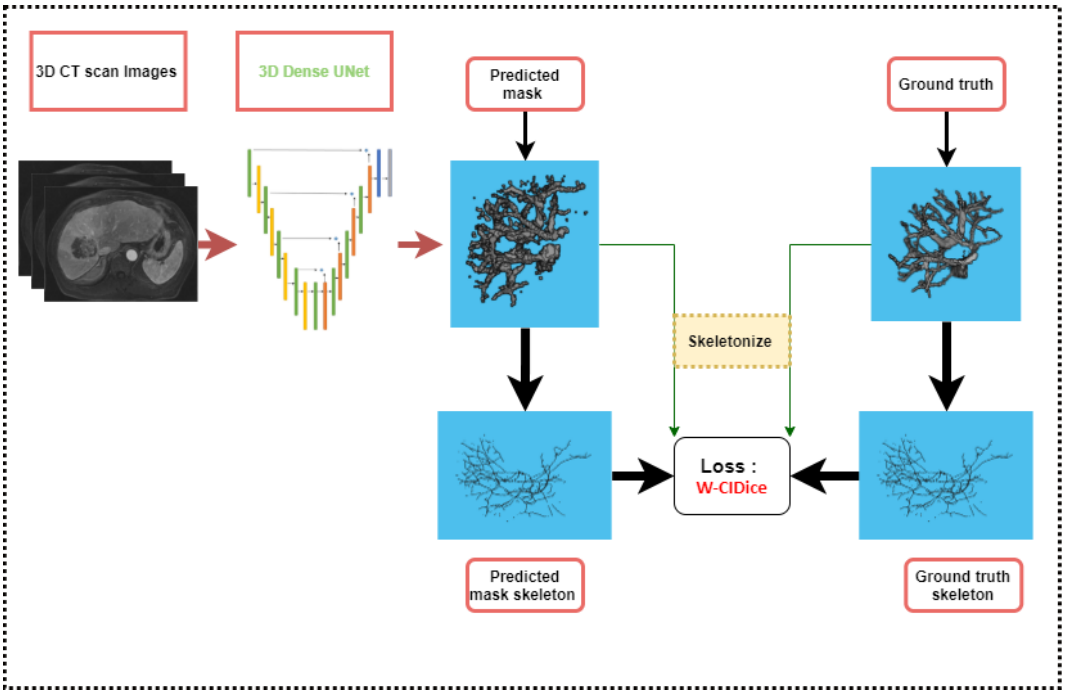

Figure 6.4: The pipeline proposed to carry out the proposed study, soft-skeletonization [76] was used to generate skeletons.

Loss weighting strategy

In highly imbalanced segmentation tasks a severe class imbalance is likely to occur between candidate labels, thus resulting in poor performance, U-Net can ignore small size vessel voxels in the training process, which results poor segmentation accuracy on small regions and bifurcations. This problem can be solved by weighting the loss of small size foreground voxels. In this study, we used a loss weighting strategy based on focal weighting coupled with a 3-D Dense U-Net.

Focal weighting

Focal weighting [79] is a method for increasing more focus on hard-to-classify class voxels based on predictive probability. The focal weighting is defined by :

$$\mathbf{W}_p^{\text{Focal}} = (1 - \mathbf{V}_p)^{\gamma} \tag{6.3}$$

where $\mathbf{V}_p$ is a predicted segmentation probability, and γ is called a focusing parameter. In this study, we used $\gamma = 1$ for Dice loss function as in the article [51].

Weighted ClDice loss function (W-ClDice)

In this part we have modified the ClDice proposed by [76] using the focal weighting presented in [79]. The ClDice measures the similarity termed centerlineDice (clDice), which is calculated on the intersection of the segmentation masks and their skeleton. We add the focal weight, which gives higher weight to class voxels with lower prediction confidence and reduces the loss assigned to well classified voxels during the training process.

We consider two binary masks: the ground truth mask $\mathbf{V}_l$ and the predicted segmentation masks $\mathbf{V}_p$. First, the skeletons $\mathbf{S}_p$ and $\mathbf{S}_l$ are extracted from $\mathbf{V}_p$ and $\mathbf{V}_l$ respectively. We calculate the fraction of $\mathbf{S}_p$ that lies within $\mathbf{V}_l$, which called Topology Precision or $\mathbf{T}_{prec}$ ($\mathbf{S}_p$, $\mathbf{V}_l$), and Conversely we obtain Topology Sensitivity or $\mathbf{T}_{sens}$($\mathbf{S}_l$, $\mathbf{V}_p$) as presented bellow:

$$\mathbf{T}_{prec}(\mathbf{S}_p, \mathbf{V}_l) = \frac{|\mathbf{S}_p \bigcap \mathbf{V}_l|}{|S_p|} \quad ; \quad \mathbf{T}_{sens}(\mathbf{S}_l, \mathbf{V}_p) = \frac{|\mathbf{S}_l \bigcap \mathbf{V}_p|}{|S_l|} \tag{6.4}$$

Where $\mathbf{V}_p$ and $\mathbf{V}_l$ are predicted segmentation mask, and ground truth mask respectively. $\mathbf{S}_p$ and $\mathbf{S}_l$ are predicted mask skeleton, and ground truth skeleton. The weighted Dice loss function W-ClDice where we added a focal weight to the

standard ClDice is defined as :

$$\textbf{W-ClDice} = 1 - \frac{2 \times \sum_{c=1}^{C} \sum_{i=1}^{N} \mathbf{W}_{i,c}^{\text{Focal}} \times (\mathbf{T}_{prec_{(i,c)}} \times \mathbf{T}_{sens_{(i,c)}})}{\sum_{c=1}^{C} \sum_{i=1}^{N} \mathbf{W}_{i,c}^{\text{Focal}} (\mathbf{T}_{prec_{(i,c)}} + \mathbf{T}_{sens_{(i,c)}})} \tag{6.5}$$

Where N and C are the numbers of pixels and classes in images for a training dataset, respectively. Note that W-ClDice formulation is not defined for $\mathbf{T}_{prec} = 0$ and $\mathbf{T}_{sens} = 0$, but can easily be extended continuously with the value 0.

6.4 Train and validate the model

In the binary segmentation tasks, we trained the 3-D Dense U-Net presented previously on each training dataset using Dice loss functions with the loss weightings. Our model was trained with 20 epochs and the Adam optimization algorithm $\alpha = 1e-5$ (learning rate), and a batch size of 1 in each training process the images size were (256x256x100). We used Keras with Tensorflow librairies designed for largest possible input images that can fit the GPU memory. The training and prediction were performed on a local server by a GPU NVIDIA GeForce GTX 1650 (12Gb) with 256 Gb of RAM, available for deep learning experiments.

We evaluated our models by randomly selecting the data distributed from IRCAD database [30] into the training, validation and testing sets in the ratio of 70%-20%-10% respectively in a cross-validation manner. For each method, all data are performed to collect experimental results with a different training set. The performance of each model was evaluated using the test set (one CT-scan following our distribution).

The result of our proposed W-ClDice for the 3-D Dense U-Net is compared to the segmentation of a baseline 3-D U-Net [69] and the 3-D Dense U-Net, and 3-D U-Net GNN [33], and CIDice [76] approaches in order to validate the best method.

6.4.1 Contributions

In this section we have presented a pipeline with the aim of developing a methodology for detecting the hepatic vascular network from abdominal CT in a images, in a 3-D approach, using topological deep learning techniques based on *a priori* knowledge of shape. Our main objective was to find a new deep learning approach based on vessel topology to obtain an accurate segmentation of the liver vascular network. To deal with this, we proposed a novel approach which coupled a 3-D Dense U-Net with accurate weighted Dice loss function (focal weigthing), and then we compared the results with ClDice [76]. This loss function is used and tested

for segmentation tasks on 2-D images, here we have created a loss function for 3-D images for binary segmentation instead of multi class segmentation. In the literature most methods used baseline U-Net, FCN or standard CNN for segmentation of curvilinear structures, in our study we used 3-D Dense U-Net for more accuracy and we couple this architecture with a new weighted Dice loss function. This method is applied on CT scan images for liver vessel segmentation.

6.5 Results

6.5.1 Results of the GNN-UNet approach

The 3-D U-Net-GNN give poor segmentation compared to standard 3D U-Net, with the lowest Dice score of 0.471. Moreover, its validation loss is the worst, without any improvement and there were no significant decrease during the optimization. The standard U-Net architectures lead to similar outcomes, with a better performance (see Figure 6.5). Our proposed 3-D U-Net reaches a Dice accuracy of 0.727. The prediction accuracy curve during validation looks much smoother (see Figure 6.5), we can see an improvement over the U-Net GNN model. Note that the loss curve does not show real improvements but still better than our proposed approach 3-D U-Net GNN.

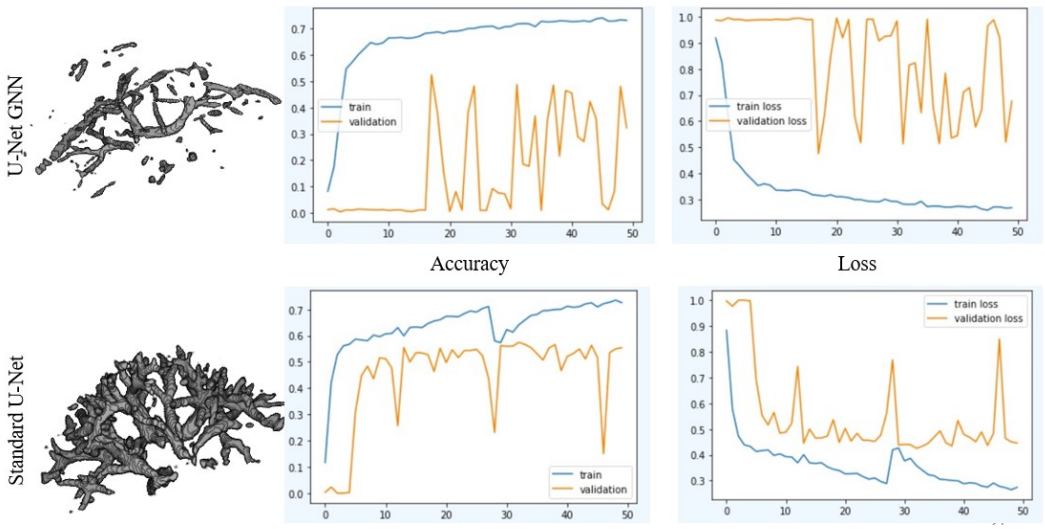

Figure 6.5: Results obtained using standard U-Net and U-Net GNN model

6.5.2 Results of the Loss function based segmentation method

Our method significantly outperforms existing methods in topological accuracy compared to the three topological models of the state of the art. Figure 6.6 shows qualitative results. Our approach demonstrates more consistency in terms of shape and topology of liver vessels. It correctly segments hepatic vascular tree, while other methods segments liver vessels but with more false positives and negatives, especially the 3-D U-Net GNN model.

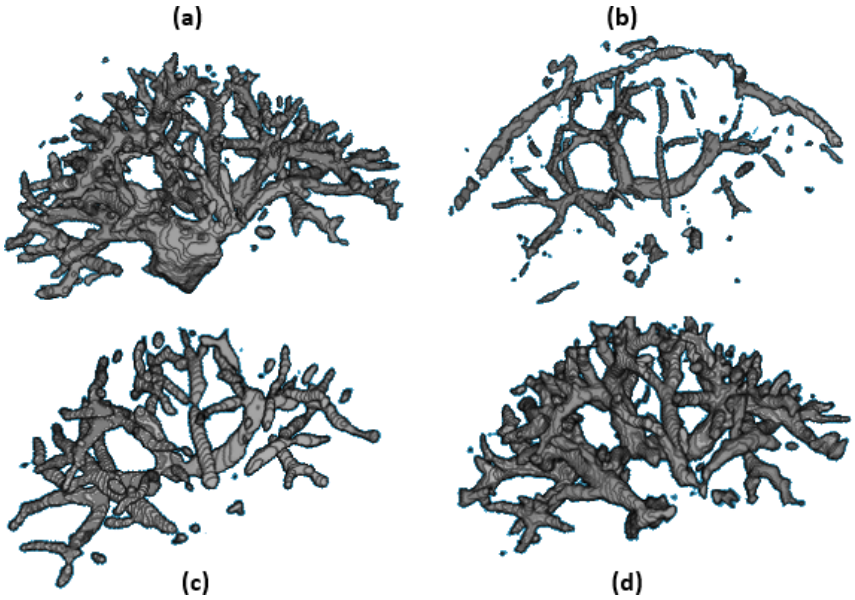

Figure 6.6: Results of 3-D topological models designed for the segmentation of liver vessels. (a) using standard 3-D U-Net, (b) U-Net-GNN, (c) ClDice loss function, (d) our proposed W-Cldice function with Dense U-Net.

The 3-D U-Net used ClDice of [76] gives good results also, but the use of focal weight to strengthen our model increases segmentation accuracy especially on small regions. Also the use of 3-D Dense U-Net instead of baseline 3-D U-Net helped us to have the most accurate results compared to the state of the art.

To explain more the rationale of W-ClDice, we first present the segmentation results and the loss function curves in Figure 6.7. Within a short period, the likelihood map and the segmentation are stabilized globally, mostly thanks to the focal weighting process. After epoch 20, topological errors are fixed by our proposed topological loss. For most vessels voxels, the network learns to make

correct prediction. However, for a small amount of data, it is much harder to learn and predict correctly, even with more annotated training images. Topological loss essentially identifies these vessel voxels during training at the expense of overfitting and consequently slightly compromised per-voxel accuracy. On the other hand, we notice that topological loss cannot succeed alone without focal weight. Focal weighting finds a correct likelihood map so that the topological loss can improve segmentation results.

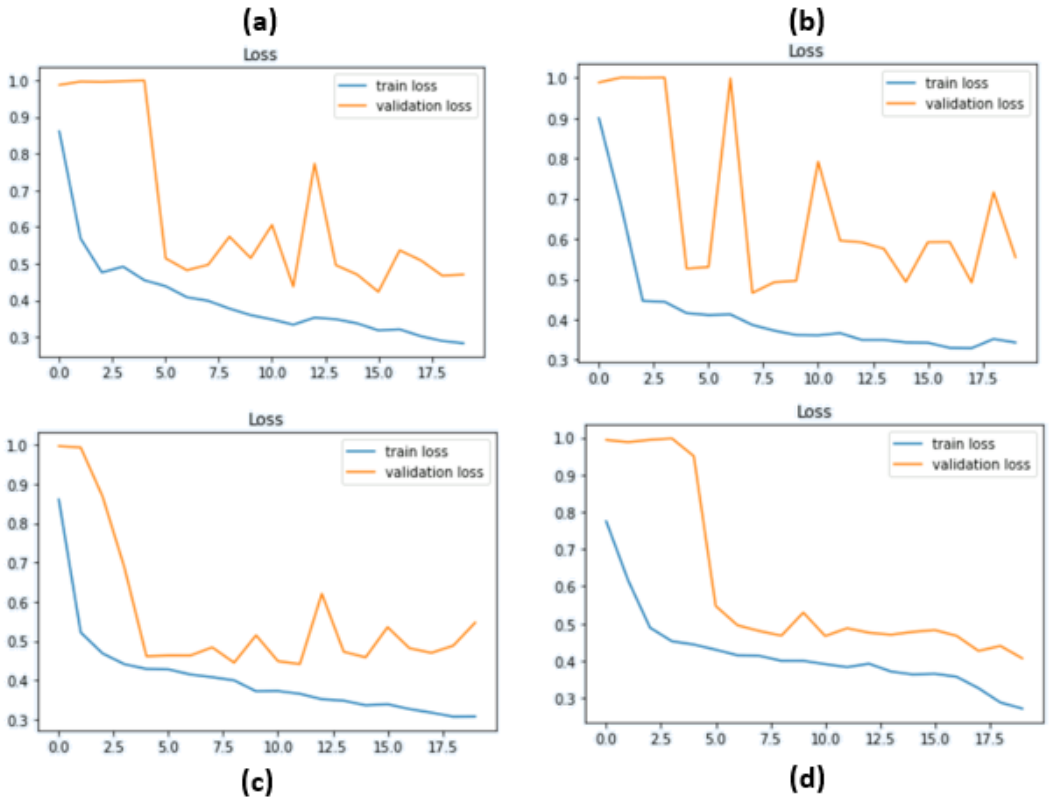

Figure 6.7: Training and validation loss optimization for the models presented in Table 6.1. (a) results obtained using standard 3-D U-Net, (b) U-Net-GNN, (c) with the ClDice loss function, (d) with our proposed W-Cldice with Dense U-Net.

6.5.3 Qualitative and quantitative comparison of results

The 3-D U-Net-GNN stands as the less efficient architecture of our study, with the lowest Dice score during training. Moreover, its validation loss is the worst, without any significant decrease during the optimization. The two other architectures lead

Table 6.1: Quantitative results for different models in state-of-the-art we have test on IRCAD public datasets for liver vessel segmentation with diffrent loss functions presented above.

Method	Weight	Loss function	Dice
3-D U-Net	No	Dice loss	0.727
3-D U-Net GNN [33]	No	Dice loss	0.527
3-D Dense U-Net	No	Dice loss	0.727
3-D Dense U-Net	No	BCE	0.702
3-D Dense U-Net	No	TI	0.676
3-D Dense U-Net	No	TFL	0.794
3-D Dense U-Net	No	ClDice	**0.813**
3-D Dense U-Net	Focal Weight	W-ClDice	**0.892**

to similar outcomes, with a better performance for our proposed 3-D Dense U-Net with W-ClDice loss, which reaches a Dice accuracy of 0.892.

The prediction accuracy curve during validation looks much smoother for our approach (d) in Figure 6.7, we can see a significant improvement over the state-of-the-art models. Note that the loss curve does not show real improvements, what is displayed is an average of the point loss values, but what is important for the accuracy of the prediction is the distribution of the loss values not their average, because the prediction accuracy is the result of a binary thresholding of the probability per class predicted by the model, so this model can continue to improve even if this is not reflected in the average loss. And in our case, we can clearly see that our method (d) has the best distribution compared to the other approaches (a, b, c) in Figure 6.7 especially for validation loss. And the segmentation results of Figure. 6.7 and Dice score in Table 6.1 confirm that our approach is the most accurate.

We compared our proposed pipeline to most methods , which has been tested on IRCAD public datasets. Our coupled 3-D Dense U-Net W-ClDice achieved higher Dice score of 0.892, compared to U-Net++ [93], V-Net [58], 3-D CNN [39] , and FCN [55] models, their Dice score was respectively 0.817, 0.689, 0.879, 0.624.

The proposed W-ClDice loss function were also compared with different loss functions proposed in litterature and presented above, results of 3-D Dense U-Net model designed for the segmentation of liver vessels using different loss functions presented in Figure 6.9, quantitative results are also presented in Table 6.1. The proposed W-ClDice achieved also better results compared to the standard ClDice of [76] (see Figure 6.8).

To evaluate the impact of focal weighting strategy we have multiplied all the loss functions presented above by the focal weight and we compared the results

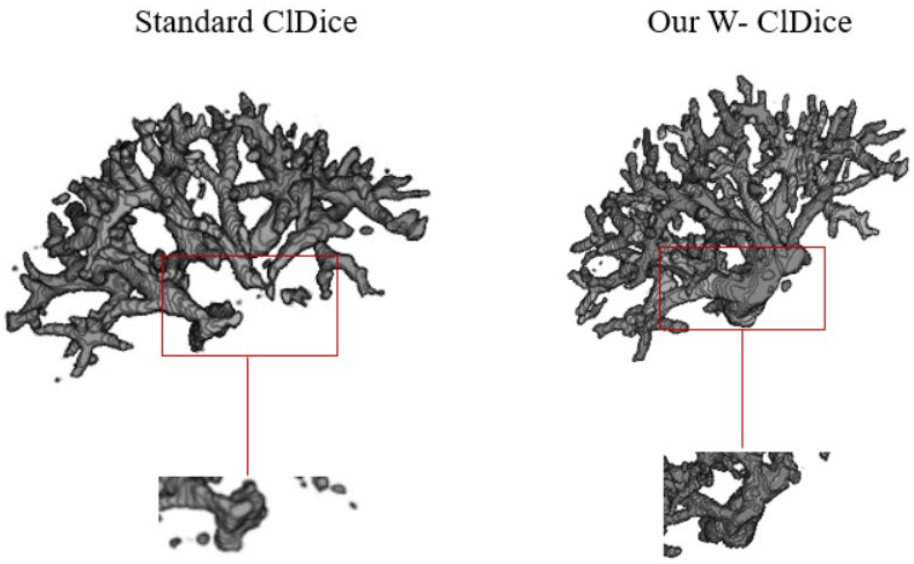

Figure 6.8: Results of 3-D topological models designed for the segmentation of liver vessels. (a) using standard ClDice loss function, (b) our proposed W-Cldice function with Dense U-Net.

before and after (see Figure 6.10). The results claim that the focal weight improved segmentation in most cases compared to the results presented in the Figure 6.9, but our W-ClDice and since it is based on the topology of the hepatic vessels. We can see that it give always the best outcomes in term of reduction of false positives and which gives the best segmentation especially on bifurcations (see Figure 6.10) .

6.6 Discussion and conclusion

We presented a joint W-ClDice with the 3-D Dense U-Net based segmentation method with an application to extract liver vessels from abdominal CT scans. By introducing a focal weight into a Dice loss function, the proposed method is able to learn and combine information from a larger region of the image. Our proposed approach shows significant improvement segmentation results with the IRCAD data set, which indicates that the proposed model can segment more complete vascular trees. Further our method was tested on few quantity of data, the performance can be more better on large amounts of data. As presented in this chapter, the

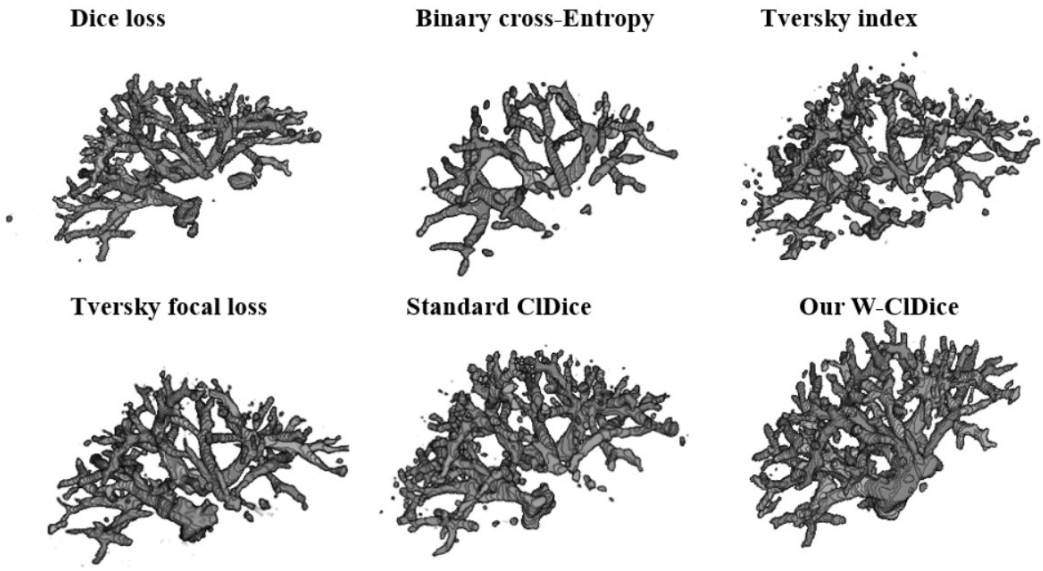

Figure 6.9: Results of 3-D Dense U-Net model designed for the segmentation of liver vessels using different loss functions on the first patient of the IRCAD dataset.

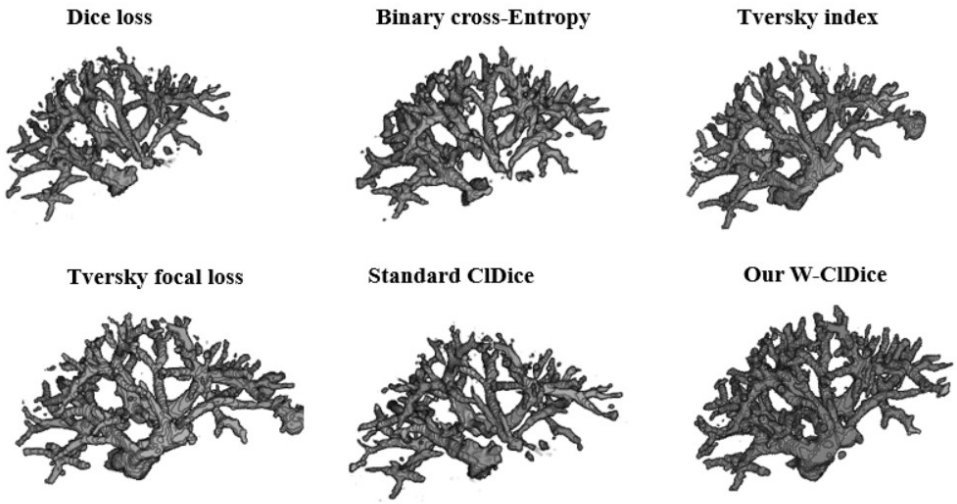

Figure 6.10: Results of 3-D Dense U-Net model designed for the segmentation of liver vessels using different weighted loss functions on the first patient of the IRCAD dataset.

standard loss function Dice ignores the small regions and loses a large amount of information. Consequently, the CT scan image has the characteristics of fewer and

smaller vessels regions. Our improved loss function can make the model focus on the vessel bifurcations and overcome the problem of the unbalanced distribution of the positive and negative samples in a single sample of the CT scan images. Our proposed loss function considerably improves the accuracy of the liver vessel segmentation compared to the state of the art approaches.

For the 3-D U-Net GNN which introduces a GNN module with graph convolutions at the deepest level of the U-Net, where the proposed method is able to learn and combine information from a larger region of the image. This model showed poor segmentation and significant appearance of false negative compared to the baseline U-Net. Several problems that can limit the performance of the 3-D U-Net-GNN model, such as 1) the GNN module was placed only at the deepest level of the U-Net, while the image underwent four downsampling operations. A more capable U-Net GNN model can be robust if it replaces all skip connections in 3-D U-Net with GCN. However, this model was not tested due to the large memory required for this task, which exceeded the GPU resources available on our local server, 2) we used a standard methods to build skeletons and this may reduce the performance of this model, 3) the calculated feature map on graph node based on neighborhood must also limit the performance especially when the GNN module try to select the exact number of significant neighbor's for each node.

For the 3-D U-Net GCN constructed of three modules, there were problems when we tried to build the inference module, more precisely when combining the feature maps obtained from the two architectures (U-Net, GCN) which are two different vectors where we could not resize or normalize them. This method could be improved in future works.

Our work focused on the design of a robust method to exploit shape information and integrate it during the segmentation process. This approach makes it possible to bring its specificity to correct segmentation errors. Classically in the literature, improving the robustness of segmentation algorithms requires defining methods designed specifically for a modality and/or using priors from databases carried out on a set of patients. Except that due to the great variability of the acquisition parameters, it is really difficult to define quantitative parameters because the acquisition is not reproducible for each patient. We seek to use topological signatures to develop which will be robust and work on CT scan images but also on liver MRI images (in our future works).

Finally, the classic approaches in the literature may solve this problem by vascular enhancement methods. Then come up against problems of disconnection in the small regions and especially the problem of noise which occurs by using these filters and since the dynamics describing the elements of anatomy are different. Our

approach, on the contrary, uses the shape of the vessels as a means of correction and is therefore immune to this type of problem.

7 Conclusions & Outlook

7.1 Contributions

During these three years of thesis, we worked on the problem of segmentation of the vascular network of the liver applied to CT scans. This work was part of the R-Vessel-X project funded by ANR which aimed to work on robust extraction of hepatic vessels. To do so during this manuscript, we have drawn up a state of the art of the methods of segmentation of complex structures as well as applied pre-processing techniques to enhance vessel contrast in raw images.

As part of this work and unlike common state-of-the-art models, we have chosen to use topological information which can improve the performance of the model and the segmentation decisions. To achieve this task we started by proposing a comparative study between three DL models for segmentation on three types of inputs (3-D full volume, 3-D slabs, 3-D patches), these models succeeded in segmenting the vascular network of the liver but the results obtained on the complete volume of the liver were better compared to slabs and boxes. And the improved versions of standard 3-D U-Net (3-D Dense U-Net and MultiRes U-Net) gave the best segmentation compared to the basic model, except that we got some disconnections in small regions and in bifurcations that need to be corrected.

For this, we have proposed a second comparative analysis based on a preprocessing step (vascular enhancement), in order to be able to distinguish the vessels from the liver, this step will improve the vascular structures before their segmentation and their visualization, and to remove the structures not vascular and image noise. We propose to test three 3-D U-Net architectures for hepatic vessel segmentation using different vessel enhancement filters as a preprocessing step. We choose four filters that improve the vascular contrasts, namely the Zhang, Sato, Jerman and RORPO filters. Then, we compared the results obtained for three 3-D U-Net models on the CT scan images hepatic whole volume and on image slabs which gave the best segmentation in the first part, the models in this stage were more efficient given the modification of their architectures compared to the first part taking into account the memory capacity which was higher. We have shown that the 3-D Dense U-Net with Jerman filter is the most suitable for the extraction of hepatic vessels on CT images. This is a promising result to promote vessel enhancement in DL pipelines for hepatic vasculature segmentation. Moreover, based

on our results, it is possible to extract different biomarkers and use them for clinical experiments, especially to detect disorders of the liver and hepatic vessels and even for the division of the liver into eight Couinaud regions previously presented, which will allow radiologists to locate HCC-like tumors within the segments.

The results obtained highlighted limitations that led us to the major contribution of this manuscript. We have proposed an approach where we have introduced several improvements to the proposed models, the first approach which is based on a combination of characteristics from two different models 3-D U-Net and GCN. This model was not functional, because the GCN can be combined with a CNN but not with a U-Net architecture because of their output vectors that are not the same so no solution has been found to solve this kind of problem. But a similar solution were proposed which is based on GNN module, where the convolutional layers at the deepest level of the U-Net are replaced by a GNN-based module, the dense feature maps was transformed into a graph input to the GNN module to improve segmentation of liver vessels. Here we noticed that the outcomes were not good and this may be due to the GNN module who operating only on the deepest level of the U-Net, where the image have undergone four downsampling operations. Outcomes of this architecture were poor compared to the baseline 3-D U-Net and this confirm that all skip connections must be replaced using GNN modules. What prevented us from carrying out this step is that it requires a very high RAM memory and is costly in terms of calculation time.

To remain within the same concept, and take advantage of the topological information of the hepatic vessels, we have proposed a joint W-ClDice with the 3-D Dense U-Net based segmentation method. By introducing a focal weight into a Dice loss function, this loss function measured the similarity which is calculated on the intersection of the segmentation masks and their skeleton. We add the focal weight, which gives higher weight to class voxels with lower prediction confidence.

This proposed approach was able to learn and combine information from a larger region of the image. Our proposed approach gave very good results on IRCAD data set, which indicates that the proposed model can segment more complete hepatic vascular trees. Our improved loss function made the model focus on the vessel bifurcations and overcome the problem of the unbalanced distribution of the positive and negative samples and considerably improved the accuracy of the liver vessel segmentation compared to the state of the art approaches.

Our proposed framework shows that the results are promising for clinical applications such as the automatic diagnosis of liver tumors based on imaging data, (see Figures 8.1, 8.3, and Figures 8.4, 8.5).

The liver vessel can be used to divide the liver into Couinaud regions, the aim is to localize the tumors on segments and to reduce the need for taking liver biopsies

to diagnose the fibrosis stage of liver. This method allows the localization of the tumors which facilitate the precocious treatment of liver cancer HCC.

7.2 Perspectives

In perspective, several solution for liver vessel reconstruction can be identified. Firstly the extension of our method to work on more CT scan images but also on MRI images where the detection of hepatic vascular tree is more difficult. We will try to adapt our models to deal with MRI data acquired thanks to the R-Vessel-X project.

Another solution is to try to replace not only the deepest part of 3-D U-Net GNN by a GNN module, but all the skip connections of 3-D U-Net using a GNN. This step requires a large RAM memory which were not available for our case, we can then couple this architecture with W-ClDice which can improve the extraction of the hepatic vascular network in MRI and CT scan images and then use them for several clinical applications.

We desire to make it possible to employ the direction of liver vessel for the reconstructions of Couinaud segments to develop a method for automatic tumor detection as radiologists do with visually. Couinaud representation serves as the validation step and will help us to realize the clinical objective presented above.

We also would like to make all the codes developed in this thesis open source, and we will try to integrate them into medical image processing software such as 3-D Slicer (as a plug-in) for example.

We desire also to combine all the developed approaches presented above together using the W-ClDice with enhanced images using vesselness filters (mostly Jerman because it is the most robust according to our results on IRCAD data set).

8 Appendix

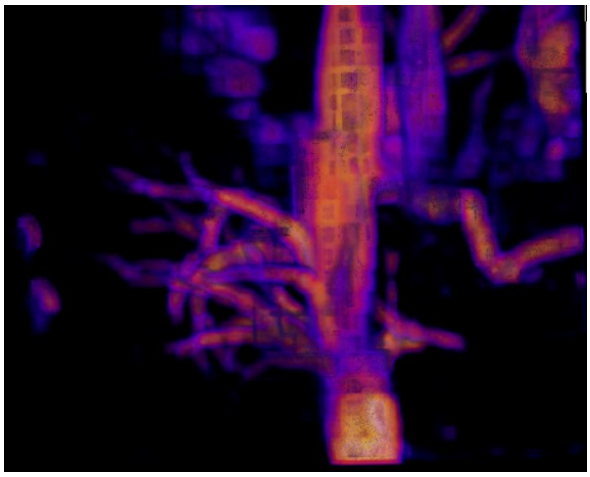

(a) U-Net

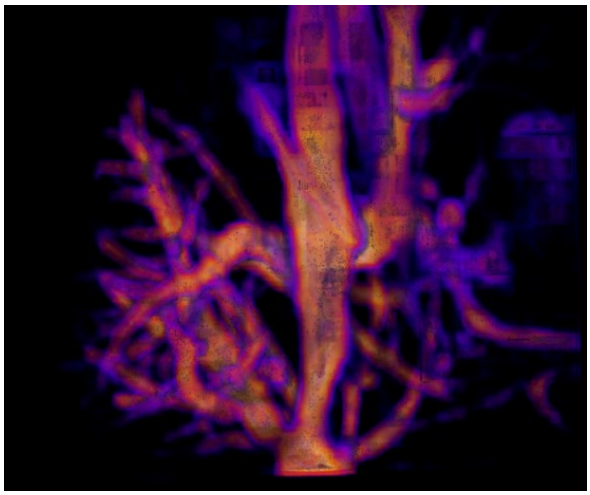

(b) MultiRes U-Net

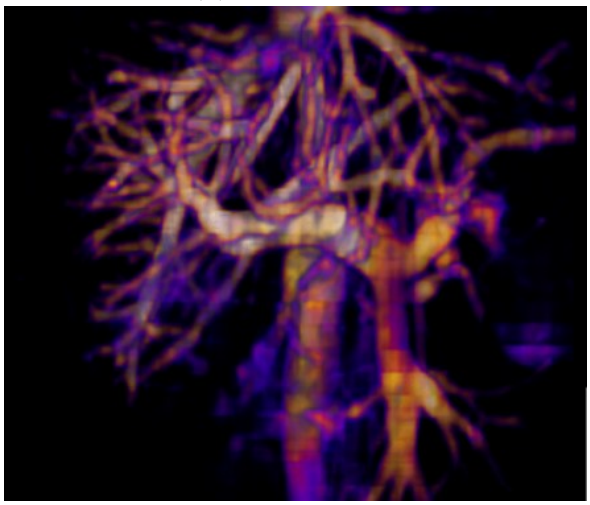

(c) Dense U-Net

Figure 8.1: 3-D ImageJ views of segmentations obtained from a patient of IRCAD dataset, with the full 3-D volume approach on abdominal CT scan before liver vessel cropping, the results are obtained using Jerman filter and W-ClDice loss function.

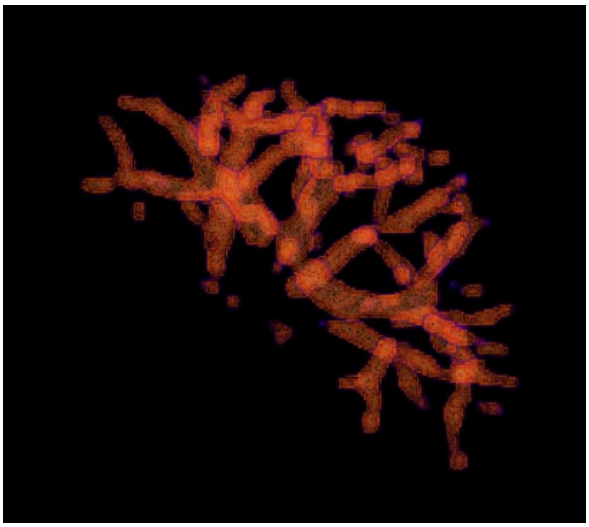

(a) U-Net

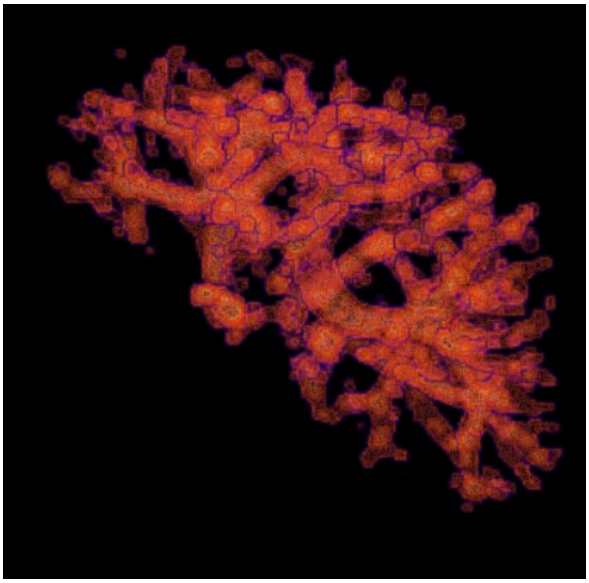

(b) MultiRes U-Net

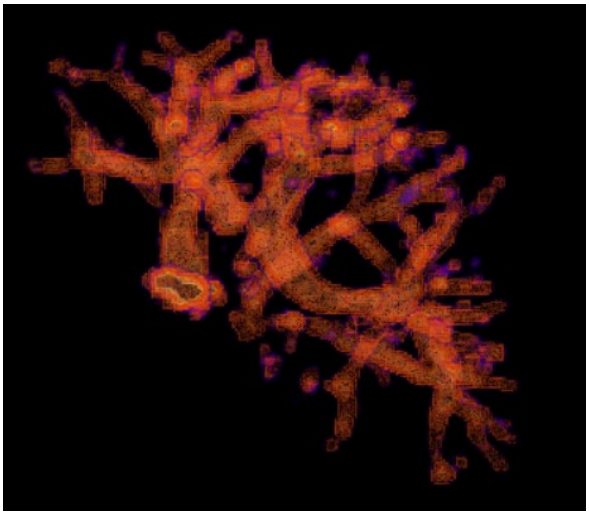

(c) Dense U-Net

Figure 8.2: 3-D ImageJ views of segmentations obtained from an other patient of IRCAD dataset, with the full 3-D volume approach, the results are obtained before preprocessing step .

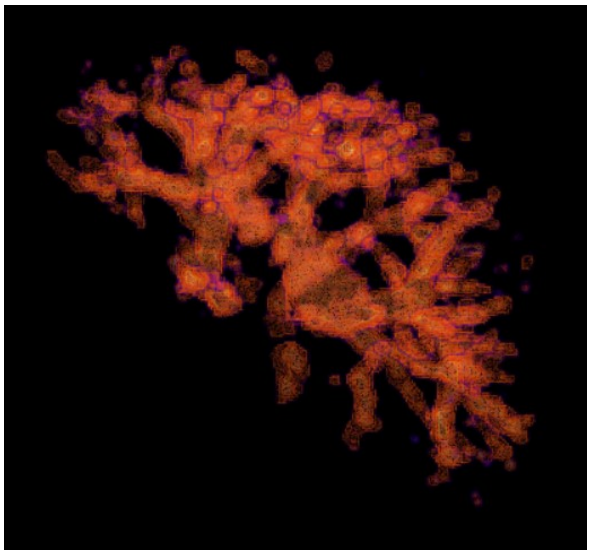

(a) U-Net

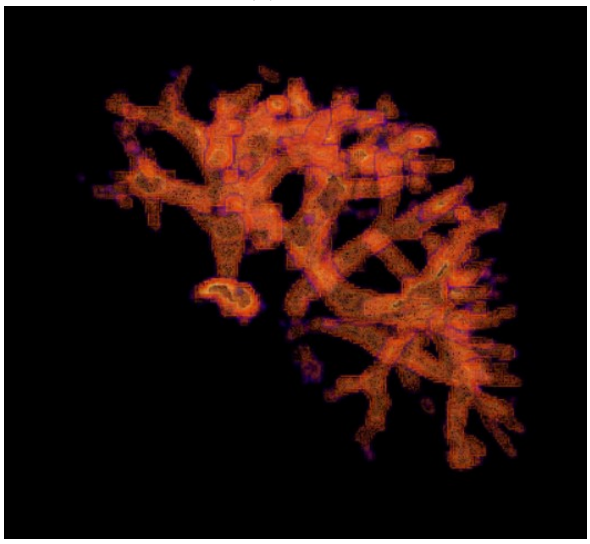

(b) MultiRes U-Net

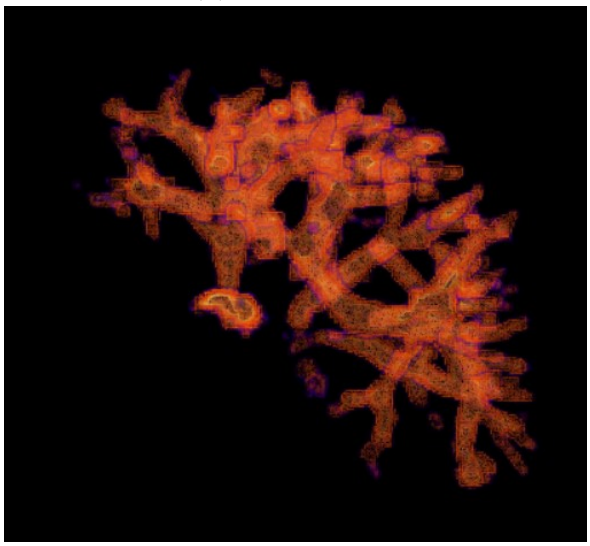

(c) Dense U-Net

Figure 8.3: 3-D ImageJ views of segmentations obtained from an other patient of IRCAD dataset, with the full 3-D volume approach, the results are obtained using Jerman filter as preprocessing step .

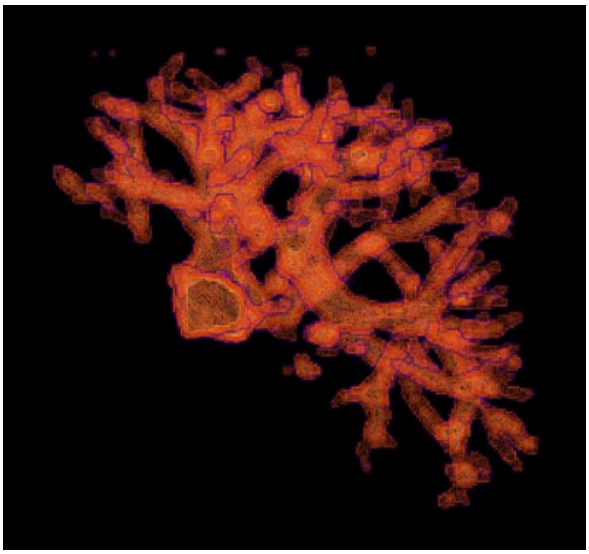

(a) U-Net

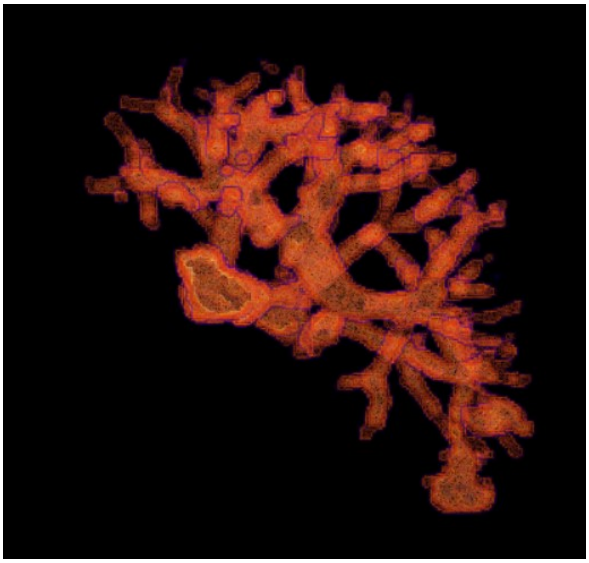

(b) MultiRes U-Net

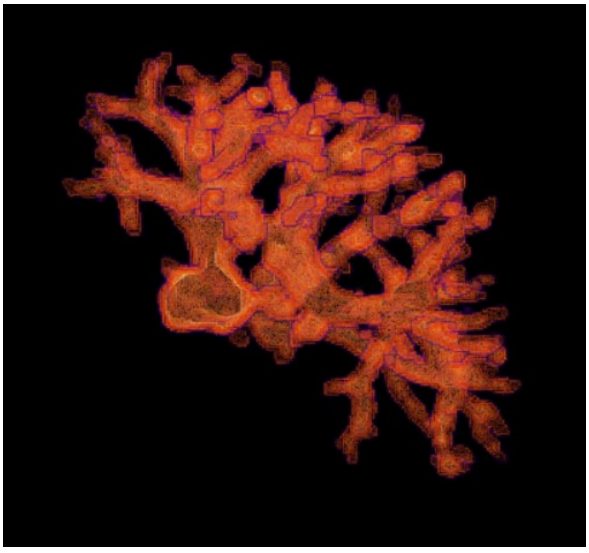

(c) Dense U-Net

Figure 8.4: 3-D ImageJ views of segmentations obtained from an other patient of IRCAD dataset, with the full 3-D volume approach, the results are obtained using Jerman filter as preprocessing step and our proposed W-ClDice as post-processing step.

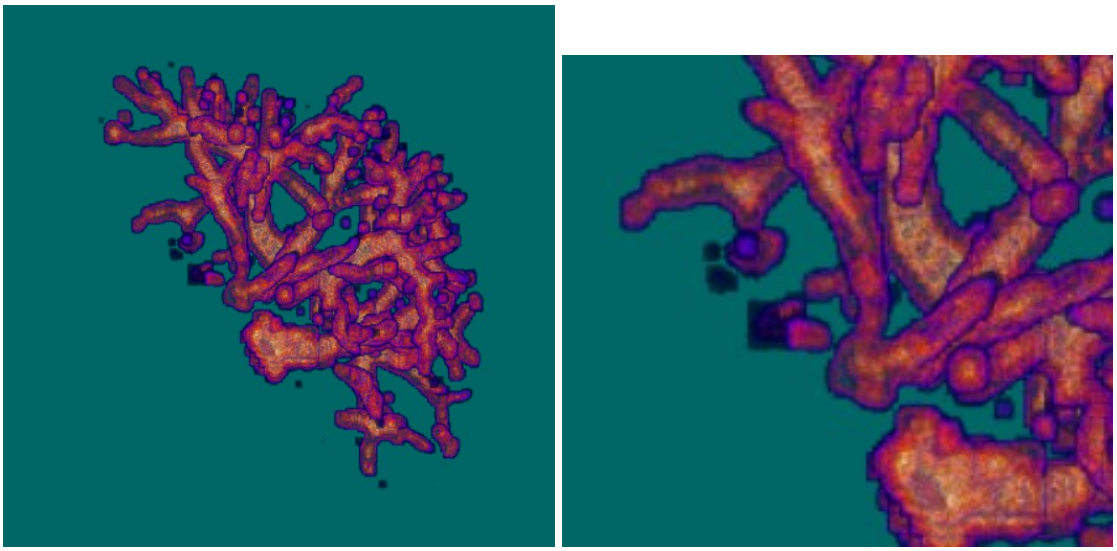

(a) 3-D U-Net

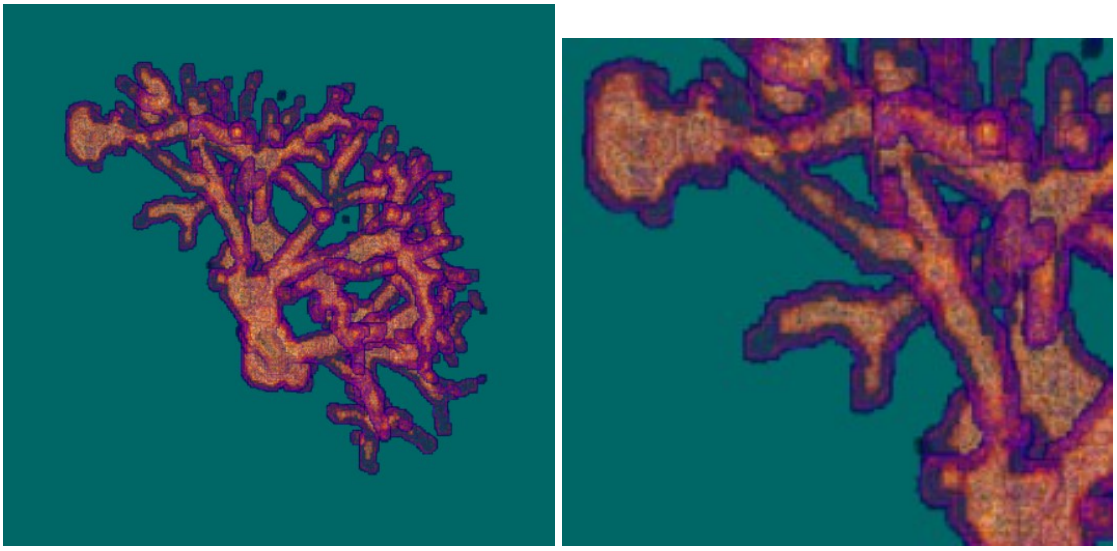

(b) 3-D MultiRes U-Net

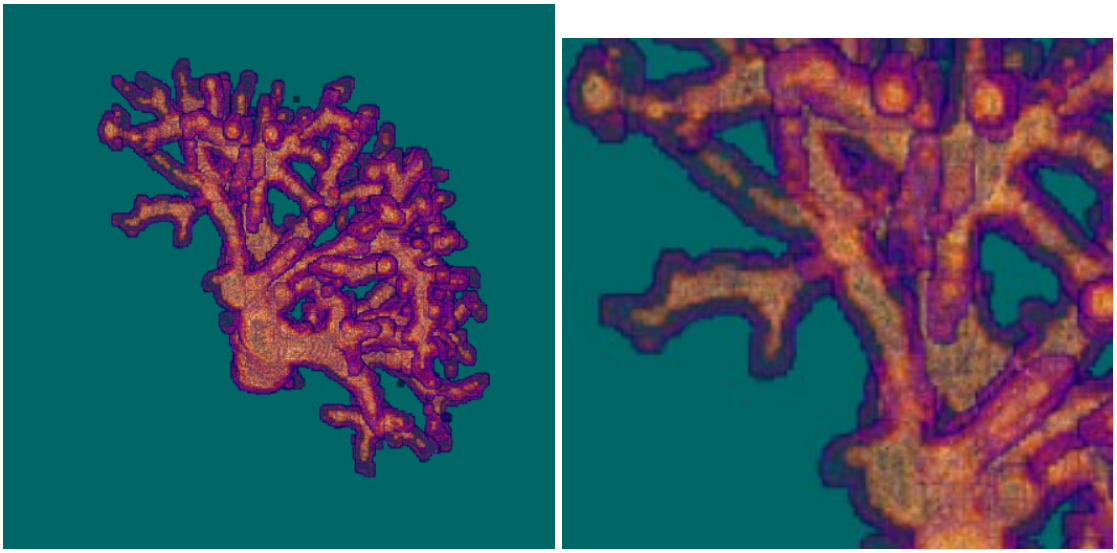

(c) 3-D Dense U-Net

Figure 8.5: 3-D ImageJ views of segmentations and their zoom on bifurcations obtained from an other patient of IRCAD dataset, with the full 3-D volume approach, the results are obtained using Jerman filter as preprocessing step and our proposed W-ClDice as post-processing step.

9 List of publications

A. Affane, A. Kucharski, P. Chapuis, S. Freydier, M.A Lebre, A. Vacavant " **Segmentation of liver anatomy by combining 3-D U-Net approaches**" MDPI Journal of Applied Sciences, 11(11): 4895, 2021.

A .Affane, M.A Lebre, U.MITTAL, A. Vacavant "**Literature Review of Deep Learning Models for Liver Vessels Reconstruction**" in IEEE, IPTA Paris, Nov 2020.

A. Affane, J. Lamy, M.A Lebre, A. Vacavant "**About the combination of vesselness filters and 3-D U-Net architectures for liver vessel segmentation**" BHI-BSN , 2021.

A. Affane, J. Lamy, M.A Lebre, A. Vacavant "**Une combinaison de filtres de rehaussement des vaisseaux avec des architectures 3D U-Net pour la segmentation des vaisseaux hepatiques**" Orasis , 2021.

A. Affane, J. Lamy, M.A Lebre, A. Vacavant "**Robust deep 3-D architectures based on vascular patterns for liver vessel segmentation**" in Informatics in Medicine Unlocked, 2022.

Bibliography

[1] Ben-Cohen A., Diamant I., Klang E., Amitai M., and Greenspan H. **Fully Convolutional Network for Liver Segmentation and Lesions Detection**. *Deep Learning and Data Labeling for Medical Applications* Springer LNCS 1008 (2016) (see page 35).

[2] Martín Abadi, Ashish Agarwal, Paul Barham, Eugene Brevdo, Zhifeng Chen, Craig Citro, Greg S Corrado, Andy Davis, Jeffrey Dean, Matthieu Devin, et al. *Tensorflow: Large-scale machine learning on heterogeneous distributed systems*. 2016 (see page 66).

[3] Abir Affane, Marie-Ange Lebre, Utkarsh Mittal, and Antoine Vacavant. **Literature Review of Deep Learning Models for Liver Vessels Reconstruction**. *IPTA* (2020), 1–6 (see pages 35, 44).

[4] S Azizaddini and N Mani. **Liver imaging**. *StatPearls* (2022) (see pages 31–34).

[5] R Banerjee, F Lui, and P Ke. **Towards Robust Perception using Topological Invariants**. *AISafety IJCAI* (2021), 1–6 (see page 39).

[6] Foie-Voies biliaires. **LES FONDAMENTAUX DE LA PATHOLOGIE DIGESTIVE**. *Editions Elesevier-Masson* (2014) (see pages 23, 27, 33).

[7] Charnchai C Butdee and N Tanpowpong P. **3D plane cuts and cubic Beizier curve for CT liver volume segmentation according to Couinaud's classification**. *Songklanakarin J. Sci. Technol* 39:6 (2017), 793–801 (see pages 18, 19, 37).

[8] G. Chlebus, A. Schenk, J.H. Moltz, B. van Ginneken, H.K. Hahn, and H. Meine. **Automatic liver tumor segmentation in CT with fully convolutional neural networks and object-based postprocessing**. *Nature Scientific Report* 8 (2018), 15497 (see page 36).

[9] François Chollet. **Deep Learning with Python**. Manning, 2017. ISBN: 9781617294433 (see page 66).

[10] Patrick Ferdinand Christ, Florian Ettlinger, Felix Grün, Mohamed Ezzeldin A Elshaera, Jana Lipkova, Sebastian Schlecht, Freba Ahmaddy, Sunil Tatavarty, Marc Bickel, Patrick Bilic, et al. **Automatic liver and tumor segmentation of CT and MRI volumes using cascaded fully convolutional neural networks**. *arXiv preprint arXiv:1702.05970* (2017) (see page 35).

[11] Marcin Ciecholewski and Michał Kassjański. **Computational Methods for Liver Vessel Segmentation in Medical Imaging: A Review**. *MDPI Sensors* 21 (2021), 6 (see pages 35, 44).

[12] James R Clough, N Byrne, I Oksuz, V. A Zimmer, Julia A Schnabel, and A. P King. **A Topological Loss Function for Deep-Learning based Image Segmentation using Persistent Homology**. *Transactions on Pattern Analysis and Machine Intelligence* (2020), 1–13 (see page 39).

[13] Claude Couinaud. **Le foie: études anatomiques et chirurgicale**. *https://www.worldcat.org/title/foi etudes-anatomiques-et-chirurgicales/oclc/912097374?referer=diht=edition* (1957) (see page 23).

[14] CS231n. **Convolutional Neural Networks (CNNs / ConvNets)**. *https://cs231n.github.io/convoluti networks/* (2021) (see page 13).

[15] R Fisher, S Perkins, A Walker, and E Wolfart. **Thinning**. *https://homepages.inf.ed.ac.uk/rbf/HIPR2/thi* (2003) (see page 81).

[16] Ponziani Francesca, Zocco Maria, and Gasbarrini Antonio. **Portal vein thrombosis: Insight into physiopathology, diagnosis, and treatment**. *insight into physiopathology, diagnosis, and treatment. World J Gastroenterol* (2010) (see page 28).

[17] Alejandro F Frangi, Wiro J Niessen, Koen L Vincken, and Max A Viergever. **Multiscale vessel enhancement filtering**. In: *MICCAI*. Springer. 1998, 130–137 (see pages 29, 65).

[18] H Fu, Y Xu, S Lin, D W K Wong, and J Liu. **DEEPVESSEL: Retinal vessel segmentation via Deep Learning and conditional Random field**. *Nature Scientific Reports* (2019) (see pages 37, 38).

[19] T. Germain, S. Favelier, J.-P. Cercueil, A. Denys, D. Krausé, and B. Guiu. **Liver segmentation: Practical tips**. *Diagnostic and Interventional Imaging* 95:11 (2014), 1003–1016. ISSN: 2211-5684. DOI: https://doi.org/10.1016/j.diii.2013.11.004. URL: https://www.sciencedirect.com/science/article/pii/S2211568413003744 (see page 26).

[20] Evgin Goceri, Zarine K Shah, and Metin N Gurcan. **Vessel segmentation from abdominal magnetic resonance images: adaptive and reconstructive approach**. *International journal for numerical methods in biomedical engineering* 33:4 (2017), e2811 (see page 17).

[21] Xiaoyu Guo, Ruoxiu Xiao, Tao Zhang, Cheng Chen, Jiayu Wang, and Zhiliang Wang. **A novel method to model hepatic vascular network using vessel segmentation, thinning, and completion**. *MBEC* 58:4 (2010), 1–16 (see page 18).

[22] Badakhshannoory H, Saeedi P, and Qayumi K. **Liver segmentation based on deformable registration and multi-layer segmentation**. *ICIP: International Conference on Image Processing* (2010), 1–8 (see page 18).

[23] Health. **Liver: Anatomy and Functions**. *https://www.hopkinsmedicine.org/health/conditions-and-diseases/liver-anatomy-and-functions* () (see page 26).

[24] https://www.geeksforgeeks.org/graph-types-and-applications/. **Graph Types and Applications**. *https://www.geeksforgeeks.org/graph-types-and-applications/* (2022) (see page 16).

[25] X Hu, L Fuxin, D Samaras, and C Chen. **Topology-Preserving Deep Image Segmentation**. *Conference on Neural Information Processing Systems* (2019) (see page 39).

[26] X Hu, Y Wang, L Fuxin, D Samaras, and C Chen. **TOPOLOGY-AWARE SEGMENTATION USING DISCRETE MORSE THEORY**. *Published as a conference paper* (2021), 1–8 (see page 39).

[27] Bulat Ibragimov, Diego Toesca, Daniel Chang, Albert Koong, and Lei Xing. **Combining deep learning with anatomical analysis for segmentation of the portal vein for liver SBRT planning**. *Physics in Medicine & Biology* 62:23 (2017) (see pages 36, 37).

[28] Nabil Ibtehaz and M Sohel Rahman. **MultiResUNet: Rethinking the U-Net architecture for multimodal biomedical image segmentation**. *Neural Networks* 121 (2020), 74–87 (see page 48).

[29] Actualité informatique. **Définition Deep Learning**. *https://actualiteinformatique.fr/intelligence-artificielle/definition-deep-learning* (2021) (see page 12).

[30] IRCAD. **3D Image Reconstruction for Comparison of Algorithm Database**. *https://www.ircad.fr/research/3dircadb/* () (see pages 45, 90).

[31] Tim Jerman, Franjo Pernus, Bostjan Likar, and Ziga Spiclin. **Enhancement of vascular structures in 3D and 2D angiographic images**. *IEEE T-MI* 35:9 (2016), 2107–2118 (see pages 29, 65).

[32] Qiangguo Jin, Zhaopeng Meng, Changming Sun, Hui Cui, and Ran Su. **RA-UNet: A hybrid deep attention-aware network to extract liver and tumor in CT scans**. *Frontiers in Bioengineering and Biotechnology* 8 (2020), 1471 (see page 36).

[33] A Juarez, R Selvan, Z Saghir, and M Bruijne. **A joint 3-D U-Net-Graph Neural Network-based method for Airway Segmentation from chest CTs**. *MICCAI* (2019), 1–8 (see pages 38, 80, 84–86, 90, 94).

[34] S Kawajiri, X Zhou, X Zhang, and T Hara. **Automatic segmentation of hepatic vessels in non-contrast X-Ray CT images**. *Radiological Physics and Technology* 1:2 (July 2008), 214–22 (see page 19).

[35] H Kervadec, J Bouchtiba, C Desrosiers, E Granger, J Dolz, and I Ben Ayed. **Boundary loss for highly unbalanced segmentation**. *MedIA deep learning special issue* (January 2021), 285–296 (see page 39).

[36] SH Kim, A Kamaya, and JK Willmann. **CT perfusion of the liver: principles and applications in oncology**. *principles and applications in oncology* 42:1 (2014), 322–44 (see pages 31, 32).

[37] T N Kipf and Max Welling. **Semi-supervised classification with graph convolutional networks**. In: *transactions on neural networks*. IEEE. 2008, 61–80 (see pages 9, 16).

[38] Titinunt Kitrungrotsakul, Xian-Hua Han, Yutaro Iwamoto, Lanfen Lin, Amir Hossein Foruzan, Wei Xiong, and Yen-Wei Chen. **VesselNet: A deep convolutional neural network with multi pathways for robust hepatic vessel segmentation**. *CMIG* 75 (2019), 74–83 (see pages 36, 37, 71).

[39] Titinunt Kitrungrotsakul, Xian-Hua Han, Yutaro Iwamoto, Lanfen Lin, Amir Hossein Foruzan, Wei Xiong, and Yen-Wei Chen. **VesselNet: A deep convolutional neural network with multi pathways for robust hepatic vessel segmentation**. *CMIG* 75 (2020), 74–83 (see pages 37, 71, 94).

[40] Devidas T Kushnure and Sanjay N Talbar. **MS-UNet: A multi-scale UNet with feature recalibration approach for automatic liver and tumor segmentation in CT images**. *Computerized Medical Imaging and Graphics* 8 (2021), 101885 (see page 36).

[41] Hyun Kwon, Hyunsoo Yoon, and Daeseon Choi. **Restricted Evasion Attack: Generation of Restricted-Area Adversarial Example**. *principles and applications in oncology* 7:1 (2019), 60908–60919 (see page 35).

[42] Hyun Kwon, Hyunsoo Yoon, and Ki-Woong Park. **Acoustic-decoy: Detection of adversarial examples through audio modification on speech recognition system**. *Neurocomputing* 417:1 (2020), 357–370 (see page 35).

[43] T Laibacher and S Jalali Weyde. **M2U-NET: Effective and efficient retinal vessel segmentation for resource-Constrained environments**. *Nature Scientific Reports* (2019) (see pages 37, 38).

[44] Jonas Lamy, Odyssée Merveille, Bertrand Kerautret, Nicolas Passat, and Antoine Vacavant. **Vesselness filters: A survey with benchmarks applied to liver imaging**. In: *ICPR*. 2020 (see pages 29, 30, 64).

[45] Jonas Lamy, Odyssée Merveille, Bertrand Kerautret, Nicolas Passat, and Antoine Vacavant. **Vesselness filters: A survey with benchmarks applied to liver imaging**. *ICPR* (2020), 3528–3535 (see pages 65, 66, 72).

[46] DeLeve Laurie D, Valla Dominique Charles, and Tsao Guadalupe Garcia. **Vascular Disorders of the Liver**. *American Association for the Study Liver Diseases* (2009), 1729–1764 (see page 28).

[47] M.-A. Lebre, A. Vacavant, M. Grand-Brochier, H. Rositi, A. Abergel, P. Chabrot, and B. Magnin. **Automatic segmentation methods for liver and hepatic vessels from CT and MRI volumes, applied to the Couinaud scheme**. *Computers in Biology and Medicine* 110 (2019), 42–51 (see page 44).

[48] M.-A. Lebre, A. Vacavant, M. Grand-Brochier, R. Strand, H. Rosier, A. Abergel, P. Chabrot, and B. Magnin. **A robust multi-variability model based liver segmentation algorithm for CT-scan and MRI modalities**. *Computerized Medical Imaging and Graphics* (2019), 74–87 (see page 44).

[49] Huang Lei, Wan Genxun, and Liu Changping. **An Improved Parallel Thinning Algorithm**. *IEEE International Conference on Document Analysis and Recognition (ICDAR)* (2003) (see page 85).

[50] D Lesage, E Angelini, I Bloch, and F Gareth. **A review of 3D vessel lumen segmentation techniques: models and features and extraction schemes**. *Medical image analysis* 13:6 (2009), 819–845 (see page 19).

[51] x Li, X Sun, Y Meng, and J Liang. **Dice Loss for Data-imbalanced NLP Tasks**. *preprint arXiv* (2020) (see page 89).

[52] Xiaomeng Li, Hao Chen, Xiaojuan Qi, Qi Dou, Chi-Wing Fu, and Pheng-Ann Heng. **H-DenseUNet: hybrid densely connected UNet for liver and tumor segmentation from CT volumes**. *IEEE transactions on medical imaging* 37 (2018), 2663–2674 (see page 36).

[53] P Liskowski and K Krawiec. **Segmenting retinal bllod vessels with Deep Neural Networks**. *IEEE TRANSACTIONS On MEDICAL IMAGING* (2019) (see pages 37, 38).

[54] Zhe Liu, Yu-Qing Song, Victor S Sheng, Liangmin Wang, Rui Jiang, Xiaolin Zhang, and Deqi Yuan. **Liver CT sequence segmentation based with improved U-Net and graph cut**. *Expert Systems with Applications* 126 (2019), 54–63 (see page 36).

[55] Jonathan Long, Evan Shelhamer, and Trevor Darrell. **Fully convolutional networks for semantic segmentation**. *IEEE CVPR* (2015), 3431–3440 (see pages 35, 44, 71, 94).

[56] Fang Lu, Fa Wu, Peijun Hu, Zhiyi Peng, and Dexing Kong. **Automatic 3D liver location and segmentation via convolutional neural network and graph cut**. *International journal of computer assisted radiology and surgery* 12 (2017), 171–182 (see page 36).

[57] Odyssée Merveille, Hugues Talbot, Laurent Najman, and Nicolas Passat. **Curvilinear structure analysis by ranking the orientation responses of path operators**. *IEEE TPAMI* 40:2 (2017), 304–317 (see pages 31, 65).

[58] F Milletari, N Navab, and S Ahmadi. **V-Net: Fully Convolutional Neural Networks for Volumetric Medical Image Segmentation**. *Computer Vision and Pattern Recognition* (2016) (see pages 71, 94).

[59] Mehrdad Moghbel, Syamsiah Mashohor, Rozi Mahmud, and M. Iqbal Saripan. **Review of Liver Segmentation and Computer Assisted Detection/Diagnosis Methods in Computed Tomography**. *Artificial Intelligence Review* 50 (2018), 497–537 (see pages 35, 44).

[60] Dominik Müller and Frank Kramer. **MIScnn: a framework for medical image segmentation with convolutional neural networks and deep learning**. *BMC Medical Imaging* 21:1 (2021), 1–11 (see pages 44, 48).

[61] H Nader, massieh A, M Mohiy, Khalid H, and Amin M. **A novel fully automatic technique for liver tumor segmentation from CT scans with knowledge-based constraints**. *nternational Conference on Intelligent Systems Design and Applications (ISDA)* 44 (2010) (see page 18).

[62] M Ô V Ngoc, Y Chen, N Boutry, J Chazalon, E Carlinet, J Fabrizio, C Mallet, and T Géraud. **Introducing the Boundary-Aware loss for deep image segmentation**. *British Machine Vision Conference* (2021), 1–13 (see page 39).

[63] Dário AB Oliveira, Raul Q Feitosa, and Mauro M Correia. **Segmentation of liver, its vessels and lesions from CT images for surgical planning**. *Biomedical engineering online* 10:1 (2011), 1–23 (see pages 18, 19, 37, 38).

[64] Ciacio Oriana and Castaing Denis. **Le Foie et les Voies biliaires : Anatomie**. *https://www.centre-hepato-biliaire.org/maladies-foie/anatomie-foie.html* (2015) (see pages 27, 28).

[65] Wei Qiang and Hu Guangmin. **Evaluating graph neural networks under graph sampling scenarios**. *ICPR* (2022) (see page 17).

[66] Wenjian Qin, Jia Wu, Fei Han, Yixuan Yuan, Wei Zhao, Bulat Ibragimov, Jia Gu, and Lei Xing. **Superpixel-based and boundary-sensitive convolutional neural network for automated liver segmentation**. *Physics in Medicine & Biology* 63 (2018), 095017 (see page 36).

[67] Li. R, Huang. YJ, Chen. H, Liu. X, Yu. Y, Qian. D, and Wang. L. **3D Graph-Connectivity Constrained Network for Hepatic Vessel Segmentation**. *IEEE J Biomed Health Inform* 26:3 (2022), 1251–1262. DOI: 10.1109/JBHI.2021.3118104 (see page 86).

[68] Shima Rafiei, Ebrahim Nasr-Esfahani, Kayvan Najarian, Nader Karimi, Shadrokh Samavi, and SM Reza Soroushmehr. **Liver segmentation in CT images using three dimensional to two dimensional fully convolutional network**. *2018 25th IEEE International Conference on Image Processing (ICIP)* 12 (2018), 2067–2071 (see page 36).

[69] 0. Ronneberger, P. Fischer, and T. Brox. **U-Net: Convolutional Networks for biomedical image segmentation**. *MICCAI* () (see pages 15, 35, 44, 48, 71, 72, 90).

[70] Rosemary. **Where Is The Location of Liver In Your Body - Left Or Right?** *https://knowinsiders.com/where-is-the-location-of-liver-in-your-body-left-or-right-33746.html* (2022) (see page 24).

[71] Mishra. S, Wang. YX, Wei. CC, Chen. DZ, and Hu. XS. **VTG-Net: A CNN Based Vessel Topology Graph Network for Retinal Artery/Vein Classification**. In: *Front Med (Lausanne)*. PMID. 2021. DOI: 10.3389/fmed.2021.750396 (see page 86).

[72] Yoshinobu Sato, Shin Nakajima, Hideki Atsumi, Thomas Koller, Guido Gerig, Shigeyuki Yoshida, and Ron Kikinis. **3D multi-scale line filter for segmentation and visualization of curvilinear structures in medical images**. In: *CVRMed-MRCAS'97*. Springer. 1997, 213–222 (see pages 19, 29, 37, 65).

[73] F Scarselli, A Gori Grover, and J Leskovec. **Scalable feature learning for networks**. In: *international conference on Knowledge discovery and data mining*. IEEE. 2016, 61–80 (see page 9).

[74] F Scarselli, M Gori, A C Tsoi, M Hagenbuchner, and G Monfardini. **The graph neural network model**. In: *transactions on neural networks*. IEEE. 2008, 61–80 (see page 9).

[75] S Shin, S Lee, D Yun, and K Lee. **Deep vessel segmentation by learning graphical connectivity. Medical Image Analysis**. *Medical Image Analysis* 58:101556 (2019), 1361–8415 (see pages 21, 37, 38, 81, 84).

[76] S Shit, J Paetzold, A Sekuboyina1, I Ezhov, A Unger, A Zhylka, J Pluim, U Bauer, and B Menze. **clDice - a Novel Topology-Preserving Loss Function for Tubular Structure Segmentation**. *CVPR* (2021) (see pages 39, 80, 87–90, 92, 94).

[77] Nripendra Kumar Singh and Khalid Raza. **Medical Image Generation using Generative Adversarial Networks**. *arXiv* (2020) (see page 35).

[78] C Sudre, W Li, T Vercauteren, S Ourselin, and M. Jorge Cardoso. **Generalised Dice Overlap as a Deep Learning Loss Function for Highly Unbalanced Segmentations**. *Deep Learn Med Image Anal Multimodal Learn Clin Decis Support* (2017), 1–5 (see page 39).

[79] T Sugino, T Kawase, S Onogi, T Kin, N Saito, and Y Nakajima. **Loss Weightings for Improving Imbalanced Brain Structure Segmentation Using Fully Convolutional Networks**. *Healthcare* (2021), 1–9 (see pages 39, 89).

[80] Changjian Sun, Shuxu Guo, Huimao Zhang, Jing Li, Meimei Chen, Shuzhi Ma, Lanyi Jin, Xiaoming Liu, Xueyan Li, and Xiaohua Qian. **Automatic segmentation of liver tumors from multiphase contrast-enhanced CT images based on FCNs**. *Artificial intelligence in medicine* 8 (2017), 58–66 (see page 35).

[81] Bart R Thomson, Jasper Nijkamp, Oleksandra Ivashchenko, Ferdinand van der Heijden, Jasper N Smit, Niels FM Kok, Koert FD Kuhlmann, Theo JM Ruers, and Matteo Fusaglia. **Hepatic vessel segmentation using a reduced filter 3D U-Net in ultrasound imaging**. *arXiv preprint arXiv:1907.12109* (2019) (see page 37).

[82] Robin Vinod. **Dealing with class imbalanced image datasets using the Focal Tversky Loss**. *https://towardsdatascience.com/dealing-with-class-imbalanced-image-datasets-1cbd17de76b5* (2020), 1–5 (see pages 82, 83).

[83] Minfeng Xu, Yu Wang, Ying Chi, and Xiansheng Hua. **Training liver vessel segmentation deep neural networks on noisy labels from contrast CT imaging**. In: *ISBI*. IEEE. 2020, 1552–1555 (see page 18).

[84] Qingsen Yan, Bo Wang, Wei Zhang, Chuan Luo, Wei Xu, Zhengqing Xu, Yanning Zhang, Qinfeng Shi, Liang Zhang, and Zheng You. **An Attention-guided Deep Neural Network with Multi-scale Feature Fusion for Liver Vessel Segmentation**. *IEEE JBHI* 58:4 (2020), 1–13 (see pages 36, 37, 71).

[85] J Yi and J Ra. **A locally adaptative region growing algorithm for vascular segmentation**. *International Journal of Imaging Systems and Technology* 13:4 (2003), 208–214 (see page 19).

[86] W Yu, B Fang, Y Liu, M Gao, S Zheng, and Y Wang. **Liver vessels segmentation based on 3D Residual U-Net**. *IEEE* (2019) (see page 37).

[87] Ye Zhan Zeng, Yu Qian Zhao, Miao Liao, Bei Ji Zou, Xiao Fang Wang, and Wei Wang. **Liver vessel segmentation based on extreme learning machine**. *Physica Medica* 32:5 (2016), 709–716 (see pages 36, 37).

[88] S Zhai, M Staring, X Zhou, Q Xie, X Xiao, M Bakker, L Kroft, P Boudewijn, F Lelieveldt, J Gudula, A Klok, and B Sotel. **Linking Convolutional Neural Networks with Graph Convolutional Networks: Application in Pulmonary Artery-Vein Separation**. *Springer International Publishing* (2019), 36–43 (see pages 37, 38, 80).

[89] Huahai Zhang, Peirui Bai, Xiaolin Min, Qingyi Liu, Yande Ren, Hui Li, and Yixuan Li. **Hepatic vessel segmentation based on an improved 3D region growing algorithm**. *Journal of Physics: Conference Serie* 1486:1 (2020), 032038 (see pages 35, 44).

[90] Rui Zhang, Zhuhuang Zhou, Weiwei Wu, Chung-Chih Lin, Po-Hsiang Tsui, and Shuicai Wu. **An improved fuzzy connectedness method for automatic three-dimensional liver vessel segmentation in CT images**. *J Healthc Eng* 2018 (2018) (see page 29).

[91] Rui Zhang, Zhuhuang Zhou, Weiwei Wu, Chung-Chih Lin, Po-Hsiang Tsui, and Shuicai Wu. **An improved fuzzy connectedness method for automatic three-dimensional liver vessel segmentation in CT images**. *J Healthc Eng* 2018 (2018) (see page 65).

[92] Yao Zhang, Zhiqiang He, Cheng Zhong, Yang Zhang, and Zhongchao Shi. **Fully convolutional neural network with post-processing methods for automatic liver segmentation from CT**. *2017 Chinese Automation Congress (CAC)* 8 (2017), 3864–3869 (see page 35).

[93] Z Zhou, M Siddiquee, N Tajbakhsh, J Liang, A Foruzand, W Xionge, and Y. Chen. **UNet++: Redesigning Skip Connections to Exploit Multiscale Features in Image Segmentation**. *Transactions on Medical Imaging* (2020), 1729–1764 (see pages 71, 94).